The Contribution of Chronic Protein Kinase C-Mediated Troponin I Phosphorylation to Cardiac Dysfunction

By

Vani Ravichandran

A dissertation submitted in partial fulfillment
of the requirements of the degree of
Doctor of Philosophy
(Cellular and Molecular Biology)
in the University of Michigan
2022

Doctoral Committee

Associate Professor Margaret V. Westfall, Chair
Professor Daniel A. Beard
Professor Daniel E. Michele
Associate Professor Scott Soleimanpour

Vani S. Ravichandran

vaniravi@umich.edu

ORCID iD: 0000-0003-2360-0837

Dedication

To my sweet Saradha Avva and Vishwanath Pedanna,

Until we meet again.

Acknowledgements

I extend my deepest gratitude to my mentor, Dr. Margaret Westfall. You have taught me far more than how to plan experiments, give strong presentations, and think about complex problems. Under your guidance, I have learned to be an independent, confident, and self-sufficient scientist. Thank you for consistently challenging me, and for having me prove to myself that I can accomplish anything. It has been an honor to train under you. While I do not think I could ever repay you for your efforts, I hope that the impact that I am able to make in my career is a reasonable start. Thank you so much for believing in me—it means more to me than you will ever know.

To the rest of my dissertation committee, Dr. Daniel Beard, Dr. Daniel Michele, and Dr. Scott Soleimanpour; thank you for always challenging me to think outside of the box in science, and for encouraging me to continually set realistic and yet aggressive goals. Each of you has given me unique gems of advice which have been instrumental in propelling me forward in my academic and career pursuits. I am grateful to be able to carry with me, the strong intellectual skillsets I developed under you all.

I extend a very special thank you to my former colleague and dear friend, Ms. Tabea Schatz. Thank you for helping me to develop my technical skills, thank you for all of your hard work and patience at the bench, and thank you for being a wonderful friend through my PhD journey. I would like to thank all other past and current members of the Westfall Laboratory; it has been a pleasure to work alongside every one of you. I would also like to thank the Cellular &

Molecular Biology (CMB) graduate program for making the PhD journey so smooth. Special thank you to the former and current CMB directors and administrators, Dr. Roberta Fuller, Dr. Manoj Puthenveedu, Patricia Ocelnik, Jessica Kijek, and Lauren Perl, who have always gone above and beyond to provide students with unmatched support.

No words can describe my gratitude for the unfailing support of my parents. Dad, your authentic love for science sparked my interest in it. To be one-tenth of the scientist you are in my lifetime would be a colossal success. Amma, to articulate your selfless dedicated service to your children would be naïve. Thank you for always rooting for me and for consistently checking in on my mental and physical health. Ashwin Anna and Ajay Anna— you are the best older brothers I could ask for. My getaway from Ann Arbor, my on-call presentation critiques, and the graceful recipients of my stressed calls and texts. Ashwin Anna, the countless hours you spent drilling cardiac pathophysiology into my brain are not taken for granted. My gratitude to you is immeasurable. Ajay Anna, I am grateful to have shared so many adventures with you from childhood to professional school. Thank you for everything.

To my high school honors biology teacher, Mrs. Jennifer Mockensturm, you were my first female-in-science role model. You inspired my scientific journey in a way that no one else could. From the bottom of my heart, thank you. To the Meyerhoff and MARC U* STAR Scholars programs at the University of Maryland, Baltimore County, thank you for giving me every imaginable tool to succeed in my pursuit of a PhD.

To all those I was unable to explicitly thank in this dissertation, there are not enough days in this eternity for me to adequately express my gratitude. My journey does not end here, and I hope to continually make you all proud.

TABLE OF CONTENTS

List of Tables

Supplemental Tables

List of Figures

Supplemental Figures

Abstract

Heart failure (HF), a leading cause of death in the United States, is characterized as dysfunction in the filling or pumping of blood from the heart. The myofilaments, a key component of the heart's muscle machinery, are directly responsible for force production and contraction of cardiac muscle cells, that are essential for the heart's pumping function. Myofilaments contain repeating units of sarcomeres, composed of highly organized arrangements of thin and thick filaments. In the absence of Ca^{2+}, the thin filament molecular switch protein cardiac troponin I (cTnI), inhibits the interaction between thin and thick filaments. When Ca^{2+} levels increase in response to an action potential, cTnI toggles from actin towards troponin C (cTnC), the Ca^{2+}-binding subunit of the heterotrimeric troponin (cTn) complex, allowing thick filament myosin to bind and slide the thin filament. The oscillatory function of cTnI can be modulated via phosphorylation by a number of kinases. This dissertation focuses on the impact of chronic protein kinase C (PKC) phosphorylation of cTnI at the S43/45 residues, to test whether it produces contractile dysfunction leading to HF.

Multiple biochemical and *in vitro* studies indicate that S43/45 phosphorylation in cTnI increases during HF, and this phosphorylation diminishes contractile function. However, there is debate about whether S43/45 phosphorylation plays a similar role *in vivo*, primarily because of the lack of mouse models studying phosphorylation at *only* cTnI S43/45. One major goal of the presented work is to determine whether *in vivo* S43/45 phosphorylation causes cardiac dysfunction. The hypothesis tested is that acute S43/45 phosphorylation acts as a master brake on

contractile function, while chronic S43/45 phosphorylation produces progressive cardiac dysfunction, and the absence of phosphorylation at this site does not change resting contractile function. As part of investigating the *in vivo* S43/45 phosphorylation role, we also sought to determine whether the amount of phosphorylation (i.e., phosphorylation "dose") in this cluster had an impact on the *in vivo* response. To address this question, transgenic mice were generated to replace endogenous cTnI with varied levels of phospho-mimetic aspartic acid (D) at *only* S43/45 (cTnIS43/45D). In these mice, cTnIS43/45D causes dose-dependent, progressive cardiac dysfunction and remodeling, leading to HF and death. Additional work tests whether sarcomere-to-mitochondrial communication is an early contributor to the progressive phenotype. Specifically, studies test the idea that early accumulation of mitochondrial reactive oxygen species (ROS) disrupts mitochondrial function and lays the foundation for progressive HF. Then, studies test whether early mitigation of mitochondrial ROS improves contractile function.

Parallel analyses using non-phosphorylatable substitutions at S43/45 bolsters the idea that chronic S43/45 phosphorylation is detrimental *in vivo*. Previously, traditional nonpolar alanine (S43/45A) substitutions at S43/45 reduced cardiomyocyte contractile function and myofilament Ca^{2+} sensitivity. These alterations indicated the A substitution is not functionally conservative at S43/45. Earlier studies also showed that novel non-phosphorylatable asparagine (N) used in place of A (S43/45N) does not alter *in vitro* contractile function. Thus, in this dissertation, *in vivo* cardiac function was analyzed by echocardiography in mice expressing cTnIS43/45N, with no change in cardiac morphology and function. Together, the studies presented here demonstrate chronic cTnI S43/45 phosphorylation causes HF via mitochondrial dysfunction, while the lack of phosphorylation does not impact cardiac function. These findings are relevant to a broad

population of patients at-risk for HF, as many pathologies are associated with increased PKC activity and presumably, downstream cTnI phosphorylation.

Chapter 1

Introduction

Heart Function

The highly muscular, beating heart pumps blood to deliver nutrients and oxygen to all vital organs [1]. Mammalian hearts have four chambers: right and left atria, and right and left ventricles (Fig. 1.1). Blood flows into the right atrium, then the right ventricle, and is then pumped to the lungs for oxygenation. Oxygenated blood then returns to the left atrium, followed by the left ventricle, which pumps oxygenated blood to the rest of the body [1]. This process is cyclical, and requires unidirectional flow provided by the four valves separating the atria, ventricles, and external circulation on each side. The heart's performance is controlled by tightly regulated contraction and relaxation of cardiomyocytes, which contain the cardiac muscle's mechanical machinery required for cyclical pumping (Fig. 1.2).

The heart is inarguably the most vital organ in the body. It is directly responsible for perfusing vital organs with blood, nutrients, and oxygen, and its performance is modulated based on the body's needs. Early observations led to the observation that the heart can inherently modify contraction. During diastole (filling), myocardial fibers are stretched as the ventricle fills with blood. According to Starling's law of the heart or the Frank-Starling relationship, increasing the length of cardiac muscle fibers increases the force with which they contract [2]. This means the heart can more forcefully contract during each cycle and therefore deliver more blood to peripheral organs. The heart's performance can be described as "cardiac output" or CO, and mathematically defined as:

*Cardiac Output (volume blood pumped per minute) = Stroke Volume * Heart Rate*

*(CO= SV*HR)*

Thus, anything that modulates 1) the amount of blood the heart can pump with each contraction, or 2) the heart rate, can impact CO. External factors also can modulate CO, such as neuro-hormonal input, endocrine and/or paracrine signaling, or the load against which the heart must work to initiate and complete systole (referred to as afterload). At the molecular level, this external modulation is mediated via several signaling pathways targeting multiple proteins to alter cardiac function, including post-translational modification of cardiac muscle proteins. While multiple pathways modulate cardiac performance, sarcomere proteins are fundamentally responsible for contraction and relaxation within the cardiomyocyte—and are a key target for these signaling pathways.

Contractile proteins in the sarcomere work together at the cellular and molecular level to dynamically regulate contractile performance within the heart. Inherited mutations in cardiac contractile proteins alter these interactions and can detrimentally impact CO. In addition, chronic post-translational modification of cardiac muscle proteins can significantly impact heart performance over time. This dissertation focuses on how chronic phosphorylation of a critical contractile protein, cardiac troponin I (cTnI), can alter heart performance, cause cardiac dysfunction and lead to heart failure (HF). More specifically, these studies establish that site-specific phosphorylation in cTnI at S43/45 is elevated in human HF, contributes to dysfunction in a mouse model, and initiates a progressive pathological response that can result in cardiac pump failure. This work builds upon *in vitro* biochemical and cellular studies conducted previously [3-5]. Here, phosphorylation is mimicked in murine animal models with a cTnIS43/45D substitution. Then, cardiac structure and function is analyzed at the *in vivo*, cellular

and molecular levels to provide insight into the role of this cluster in causing cardiac dysfunction.

The heart is an excitable organ

The heart is rich with excitable cardiomyocytes (excitable cells). Like any other cell, the cardiomyocyte contains a plasma membrane (termed "sarcolemma") which provides a barrier between the contents of the cell and the surrounding environment (Fig. 1.2). Pump function in the heart relies on an endogenous pacemaker located in the right atrium, and the spread of this initial electrical stimulus via subsidiary pacemakers distributed throughout the heart. These pacemaker cells spread the electrical stimulus to produce an action potential in every contractile cell in the heart. Cardiomyocytes are elegantly arranged in a functional syncytium to allow for rapid spread of this electrical stimulus [6]. Specifically, end-to-end connection of cardiomyocytes via gap junctions allows rapid transmission of electrical impulses throughout the heart.

Cardiac contractile function is initiated by electrical excitation of the cardiomyocyte in the form of an action potential. During an action potential, myocytes undergo depolarization, which is the first step in initiating coordinated contraction (or systole) by the heart. Repolarization of each myocyte also is required for relaxation (diastole) [6]. Multiple currents contribute to the action potential, including Ca^{2+} influx via sarcolemmal voltage-gated L-type Ca^{2+} channels, which then triggers a larger release of Ca^{2+} from the endoplasmic reticulum (termed sarcoplasmic reticulum or SR in muscle). This process is known as calcium-induced calcium release, or CICR (Fig. 1.2), and these steps are critical for linking excitation (e.g. action potentials) to contraction. The rapid rise in cytosolic Ca^{2+} produced by CICR results in Ca^{2+} binding to troponin's Ca^{2+} binding subunit, troponin C (TnC) within the myofilaments. Then,

Ca^{2+}-bound TnC initiates conformational changes within the myofilaments to generate a contraction (systole) [6, 7]. The translation of an electrical impulse into a mechanical contractile event is collectively termed "excitation-contraction coupling" (E-C coupling). As the myocyte repolarizes, relaxation (diastole) begins as Ca^{2+} is released from the myofilament, and Ca^{2+} levels return to baseline via a Ca^{2+} pump in the SR as well as Ca^{2+} extrusion via sarcolemmal transporters [6]. While action potentials are needed to initiate the electrical events prior to contraction, *pump function in the heart is a direct result of the work of myofilaments within the excitable cardiomyocyte.*

HF: Progressive dysfunction and remodeling

HF is a leading cause of death in the United States affecting >6 million Americans annually [8]. HF is a disease of many etiologies, wherein the heart's filling and/or ejection capabilities are compromised. While numerous therapies exist to provide palliative care for HF, currently there is no cure for the disease other than transplantation.

Typically, HF is categorized into left, right, or dual-sided HF—referring to the most severely-impacted ventricle(s). In healthy adult individuals, the ejection fraction (volume of blood pumped/volume of blood received in the ventricle) typically remains over 50%. A decrease in this ratio (as seen in HF) indicates a decrease in the heart's pump function. HF has many causes including tissue damage due to myocardial infarction, hypertension, inherited myopathies, aging, and more [9-11], but ultimately, the failing heart is unable to keep up with the metabolic demands of the body. Preceding the ultimate failure of the heart are a series of cellular, interstitial, and whole-organ compensatory changes to maintain heart function, some of which will be explored in Chapter 4.

A heart compensating for dysfunction undergoes cardiac remodeling to maintain function. This response includes hypertrophy of the afflicted ventricle, fibrosis, stiffening of the ventricle, endothelial dysfunction, and inflammation, until the heart is no longer able to compensate and the changes become maladaptive [12]. HF is broadly categorized into two types: HF with reduced ejection fraction (HFrEF) and preserved ejection fraction (HFpEF) [13]. Two types of pathological remodeling commonly observed are “hypertrophy” and “dilation”, which are predominantly responsible for HFpEF or HFrEF, respectively. In a hypertrophic phenotype, ventricular walls “thicken” to compensate for enhanced systolic (pumping) function, and this most often results in HFpEF. In these hearts, sarcomeres are added to each cardiomyocyte in parallel (one next to another) to produce concentric hypertrophy, increase ventricular wall thickness, more muscle for pumping and a hypercontractile ventricle, but this remodeling also slows relaxation, leading to HFpEF. In contrast, an individual with a dilated phenotype experiences eccentric hypertrophy that results in an enlargement of the ventricular chamber, to accommodate more blood during diastole (filling). In this situation, systolic function becomes impaired and results in HFrEF, or inadequate pumping of blood during systole. Inherited cardiac muscle defects (cardiomyopathies) also can cause either of these phenotypes (hypertrophic cardiomyopathy is termed HCM and dilated cardiomyopathy is termed DCM). Documented examples of inherited cardiomyopathy mutations develop in sarcomere proteins such as the thin filament protein cardiac troponin I (cTnI), and include R21C, P82S, R145G/Q, G203S and K206Q that are linked to HCM [14-16], and K36Q and N185K that are associated with DCM [17, 18]. Currently, most therapies exist to target HFrEF, though roughly half of HF cases have preserved EF [19].

While cardiomyocytes contribute to 75% of myocardial tissue, other cells are present in the heart and can play important roles in the development of HF. A majority of the remaining cells in the heart are fibroblasts [20]. Fibroblasts typically produce components of the extracellular matrix such as collagen, periostin, vimentin, and fibronectin [21]. Fibroblasts, an abundant cell type within the heart provide structural support, and also contribute to remodeling in the diseased heart [22]. Upon injury, fibroblasts differentiate into hybrid fibroblast-smooth muscle cells called "myofibroblasts" that secrete extracellular matrix components, namely collagen, to preserve the structure of the ventricular wall as injured cardiomyocytes die [23]. However, the accumulation of extracellular matrix—termed "fibrosis" is not a suitable environment for efficient spread of electrical impulses through the myocardium's functional syncytium. Combined with the death of contractile cells in the heart, this pathologically compromises heart function. These changes contribute to the presentation of a stiffer heart, inability to efficiently spread electrical impulses from the sinoatrial node through the rest of the heart, and finally, a fatal arrhythmia.

The endothelium, a layer of squamous cells that lines blood vessels (in this case arteries and veins such as the aorta and pulmonary vein) also plays a role in the progression of HF. The primary role of the endothelium is to regulate structural integrity of the vessel, blood flow, vascular permeability, and to respond to injury [24]. Endothelial dysfunction is routinely noted in HF, where the delicate balance in endothelial function is dysregulated [24]. Inflammation is also commonly noted in HF, however, its precise role in the pathogenesis is unclear [25]. In summary, changes in multiple cell types occur during HF. However, the fundamental ability to pump blood depends on the myofilament in cardiomyocytes.

Myofilament Organization: The master regulator of contractile function

The myofilament is comprised of highly structured, overlapping thin and thick filaments which are collectively organized into sarcomeres, and the functional units of the contractile machinery in the myocyte (Fig 1.2). The region of the sarcomere spanning the thick filament is called the A-band, and the M-band resides in the center of the A band, flanked by ribbons of myosin binding protein C (MyBP-C). The contractile proteins in the thick filament include the motor protein myosin heavy chain (MHC) containing the myosin head (a Mg^{2+}-ATP hydrolyzer or ATPase) plus the myosin light chains (MLC) which modulate myosin's function and movement along with MyBP-C [26]. Anchoring the sarcomere on either end is a Z-band (or Z-disk), and I-bands containing the thin filament span the region of the sarcomere flanking the Z-bands (Fig. 1.2) [27]. Filamentous actin is arranged in a coiled-coil and forms a backbone for the thin filament proteins contributing to contraction. Important accessory proteins are integrated into this actin backbone including tropomyosin (Tm) and heterotrimeric troponin (Tn) regulatory proteins in a 7:1:1 molar ratio [28] (Fig. 1.3A). The Tm-Tn complex is crucial for transduction of the E-C-induced Ca^{2+} signal into mechanical contraction [29]. The Tn complex is a heterotrimer consisting of a Ca^{2+}-binding subunit (TnC), a Tm-binding subunit (TnT), and an inhibitory subunit (TnI) [30] [31-33]. Assembly of the sarcomere is unique; while tropomyosin and actin are assembled in an ordered manner, troponin is incorporated into the sarcomere stochastically [34, 35]. In this way, the sarcomere is highly organized and tightly regulated, and strictly adheres to this stoichiometric arrangement. This information becomes critical later on when genetic manipulation of the heart is discussed.

During diastole (relaxation) and/or in the absence of calcium, the myosin motor does not produce force because its interaction with actin is limited. The thin filament directly prevents

interactions between actin and myosin in the absence of Ca^{2+}. Specifically, Tm and the cTnI subunit of Tn occupy positions to prevent the myosin head from forming strong, force-generating crossbridges (XBs) with actin. To initiate systole (contraction) the action potential-induced sarcolemma Ca^{2+} current and CICR SR Ca^{2+} release produce a rapid increase in cytosolic Ca^{2+}. This cytosolic Ca^{2+} binds to a divalent cation binding site within the N-lobe of TnC which elicits a conformational change in the Tn complex. This conformational change causes a coordinated increase in the affinity of TnI for TnC, and decreased affinity of TnI for actin. The switch of TnI from actin to TnC produces a coordinated change throughout the Tn complex and positioning of Tm on the actin surface [36] (Fig. 1.3B). Most importantly, this Ca^{2+} signal initiates changes in thin filament Tn-Tm which now allows myosin to form a strong, force-generating interaction with actin and generate the power stroke necessary to cause thin filament sliding for mechanical contraction. This is the key underlying mechanism for cardiac pump performance. TnI is therefore considered a "switch" protein responsible for regulating contraction in the heart and other striated muscles.

Also during systole, the XB hydrolyzes ATP into ADP and P_i [37]. The "power stroke" is triggered during this transition to ADP and Pi and the XB binds to actin and slides the thin filament (Fig. 1.3A). The power stroke is the fundamental step required for pressure generation by the ventricles within the heart as the sarcomere generates force and/or shortens. Upon ADP dissociation from the myofilament and replacement by ATP, the XB is released from the thin filament, and the sarcomere relaxes (diastole).

A two-state Hill model showing the cycle of ATP, ADP and P_i for attachment and detachment between myosin plus actin is traditionally used to explain muscle contraction. A newer model now incorporates steps in thin filament activation [38, 39] based on observations

showing that contraction and relaxation are mediated by Ca^{2+} binding to TnC in addition to the XB [40, 41]. In the more recent model, Tm can exist in at least 3 states or positions to alter XB interactions with the thin filament (Fig. 1.3) [37, 39]. The three positions are "blocked" (B) with no Ca^{2+} bound to the thin filament (TF), "closed" (C) with Ca^{2+} bound to the TF and a XB weakly bound to the thin filament, and "open" (M) where the XB is now strongly bound to thin filaments to develop force within the myofilament [37]. Apart from just hydrolysis of ADP and release of P_i, the strongly bound XB in the third state can also increase the affinity of a neighboring XB for the thin filament to produce another open, strongly bound XB, and thus, cooperatively activates the force generated by the sarcomere [37]. Though still debated, Tm is postulated to revert to the C state before transitioning to the B state, as Ca^{2+} is released from the myofilament and intracellular Ca^{2+} decreases to a diastolic baseline [6, 7]. In summary, Tn-Tm can dynamically occupy three different positions, and the position in which it resides is largely determined by the presence of Ca^{2+} and neighboring XB's. The idea of 3 states has since been corroborated and expounded by experimental findings [40-43]. While this dissertation work focuses on the thin filament, it is crucial to note that contraction and relaxation results from coordinated work between thin and thick filaments. Recent literature supports the idea that thick filament myosin can also exist in at least 3 states; 1) an ordered- or super-relaxed state with inactive myosin having low ATPase activity, 2) a disordered-relaxed state with ATPase activity and myosin heads "eligible" for interaction with the thin filament), and 3) an active state with ATPase activity and strongly bound to actin [44]. The apparent complexity of muscle activation, and newer models of sarcomere activation rely on multiple states, and occupancy of these states are likely modulated via a variety of processes. For example, key mechanisms of coordinated muscle contraction delineated above can be modified or modulated by post-translational

modifications (PTMs) of contractile proteins. The focus of this dissertation is on a specific PTM within cTnI and its *in vivo* role in both sarcomere and cardiac pump performance.

Troponin I: A critical regulator & modulator

There are three isoforms of troponin I (TnI): cardiac (cTnI), fast (fsTnI), and slow skeletal (ssTnI) [45, 46], and each act as a molecular switch within the sarcomere that prevents strong XB interaction with actin in the absence of Ca^{2+}. Slow skeletal TnI is expressed in the heart during embryonic development, and the heart irreversibly transitions to expressing cTnI perinatally in mammals [47-50]. The 25kDa cTnI protein has multiple distinct regions—a unique and flexible N-terminus, two sets of α-helices (H1 and H2), an inhibitory peptide (IP) region, a regulatory domain (H3 helix) and a H4 helix containing a mobile domain [51] (Fig. 1.4A-C). Ca^{2+} binding to the N-lobe of cTnC initiates conformational changes in cTnI followed by an array of conformational changes in the thin filament. Within cTnI domains, the IP region is notable because it is highly flexible and dynamically oscillates between strong binding to actin in the absence of Ca^{2+} to strong binding to cTnC upon Ca^{2+} binding to cTnC. In addition, the amphiphilic H3 helix of cTnI is important because its insertion into a hydrophobic patch within cTnC is a necessary step for Ca^{2+} to bind to TnC in cardiomyocytes. Together, these conformational changes shift from disinhibiting the actomyosin interaction to allowing a force generating XB attachment to actin as Ca^{2+} binds to TnC. Less is known about the specific roles played by the H1, H2 and H4 helices of cTnI. Currently, the cTnI H2 helix is known to form an IT-arm with the cTnT C-terminal helix; a well-conserved antiparallel coiled-coil structure [52]. While the IT-arm does not have direct contacts with actin or tropomyosin, it is predicted to optimize positioning of the Tn complex within the thin filament by providing structural rigidity

[51]. A portion of the H4 helix also anchors cTnI to the azimuthal actin on the actin backbone [53]. The cTnI phosphorylation cluster of interest in this dissertation is S43/45, which is positioned at the N1 and N3 positions of the H1 helix [51]. It is possible, therefore, that phosphorylation at these sites could alter the rigidity of this H1 helix to alter the function of the downstream I-T arm and/or communication to cTnT-Tm, and result in alterations in pressure generation and/or relaxation by the ventricle [54]. In addition, the S43/45 site is located near the IP domain in the 3-dimensional structure of Tn [51] (Fig. 1.4), and this could modify the ability of the IP region to disinhibit the actomyosin interaction, though no studies prove there is this local impact of S43/45 phosphorylation. Based on this background, cTnI switch function is incompletely understood. Post-translational modification (PTM) of cTnI also modifies cTnI switch function, but the mechanism(s) are incompletely understood. This dissertation work specifically focuses on the phosphorylation of cTnI as a means of fine-tuning or modulating function within the heart. Information about the kinases responsible for phosphorylation, as well as the known downstream impact of phosphorylation, are therefore critical to know for this project.

AGC kinases and the myofilament

To date, over 60 AGC kinases in the human genome have been identified. In 1995, Steve Hanks and Tony Hunter classified AGC kinases as protein kinases with considerable sequence homology to PKA, PKG, and PKC (cyclic AMP-dependent, cyclic GMP-dependent, and nucleotide-independent protein kinases, respectively) [55]. Early studies indicated that short primary sequences flanking a substrate's phosphorylation site provided substrate specificity for a kinase [56, 57]. AGC kinases target serine and threonine (S/T) residues that lie within specific

consensus sequences that confer kinase-specificity [58]. Structurally, AGC kinases possess a catalytic (C) and non-catalytic regulatory (N) lobe which "hold" the ATP required for phosphorylation of AGC kinase substrates [59, 60]. The AGC kinases are typically activated by site-specific phosphorylation in the catalytic domain and a hydrophobic motif in the non-catalytic domain. Phosphorylation of the catalytic domain initiates conformational changes that coordinate the appropriate organization of the N lobe, C lobe, and ATP for catalytic activity [61, 62]. In fact, in the non-phosphorylated state, some AGC kinases lack the hydrophobic motif and catalytic segment organization necessary to prevent interactions with ATP [61]. This suggests that these site-specific phosphorylation regions within AGC kinases maintain the appropriate structural conformation needed to achieve maximal activation of the kinase.

AGC kinases play an important role in the physiological and pathophysiological modulation of cardiac function via the myofilament. For instance, β-adrenergic stimulation activates PKA to phosphorylate S23/24 within cTnI, because both serines meet PKA's minimal consensus sequence [63, 64]. Upon S23/24 phosphorylation, myofilament Ca^{2+} sensitivity decreases, Ca^{2+} release from cTnC is accelerated, and relaxation in the heart is enhanced [64-67]. Conversely, increased PKC (another member of the AGC kinase family) activity develops during pathologies such as HF [68] and increases downstream phosphorylation of multiple residues within the myofilament, including cTnI S43/45 [69]. When S43/45 are phosphorylated, myofilament Ca^{2+} sensitivity decreases along with enhanced Ca^{2+} dissociation from cTnC, and slowing in the rate of *in vitro* contraction and relaxation [5, 70]. The above two examples highlight the opposing roles that AGC kinases can play in modulating myofilament function. Given what is known about cTnI S23/24 vs S43/45 phosphorylation, it is conceivable that PKA serves as an acute accelerator in response to sympathetic stimulation, while PKC acutely serves

as a master break on contractile function to extrinsically coordinate modulation within the sarcomere. While there is no universal approach for targeting AGC kinases in the treatment against HF, an improved understanding of how AGC kinases modulate cardiac function has led to the identification of therapeutic targets for HF such as β-blockers [71]. Later chapters of this dissertation stress the need for a deeper understanding of how site-specific PKC phosphorylation of the myofilament impacts cardiac function. Studies in this dissertation test the idea that PKC activity becomes pathological when chronically upregulated and targeting cTnI S43/45 in cardiac-related diseases such as HF, diabetes, and hypertension [9, 11, 68].

PKC and the Heart

Nishizuka first discovered PKC in 1977 by partially purifying the enzyme from bovine cerebellum [72]. He described it as a cyclic nucleotide-independent serine-threonine protein kinase [72]. While the protein possessed similar kinetic and phosphorylation properties to PKG and PKA, chromatography data revealed this kinase depended on calcium and phospholipids for activation [72, 73]. Since then, twelve isoforms of PKC have been identified and categorized based on their second messenger requirements for activation [74] (Fig. 1.5).

The catalytic domains of PKC isoforms are highly homologous, but the non-catalytic domains confer their regulatory response to second messengers. After phosphorylation of the catalytic segment and hydrophobic motif, PKC is competent to achieve full activation by the second messengers Ca^{2+} and/or diacylglycerol (DAG). Isoenzymes are sub-grouped into conventional, novel, and atypical classes based on their regulatory characteristics. The conventional PKC's (cPKC's) include PKCα, PKCβ1, PKCβ2, and PKCγ, and they are activated by elevated Ca^{2+} plus a 2^{nd} messenger in the form of diacylglycerol (DAG), in the presence of

membrane phospholipids such as phosphatidylserine [75-77]. This activation pattern requires the C1 and C2 binding domains within the cPKC amino-terminal regulatory domain that function as sensors for DAG and Ca^{2+}/phospholipids, respectively. Novel class PKCs (nPKCs) consist of related PKC δ/θ, and ε/η isoforms containing a DAG regulatory domain similar to cPKC's, which renders them responsive to DAG and phospholipids but not Ca^{2+}. Atypical PKC (aPKC) isoforms include ι/λ and ζ, which contain a domain similar to the DAG-binding region found in c- and n-PKC isoforms, but this domain is unable to respond to DAG and instead responds to lipid-derived second messengers [76-79]. After discovery of PKC isoenzymes, gene expression studies revealed that PKC's are ubiquitously expressed and comprise about 2% of the entire human kinome [76, 80]. However, each tissue and organ system expresses a unique complement of PKC isoforms. As a result, the reason for the unique functions of each isoenzyme remain a question, and continues to be investigated to understand the role PKC plays in multiple cellular processes and in disease.

PKC Studies: Approaches & limitations

PKC has several modulatory functions within the heart including development, cell proliferation, migration, and remodeling, as well as in most other vital organs throughout the body [81-83]. Therefore, alterations in PKC may be involved in both physiological and pathophysiological processes. In 1981, Nishizuka's group suggested that tumor-promoting phorbol esters activated PKC [77], spurring a deep interest in the scientific community as to the potential pathological role of PKC.

Much of the research conducted on the potential role of PKCs in various pathologies employs techniques such as RNA interference and adenoviral gene transfer. Unfortunately, the

impact of multiple inputs and outputs in a single cell, together with adaptive regulation of specific PKC isoenzyme expression and activity often prove to be critical limitations in the study of PKC within a given tissue or organ. Pharmacological approaches are also employed to study the role of PKC in disease and potentially pursue PKC as a therapeutic route. Because of the clear association between PKC and certain pathologies, multiple PKC inhibitors have been designed and tested for their clinical potential in disease inhibition. Two immediate obstacles arising from this approach are: i) inhibition of this ubiquitous enzyme can disrupt other important physiological processes and ii) altered expression or activity of one isoenzyme can modify expression or activity of other PKC isoforms [79]. In addition, most PKC inhibitors target PKC's catalytic domain, thus failing to achieve isoform specificity and increasing the risk for off-target effects. More recent efforts targeting the unique noncatalytic domain provide researchers with a powerful tool to study the role of individual PKC isoenzymes, and may translate into successful and effective therapeutics in the future [84]. Adding to this complexity is that activation of a specific PKC isoform changes dramatically with cellular conditions. For example, the Ca^{2+} level required for cPKC activation varies 10 fold depending on the level and type of diacylglycerol and/or phospholipid [77, 85]. Collectively, these earlier studies point to the complexity and versatility of PKC signaling to play important tissue-specific roles in the body.

In the heart, PKC modulates a variety of targets including transcription factors, enzymes, calcium transients underlying contraction, and contractile proteins [86, 87]. Chronic modulation of these downstream targets can induce architectural remodeling via hypertrophy, fibrosis, and inflammation, and direct changes in electrical impulses and pump function. Substantial evidence suggests PKC is upregulated and plays a role in cardiac pathologies such as myocardial ischemia

(restricted blood supply causing oxygen deprivation) and HF [86]. However, it is currently unclear how PKC modulates these outputs under chronic activation.

PKC and HF

In HF, the CO produced by the heart is inadequate to meet the metabolic demands of the body [88]. Additionally, the myriad of etiologies from which HF can originate has made identifying *one* therapeutic target impossible. However, one commonality in end-stage HF along with other vascular pathologies such as hypertension and diabetes is the upregulation and activation of PKC [68, 89]. Earlier studies showed that PKCα and β are both upregulated in the failing heart [68]. In HF, PKCα is the dominant isoform and its upregulation is linked with dysfunction [90]. To determine the relationship between up-regulated PKCα and dysfunction, chapter 2 of this dissertation tests whether adenoviral transduction of dominant negative PKCα rescues contractile function in human failing myocytes [91]. The findings in this chapter support the idea that cardiac function is maintained under pathophysiological processes after deleting the PKCα gene in mice [92]. Additional studies conducted with PKCβ overexpression in mice showed the development of cardiac hypertrophy [93]. While other isoforms of PKC have not been shown to be as prominently upregulated in HF, PKCε overexpression in mice caused cardiac remodeling and HF along with a decline in contractile reserve [94, 95]. Overall, prior studies indicate that the PKC family plays a critical role in initiating progressive cardiac dysfunction. However, because of its ubiquitous expression throughout the body and close homology between isoforms, targeting PKC in the treatment of HF has been challenging [79].

PKC-induced phosphorylation of the contractile apparatus and the reduced cardiac function observed in mouse models suggests that PKC targeting of the sarcomere may be an

important causative contributor to pump dysfunction in the development of HF [96]. This idea is based on the potential for deficits in the function of the cardiac contractile apparatus to translate to an inability to meet the body's oxygen demands, thus resulting in adaptive but ultimately pathological structural and functional remodeling. PKC has been long-associated with pathways that may contribute to such adaptive responses, and elevated PKC has been associated with hypertrophy leading to HF[68, 93, 97]. In fact, an increase in expression of PKC isoforms α and β was consistently observed in the myocardium from failing compared to nonfailing explanted human hearts [68]. Despite this clear association by which PKC may impair contractile function and lead to HF, the mechanism(s) responsible for the continued deterioration in pump function and the remodeling accompanying HF are not well understood.

PKC phosphorylation of cTnI: *in vitro* studies and phospho-mimetics

The impact of each kinase on function depends on posttranslational modification (PTMs) such as phosphorylation of target proteins including cTnI. This dissertation work specifically focuses on the phosphorylation of cTnI as a means of fine-tuning or modulating function within the heart. The cTnI protein has at least 17 phosphorylation sites and each phosphorylation site modulates contractile function and the ability of cTnI to act as a switch protein differently [50]. The kinases known to phosphorylate cTnI and the impact of phosphorylation are described in more detail below.

Perhaps the most well-understood phosphorylation cluster within cTnI, S23/24 sits within a unique, and highly flexible 32 amino acid extension on the N-terminus of cTnI. PKA, PKC and PKG can each phosphorylate this cluster [98, 99]. Post-translational site-specific phosphorylation of cardiac TnI (cTnI) by PKA was first described by Solaro and colleagues, and

phosphorylation of this site is now established to play a crucial role in modulating relaxation in response to β-adrenergic activation [64, 67, 100]. The S23/24 resides within the flexible N-terminus of cTnI and mediates relaxation in response to beta-adrenergic stimulation—increasing the rate of relaxation in cardiomyocytes while decreasing Ca^{2+} sensitivity in the myofilament [66, 101]. β-adrenergic stimulation (or sympathetic activation) activates adenylyl cyclase to increase activity of PKA, and PKA subsequently phosphorylates cTnI S23/24 [98, 100, 102]. The cTnI S24 residue is thought to be constitutively phosphorylated but both S23 and S24 require phosphorylation to accelerate contractile function [103]. Phosphorylation at cTnI S23/24 decreases the myofilament's Ca^{2+} sensitivity, resulting in an increased off-rate of Ca^{2+} from cTnC, and thus accelerating relaxation [64, 65]. Phosphorylation of residues S23/24 within this extension limits access of the H3 region to the hydrophobic patch and this translates into reduced Ca^{2+} sensitivity in the myofilament and accelerated relaxation in the intact heart.

In addition to S23/24, studies by J. F. Kuo and colleagues indicated that PKC also phosphorylates TnI at additional residues to modify contractile properties. These experiments were carried out by extracting contractile proteins from bovine ventricles, reconstituting the troponin complex with mutations at specific phosphorylation sites on TnI, and then adding specific PKC isoforms to determine the extent of phosphorylation, plus the calcium sensitivity, and maximum activity of actomyosin Mg^{2+}-ATPase [101, 104]. Their findings showed PKC differentially phosphorylates at least five specific TnI residues [67, 101]. Specifically, PKC α, δ, and ε also phosphorylate cTnI at S43/45 and T144, while PKCδ preferentially phosphorylates S23/24 [101, 105, 106], and collectively these sites modulate myofilament and overall contractile performance. The cTnIS43/45 phosphorylation reduced both maximum Ca^{2+}-stimulated Mg^{2+}-ATPase activity and Ca^{2+} sensitivity of myofilaments. Later studies also showed PKC

phosphorylates S199 in cTnI, which enhances *in vitro* myofilament Ca^{2+} sensitivity [107]. These findings are significant because PKC activity and expression are increased in various disease states—specifically in HF—along with downstream phosphorylation of cTnI [10, 69, 108].

The S43/45 cluster of residues in cTnI is important because its phosphorylation is elevated in human HF along with PKC activity [68, 69]. While it is not clear whether S43/45 phosphorylation is directly linked with HF, it is known that phosphorylated cTnI S43/45 diminishes contractile function *in vitro* and in biochemical assays [3, 5]. The easiest way to study chronic, site-specific phosphorylation is through substitution of S/T with a negatively charged amino acid such as aspartic (D) or glutamic (E) acid. Much *in vitro* work has been conducted to elucidate the impact of S43/45 phosphorylation on different aspects of myofilament function. In reconstituted thin filaments containing phospho-mimetic cTnI S43/45D, Ca^{2+} dissociated from cTnC faster than wildtype controls, and ATPase activity of the myofilament decreased along with maximal activity [70, 101]. Additionally, in skinned papillary muscles, cTnIS43/45D decreased peak tension and myofilament Ca^{2+} sensitivity (or pCa_{50}, the Ca^{2+} concentration required for half-maximal activation as shown in Fig. 1.7) and reduced sliding speed of the myosin head during *in vitro* motility assays [3]. Previously, adenoviral constructs containing cTnI expressing S43D (serine 43 replaced with aspartic acid), S45D, and S43/45D were transduced into rat cardiomyocytes [5]. It is important to note that these studies resulted in replacement rather than overexpression of cTnI with phospho-mimetic substitutions, due to the strict maintenance of thin filament stoichiometry in the dynamic sarcomere [109]. Within four days post gene transfer, replacement of endogenous cTnI with each phospho-mimetic cTnIS43D and/or cTnIS45D reached 65-85% in cardiomyocytes, and when myocytes were electrically stimulated, their peak shortening decreased significantly, along with transient reductions in

shortening and re-lengthening rates. The observed decreases in both shortening *and* re-lengthening challenges the historical two-state model for thin filament activation (e.g., if thin filament activation were a simple ON-OFF switch, the impact of S43/45D on shortening should oppose the impact on re-lengthening). Collectively, these earlier *in vitro* biochemical and cellular studies suggest that cTnI S43/45 phosphorylation acts to acutely reduce function. However, the *in vivo* role of cTnI S43/45 phosphorylation remains unclear. Discerning the functional impact of chronic cTnI S43/45 phosphorylation in the intact heart is a primary focus of this dissertation research.

In vivo mouse models with cTnI phospho-mimetics

Several groups have attempted to study the role of PKC-induced cTnI phosphorylation in mice through the use of transgenic (tg) animals. Expression of these transgenes are largely under the control of the α-MHC promoter to confer cardiac specificity in the adult heart. Just as in transduced myocytes, transgenesis in the sarcomere results in *replacement* of endogenous cTnI, rather than in overexpression [109]. Because sarcomere phosphorylation is meant to *modulate* function rather than serve as an ON-OFF switch, the use of transgenesis provides a useful tool to study the impact of phosphorylation of proteins in the sarcomere. As mentioned before, the primary focus of this dissertation research is the *in vivo* role of cTnI S43/45 phosphorylation, because there is evidence that chronic phosphorylation of this cluster results in contractile dysfunction, and that this cluster is phosphorylated in human end-stage HF along with elevated PKC activity [69, 91]. However, a detailed overview of existing mouse models with cTnI S43/45 substitutions is provided below and in Table 1.1, to indicate gaps and clarify the research questions addressed in this dissertation.

Sadayappan and colleagues created a tg mouse model which contained a phospho-mimetic cTnIS23/24D substitution ($cTnI_{PP}$) [66]. As mentioned previously, this cluster is phosphorylated in response to β-adrenergic stimulation, and consistently reduces myofilament Ca^{2+} sensitivity of tension *in vitro* which results in accelerated relaxation [101, 110]. In the $cTnI_{PP}$ tg mouse, there was 100% replacement of endogenous cTnI with $cTnI_{PP}$ as well as the expected acceleration of *in vivo* relaxation. Thus, the cardiac phenotype is consistent the known modulatory role played by cTnIS23/24 phosphorylation [66].

The Sadayappan group also generated a separate tg mouse possessing phospho-mimetic D substitutions at 3 cTnI clusters of PKC-targeted residues, S23/24, S43/45, T144 (S23/24D, S43/45D, T144D, or $cTnI_{AllP}$) [66]. Once again there was 100% replacement of endogenous cTnI with phospho-mimetic cTnI in these tg mouse hearts. These mice developed decreased Ca^{2+} sensitivity and diminished maximum actomyosin ATPase activity in myofibrils. These *in vitro* findings suggest that these tg hearts could develop reductions in peak pressure and accelerated relaxation. Instead, *in vivo* measurement of peak pressure did not differ from ntg littermates, relaxation was not accelerated, and mice developed a slightly diminished rate of left ventricular pressure development (dP/dt_{max}). Based on these findings, 1) diminished myofilament Ca^{2+} sensitivity does not necessarily translate into accelerated *in vivo* relaxation; and 2) there is likely crosstalk between the 3 PKC-targeted clusters, but the role played by each cluster is unclear. Later studies performed in isolated cardiomyocytes were used as a bridge between the functional outcomes in myofilament and *in vivo* mouse models and support these conclusions [4].

A tg mouse expressing S23A/S24D+S43/45D also was generated to gain further insight into the functional impact of PKC-targeted cTnI residues on cardiac function. The rationale for the S24D substitution is based on previous work showing constitutive *in vivo* phosphorylation of

S24 in cTnI [103], and the requirement for phosphorylation of both S23 and S24 in order to reduce myofilament Ca^{2+} sensitivity [103, 111]. Thus, the cardiac contractile phenotype in this mouse was expected to reflect the modulatory role of S43/45 phosphorylation on function. Indeed, myofilament Ca^{2+} sensitivity decreased in permeabilized trabeculae, and hemodynamic measurements revealed diminished dP/dt_{max} and dP/dt_{min} in tg mice with 23% replacement vs wild-type mice. This study in combination with results obtained from the $cTnI_{AllP}$ mouse indicates that phosphorylation of cTnI S43/45 slows *in vivo* contraction rates, which was not previously predicted in earlier *in vitro* studies [3]. These tg mice also experienced impaired frequency-dependent contractile dysfunction compared to ntg mice, but it was unclear whether this response resulted directly from the phospho-mimetic substitutions within the sarcomere or instead developed in response to ongoing cardiac remodeling as the heart progressed to failure.

The functional differences between the $cTnI_{AllP}$ versus cTnIS23A/24D/43/45D could be due to differences in the role played by cTnI T144. Thus, a tg mouse expressing phospho-mimetic glutamic acid (E) was generated to change PKC-targeted S43/45 and T144 to S43/45E+T144E (PKC-P) [112]. Only 7% replacement of endogenous cTnI with cTnI S43/45E+T144E was achieved in this tg mouse, and yet maximal force generation decreased in permeabilized papillary muscles without a change in myofilament Ca^{2+} sensitivity. The PKC-P mice also developed slowed dP/dt_{max}, dP/dt_{min}, plus reductions in maximal pressure development, and an impaired Frank-Starling relationship—where increases in diastolic volume resulted in decreased pressure development. The severely slowed contraction and relaxation rates, along with the decreased maximal pressure development highlighted the ability of chronically phosphorylated PKC-targeted cTnI residues to diminish contractile function, but

failed to define the specific functional roles played by S43/45 versus T144. Thus, a significant question remains about the *in vivo* functional impact of chronic S43/45 phosphorylation alone.

In summary, these models add a layer of uncertainty about whether cTnI S43/45 phosphorylation diminishes *in vivo* contractile function. Results from these mice also fail to determine whether cTnIS43/45 modification is functionally dominant against PKC-targeted S23/24 and T144 phosphorylation sites. Further work needs to be done to study the specific *in vivo* role of S43/45 phosphorylation. Questions of specific interest are 1) does chronic S43/45 phosphorylation cause HF? 2) Does the level of phosphorylation (phosphorylation "dose") have an impact on the observed phenotype? 3) What cellular mechanism(s) underlie the progression of contractile dysfunction and HF?

In the context of the dissertation work presented here, downstream consequences of PKC phosphorylation of cTnI S43/45 are postulated to initiate and contribute to progressive cardiac dysfunction. By testing this idea, this dissertation work is expected to provide insight into the role played by one phosphorylation target for PKC on cTnI and its impact on cardiac dysfunction and progressive HF. An essential goal of this project is to gain insight into the impact chronic PKC activation could have on contractile function via cTnI phosphorylation [9, 11, 68]. Specifically, studies test whether the S43/45 site on cTnI produces *in vivo* and cellular contractile dysfunction and in turn, initiates progressive HF. The progressive process leading to end-stage HF in response to cTnIS43/45 phosphorylation is hypothesized to develop via early communication with mitochondria, which is explored in chapter 4.

Studies with phospho-deficient cTnI substitutions

Investigation of the role of a targeted phosphorylation site is strengthened by studying the impact of phospho-deficient substitutions. Previous studies using a knock-out and knock-in strategy to achieve complete replacement of endogenous cTnI with a phospho-null cTnI S23/24A (Ala_2^{nb}), showed that exogenous PKA activation did not change basal myofilament Ca^{2+} sensitivity compared to untreated Ala_2^{nb} myocytes [113]. This supported current knowledge of the cTnIS23/24 site as a phosphorylation target for PKA during the β-adrenergic response. However, attempts to add phospho-null S43/45 and T144 produced results that were equally complex as those produced in tg mice with phospho-mimetic cTnI substitutions at S43/45 plus S23/24 and/or T144. Specifically, a knock-out/knock-in mouse generated to achieve complete replacement of wildtype with A substitutions in all 3 cTnI clusters (S23/24/43/45A+T144A; Ala_5^{nb}) developed decreased myofilament Ca^{2+} sensitivity [114]. However, the authors did not comment on the decrease in Ca^{2+} sensitivity observed in Ala_5^{nb}. In contrast to the consistently observed PKC-induced decrease in myofilament Ca^{2+} sensitivity reported by multiple investigators [3, 115], exogenous PKC activation also increased Ca^{2+} sensitivity in cardiomyocytes from Ala_5^{nb} mice [114]. This PKC-induced increase in Ca^{2+} sensitivity translated into slowed re-lengthening rates in isolated cardiomyocytes. Although the *in vivo* contractile phenotype is not known for these mice, their hearts developed remodeling resulting in a cardiomyopathy. We speculate that the increased Ca^{2+} sensitivity and slowed re-lengthening rates could result from other PKC targets and/or be caused by secondary changes in the cellular response to PKC in Ala_5^{nb} mice.

To add to the ambiguity surrounding the role of cTnI S43/45, conventional A substitutions at S43/45 also caused *in vitro* functional changes similar to phospho-mimetic

substitutions. The goal of a non-phosphorylatable residue is to achieve functional quiescence, meaning there are no changes compared to function in wildtype mice under basal conditions, and this substitution also prevents the functional response produced by phosphorylation [116]. A tg mouse model was created with A in place of S43/45 [117]. With a predicted 50% replacement of endogenous cTnI, ATPase activity and tension development in the myofilament decreased compared to wildtype controls. Our laboratory sought to confirm these results, by adenoviral gene transfer of S43/45A into rat cardiomyocytes [116]. As predicted, cTnIS43/45A decreased peak sarcomere shortening and the rate of re-lengthening in rat myocytes. These findings support the idea that A substitution at S43/45 in cTnI, produces changes in myofilament contractile function.

Alanine is often an ideal phospho-null substitution because it is tiny, nonpolar, and the methyl group on the second carbon makes A inflexible. While it is unclear why the A substitution causes an overt phenotype at S43/45, it is postulated that the nonpolar characteristic of A potentially alters interactions between cTnI and the N and C lobes of cTnC, a phenomenon that has been reported with more polar R groups at cTnI S43/45 [118]. Our laboratory sought to find a non-phosphorylatable substitution at S43/45 that does not change basal contraction, and is therefore functionally quiescent or conservative in place of an A. Therefore, the amide R group in asparagine (N), with a polarity somewhat similar to the hydroxyl group in serine, could make N a reasonable phospho-deficient substitute without overt effects on basal wild-type function. To initially test the N substitution, wild-type rat cardiomyocytes were transduced with adenovirus containing S43/45N. Indeed, by 4 days in culture and nearly 80% replacement of endogenous cTnI with S43/45N, there were no detectable changes in paced myocyte shortening, re-lengthening, or Ca^{2+} transients, nor were there detected adaptive changes occurring within the

myocytes as a result of the S43/45N substitution [119]. As part of Chapter 5 of this dissertation, the use of N substitutions at S43/45 is used to test whether there is an *in vivo* impact of the same N substitution studied in earlier myocyte work.

The Sarcomere and Mitochondria

The prediction that phospho-mimetic cTnIS43/45D initiates a progressive spiral leading to HF also will address ongoing questions about the mechanism(s) whereby a change in the sarcomere leads to progressive cardiac dysfunction and remodeling. As a result, studies in mice expressing phospho-mimetic cTnI S43/45D test the idea that sarcomere "stress" is communicated early to mitochondria, to lay the foundation for progressive cardiac dysfunction. Mitochondria, the famous "powerhouse of the cell" is a critical regulator of eukaryotic cellular energy and metabolism. The Endosymbiotic Theory suggests that mitochondria were bacterial descendants that, upon being symbiotically engulfed by prokaryotes, became critical components of the cell [120, 121]. These now-crucial organelles contain a permeable outer membrane surrounding an impermeable inner membrane from which complexes I-V of the electron transport chain (ETC) protrude and generate ATP [122]. The inner membrane is folded into cristae to provide increased surface area within the mitochondria to accommodate multiple ETC's and maximize ATP production [123].

In addition to providing cellular energy in the form of ATP, mitochondria are the site of carbohydrate and fatty acid metabolism [121]. Pyruvate derived from glycolysis and fatty acids are oxidized to produce acetyl CoA, which is the substrate for the tricarboxylic acid (TCA) cycle. In this cycle, reducing equivalents (NADH and $FADH_2$) are produced, providing electrons for the ETC. Specifically, NADH is oxidized by ETC complex I, whereas $FADH_2$ is oxidized by

the ETC complex II (Fig. 1.9). As electrons pass through complex I, III, and IV, protons are extruded into the intermembrane space, establishing an electrochemical gradient and proton motive force for the ETC. At complex IV, molecular oxygen is reduced to water, thus making complex IV a source of reactive oxygen species (ROS) production in addition to complexes I and III. Complex V (also called ATP synthase) uses the energy from the electrochemical gradient across the inner membrane, to create ATP from ADP and inorganic phosphate.

Myofibrils are surrounded by mitochondria, providing physical proximity to the myocyte's primary energy source, ATP. In fact, early calorimetric analysis revealed that the >75% of mitochondrial ATP in a cardiomyocyte is used by the myosin head during the power stroke [124]. Thus, it makes sense that issues with mitochondrial health and functionality are routinely noted in end-stage HF, as the diseased heart is energetically compromised [125]. While many studies have noted changes in mitochondrial function occurring in HF, none have studied whether alterations within the sarcomere trigger early changes in mitochondrial health and function during the course of progressive cardiac disease, and could be a focal point for *early* therapeutic treatment of sarcomere-linked cardiac dysfunction. The potential for mitochondria to serve as an early therapeutic target in the treatment against HF will be discussed in more detail in chapter 4 of this dissertation.

PKC as a link between oxidative stress and HF

Because cardiac myosin uses a majority of the ATP produced by mitochondria for contraction, it is hypothesized that PKC-induced reductions in contractile function may lead to stress signaling. Although multiple stress responses are produced by myocytes, one important stress signal that may be linked to the need for ATP is oxidative stress produced by

mitochondria. Thus, many researchers are investigating the potential link between PKC and oxidative stress in the context of HF.

Since the heart is rich in mitochondria, myocytes are a prime candidate for oxidative stress-induced injury. It is well-established that oxidative stress is a contributing factor in the development and progression of HF as well as many other pathologies [126, 127]. Oxidative stress is caused by greater accumulation of reactive oxygen species (ROS) than cellular antioxidant systems can handle. Reactive oxygen species are unstable free radical byproducts of cellular metabolism. Studies have shown that oxidative stress may trigger many hypertrophy-initiating pathways, as well as pathways involved in apoptosis [128]. In fact, an increase in ROS production has been demonstrated in failing human myocardium [129]. Evidence suggests that PKC may activate downstream targets that mediate H_2O_2/ROS generation in mitochondria, suggesting PKC plays a role in directly activating mitochondrial ROS [130-132]. The PKC effect on contractile function may also indicate an indirect role of PKC in activation of ROS via altered communication between the sarcomere and mitochondria.

Hypothesis and Aims

Elevation in PKC signaling is associated with cTnI phosphorylation in HF but it is not clear whether elevated cTnI S43/45 phosphorylation is linked to HF [69, 91, 133]. *In vitro* studies showed that PKC phosphorylates cTnI at three clusters: S23/24, S43/45 and T144 [101] (Figure 1.3). The S43/45 and T144 phosphorylations are elevated in HF [69], and the S23/24 is also a target for PKA [100, 134]. In cellular studies, PKC-phosphorylation of cTnI S43/45 reduced contractile function [3, 5, 69, 101, 104]. However, these studies failed to determine the impact of *only* S43/45 phosphorylation because variable *in vivo* phenotypes emerged when

S43/45 phosphorylation was combined with other residues [66, 111, 112]. Further, no studies addressed whether the amount of phosphorylation dictates the observed phenotype in existing animal models, nor the cellular events that lead to the observed phenotype. Thus, the role of this PKC-induced cTnI phosphorylation in modulating cardiac function continues to be debated.

This dissertation will fill these critical gaps using a mouse model which specifically analyzes cTnI S43/45 with different levels of phospho-mimetic replacement. Prior cellular work showed S43/45 phospho-mimetics cause myocyte dysfunction along with secondary cellular responses [5] that could include mechanism(s) responsible for progressive dysfunction. The overarching hypothesis of this dissertation work is that cTnI S43/45 serves as a central node for modulating contractile function, and when phosphorylated chronically, it reduces *in vivo* contractile function and initiates early mitochondrial alterations which lay the foundation for progressive dysfunction leading to HF.

Experiments in chapter 2 test whether there is a strong association between HF in rodents and end-stage human hearts, up-regulation of PKC isoforms and downstream phosphorylation of cTnI S43/45 in human and animal models of HF. Work in this chapter addresses whether this phosphorylation is elevated in human HF as well as in aging—which provides a broader implication for the impact of cTnI S43/45 phosphorylation with respect to aging. This study also shows that elevated cTnI S43/45 phosphorylation accompanies the contractile dysfunction observed in HF, and that adenoviral transduction of failing human myocytes with a dominant negative version of PKCα partially rescues the HF phenotype. Later work focuses on cTnIS43/45 modifications in a mouse model. Thus, chapter 3 lays out the methodology for mouse cardiomyocyte isolation and gene transfer, as isolating and maintaining mouse myocytes in culture requires attention to detail and yet is a method utilized throughout this dissertation.

This chapter provides insight into some of the technical difficulties of maintaining mouse myocytes in culture, as it is important to acknowledge limitations that this methodology imposes (e.g., it is difficult to transduce or transfect delicate mouse cardiomyocytes). Additionally, this technique was important to optimize because it enabled our group to expound upon studies conducted previously in our laboratory on rat myocytes. Since results obtained in mouse myocytes reflected rat myocyte findings, the use of this technique provided further confirmation about the role of cTnI phosphorylation.

We proposed that cTnI S43/45 phosphorylation disrupts contractile function and initiates progressive cardiac dysfunction and HF when present chronically. Chapters 4 and 5 directly test this hypothesis, as well as uncover a novel cellular mechanism by which this sarcomere modification causes cardiac dysfunction. Chapter 4 places a heavy emphasis on evaluating whether the phospho-mimetic cTnI S43/45D substitution causes cardiac dysfunction and HF, and whether the level of phospho-mimetic expression determines the severity of the phenotype. Most importantly, the work presented in Chapter 4 also investigates early mitochondrial dysfunction as a novel mechanism by which S43/45 phosphorylation causes HF. This is particularly important because while mitochondrial dysfunction is well-documented in HF [125], its role in early disease progression is unclear. Then, Chapter 5 tests the use of a phospho-deficient asparagine (N) residue at S43/45 is functionally conservative and therefore a superior alternative to the traditionally used alanine (A) substitution at this site, given that S43/45A produced cardiac dysfunction in previous studies [113, 114]. A strength of chapters 4 and 5 are that the mice are studied from adolescence into adulthood, enabling the study of the progression of HF, which can reveal novel and unique therapeutic targets in the treatment of the disease.

Taken together, the studies presented in this dissertation work address important gaps existing within the field of cardiac muscle biology. This work demonstrates the critical role played by cTnI in modulating contraction on a beat-to-beat basis and thus, serves as a master regulator of contractile function. Results from this project also test the unique idea that early mitochondrial responses underlie progressive S43/45 phosphorylation-induced dysfunction. Given that our work and the work of others show that PKC activity and downstream cTnI S43/45 phosphorylation are present in aging, HF, hypertension, and diabetes [9, 11, 68, 91], the presented work serves as an invaluable platform to begin understanding how to target and mitigate the detrimental effects of S43/45 phosphorylation in a larger population.

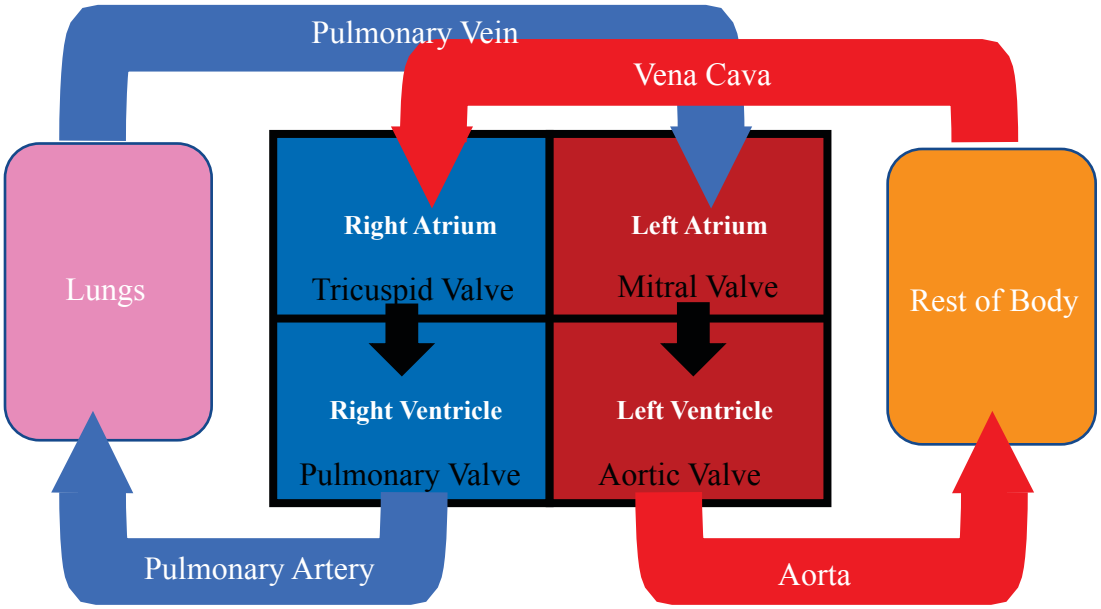

Figure 1.1 Blood flow in the heart. A schematic depiction of cyclical blood flow into and out of the heart. Important valves that establish unidirectional flow are labeled throughout the diagram.

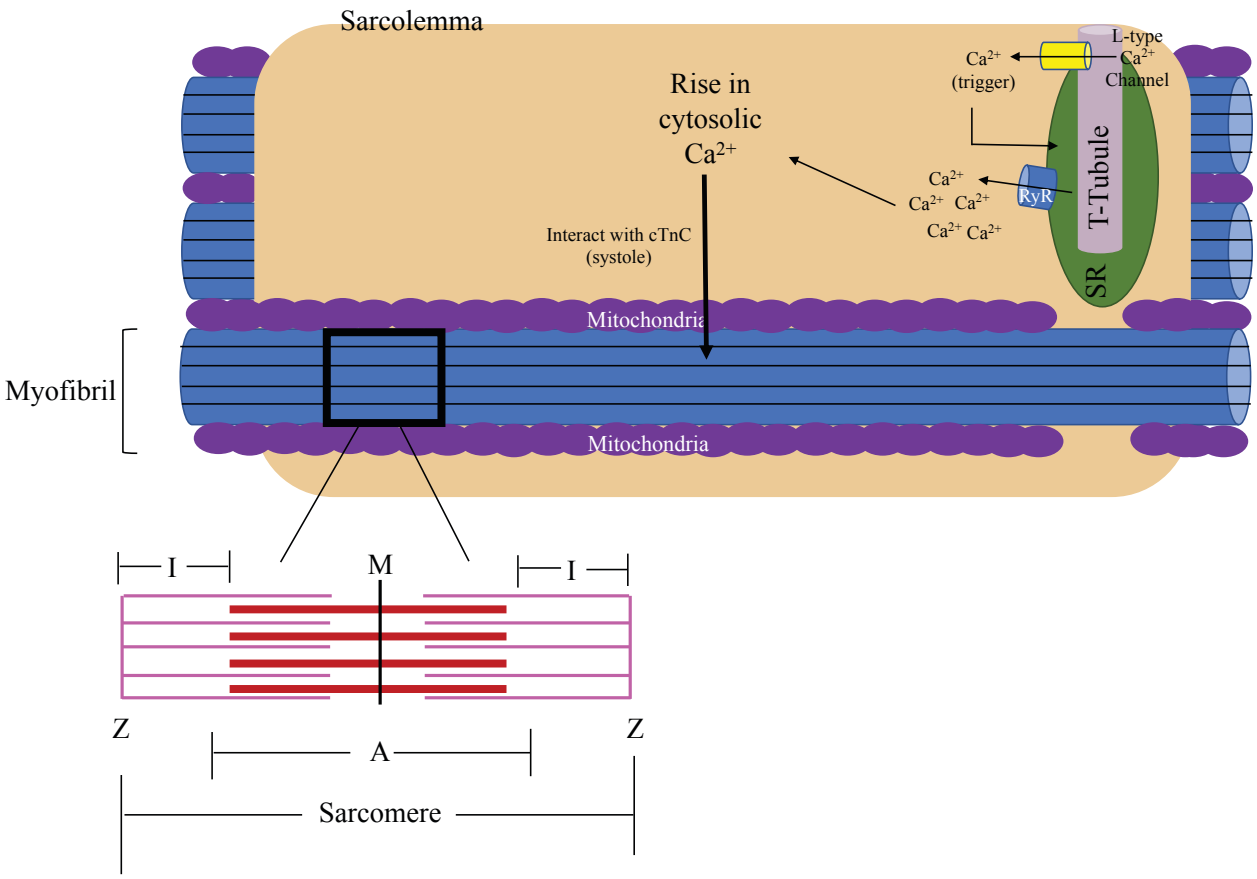

Figure 1.2 Cardiomyocyte and Ca^{2+}-induced Ca^{2+} release (CICR). A schematic depiction of the organization of myofibrils, mitochondria, and sarcoplasmic reticulum (SR) in the cardiomyocyte. Myofibrils contain myofilaments, which are made up of repeating sarcomeres (the functional unit of the contractile apparatus). Myofibrils are abundantly surrounded by mitochondria as their source of ATP. Following an action potential, Ca^{2+} influx through the L-type Ca^{2+} channel serves as a trigger to release more Ca^{2+} from the SR (CICR) through ryanodine receptors (not pictured). The newly released cytosolic Ca^{2+} is free to interact with myofilaments before being taken up by the sarcoplasmic reticular Ca^{2+}-ATPase (SERCA; not pictured). A sarcomere undergoing isotonic contraction (systole) and relaxation (diastole) is depicted beneath the cardiomyocyte, with each Z band labeled to denote the ends of the sarcomeres.

A

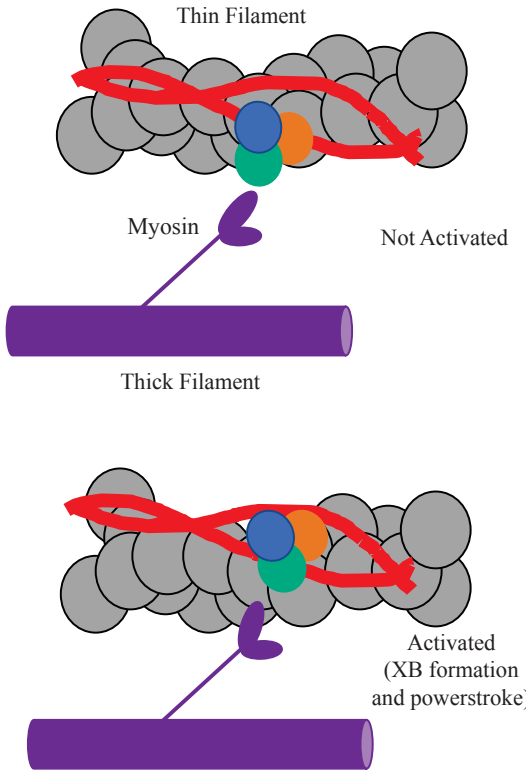
Thin Filament
Myosin
Not Activated
Thick Filament
Activated
(XB formation
and powerstroke)
Actin
Troponin
different conformations
Troponin T (cTnT)
Troponin C (cTnC)
Troponin I (cTnI)
Tropomyosin (Tm)
Myosin Rod
Myosin

B

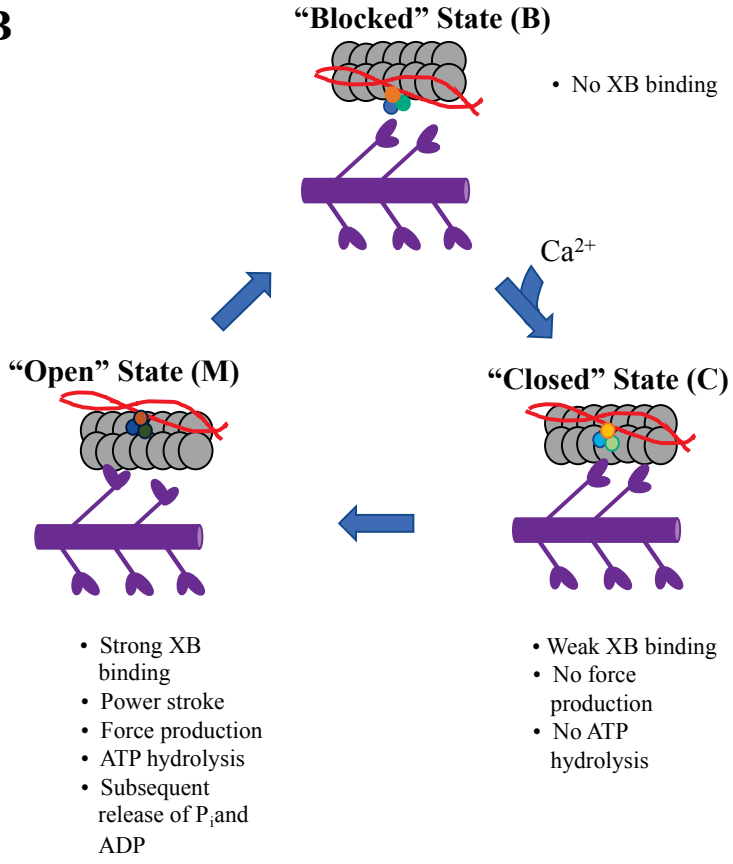
"Blocked" State (B)
• No XB binding
Ca^{2+}
"Open" State (M)
"Closed" State (C)
• Strong XB binding
• Power stroke
• Force production
• ATP hydrolysis
• Subsequent release of P_i and ADP
• Weak XB binding
• No force production
• No ATP hydrolysis

Figure 1.3 Sarcomere and cardiac troponin (cTn) complex. A, Schematic depiction of thin and thick filaments. A thick filament myosin rod section is depicted with the MgATPase myosin head in close proximity to the thin filament. The thin filament consists of coiled-coil actin, coiled-coil tropomyosin, and the heterotrimer troponin (cTn or Tn) complex. The cTn complex consists of troponin C (cTnC) which binds Ca^{2+}, troponin T (cTnT) which binds tropomyosin, and troponin I (cTnI), which is the inhibitory subunit responsible for inhibition of the acto-myosin interaction in the absence of Ca^{2+}. The bottom panel shows a two-state model of thin filament activation, where Ca^{2+} binding to cTnC results in a force-producing contraction. **B,** the newer model of thin filament activation (3-state model) is depicted. In a blocked (B) state, no crossbridge (XB) formation occurs, as Ca^{2+} has not bound to cTnC. Upon Ca^{2+} binding, a closed (C) state is generated, where weak XB formation can occur, though no force is produced. In the open (M) state, a strong XB which produces force is generated, and ATP is hydrolyzed. Important conformational changes occur within cTn which are denoted by alterations in color of each subunit of cTn. Additionally, different positions of Tm exist in each state and are depicted.

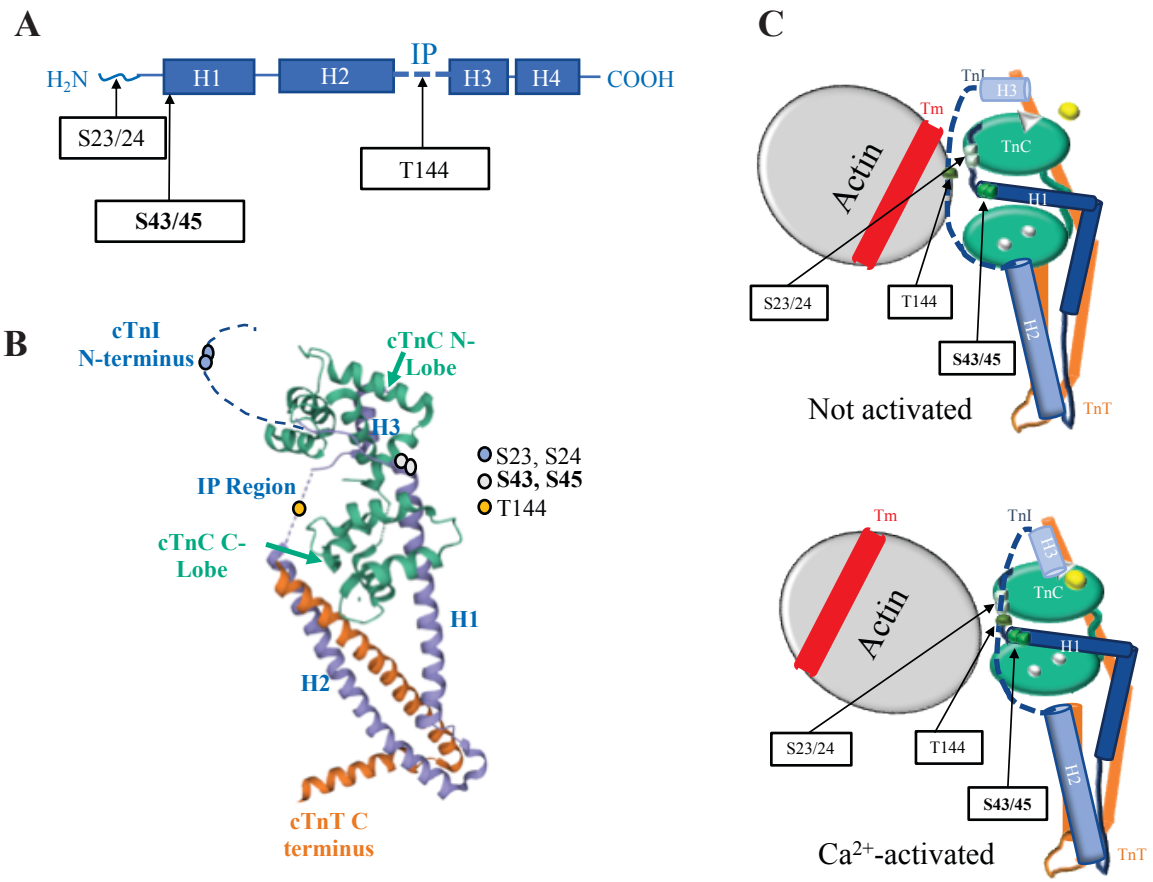

Adapted from Takeda et al., *Nature*, 2003 Jul 3;424(6944):35-41.
PDB entry 1J1E

Figure 1.4 Cardiac troponin I (cTnI) and the cTn complex. A, A linearized depiction of important regions of cTnI is shown. A flexible N-terminal region is followed by the H1 and H2 alpha-helices, the inhibitory peptide (IP) region, and then the H3 and H4 alpha helices. **B,** cTn crystal structure is shown with important regions labeled and color-coded according to the protein shown. **C,** A schematic of the troponin complex is shown as it sits within actin. Activation of the cTn complex is depicted in the lower panel, as Ca^{2+} binds to cTnC, and a series of conformational changes occur within the thin filament. Of note, the IP region (dashed line) of cTnI disinhibits actin from interacting with myosin, and tropomyosin (Tm) moves to aid in myosin-binding. In every schematic, PKC-targeted phosphorylation sites on cTnI are labeled, with the cluster of interest, S43/45, in bold. Legend; **B** and **C**, cTnI is denoted in blue, cTnC is in green, and cTnT is in orange.

PKC Subgroup	PKC isoform	Activators
Conventional (cPKC)	α, β1, β2, γ	Diacylglycerol, phospholipids, Ca^{2+}
Novel (nPKC)	δ, θ, ε, η	Diacylglycerol, phospholipids
Atypical (aPKC)	ι, λ, ζ	Lipid-derived second messengers

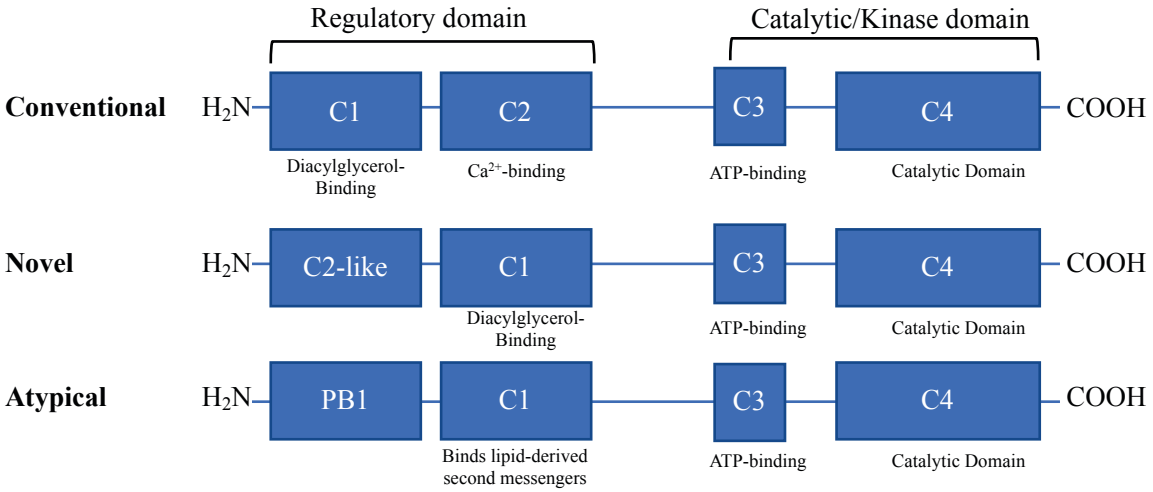

Figure 1.5 Protein Kinase C's (PKC's). Schematic depiction of mammalian PKC isoforms. Conventional and novel PKC's (cPKC's and nPKC's) possess a C1 which is a sensor for phorbol esters and DA. The C2 domain in cPKC's contain critical Ca^{2+}-binding residues and serves as the Ca^{2+}-dependent phospholipid binding site. While a similar C2-like domain exists within nPKC's, it lacks critical residues needed for Ca^{2+}-binding. Additionally, the C1 domain in atypical PKC's (aPKC's) does not bind DAG or phorbol esters, and instead is responsive to lipid-derived second messengers.

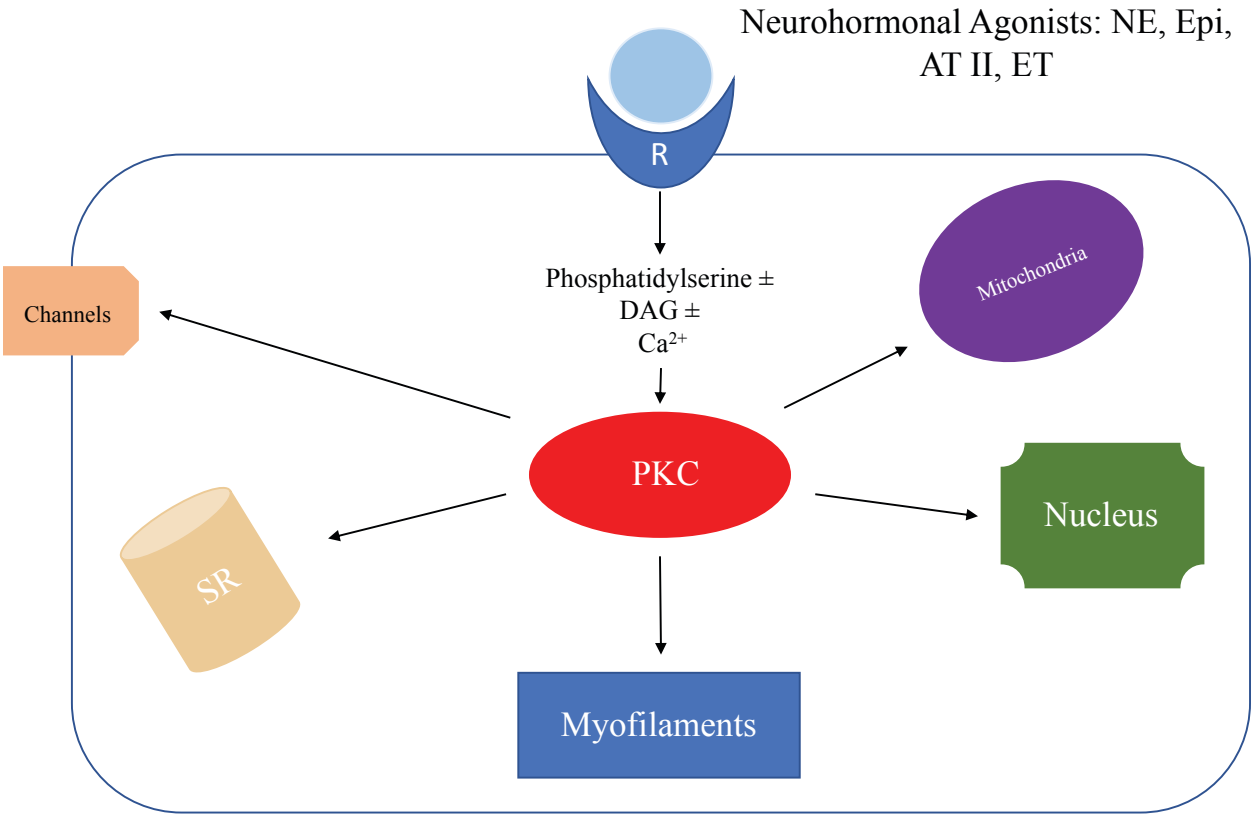

Figure 1.6 A *simplified* view of PKC signaling: multiple inputs and outputs. Ligands such as norepinephrine (NE), epinephrine (Epi), Angiotensin II (AT II), and Endothelin (ET) each bind to specific receptors (R) to ultimately activate PKC. Each receptor activates a specific spatial and temporal pattern of PKC isoforms to modulate the function and/or activity of several downstream targets including Ca^{2+} (e.g., channels, sarcoplasmic reticulum or SR), mitochondria, and the myofilament. The effects of PKC modulation may have important implications in cardiac contractile function and dysfunction.

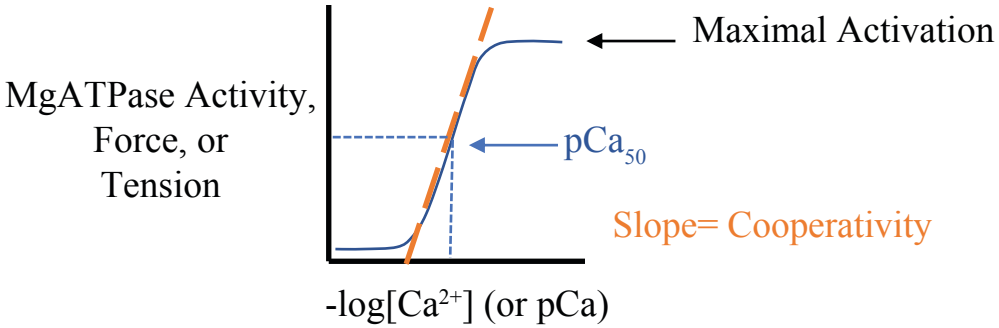

Figure 1.7 *In vitro* myofilament studies. A representative graph of data obtained from *in vitro* myofilament studies is shown. By permeabilizing cardiomyocytes or muscle fibers, force or tension generation, as well as the activity of the MgATPase can be studied over a range of fixed Ca^{2+} concentrations. Important pieces of information such as maximal activation, pCa_{50}, and cooperativity can be derived from this graph.

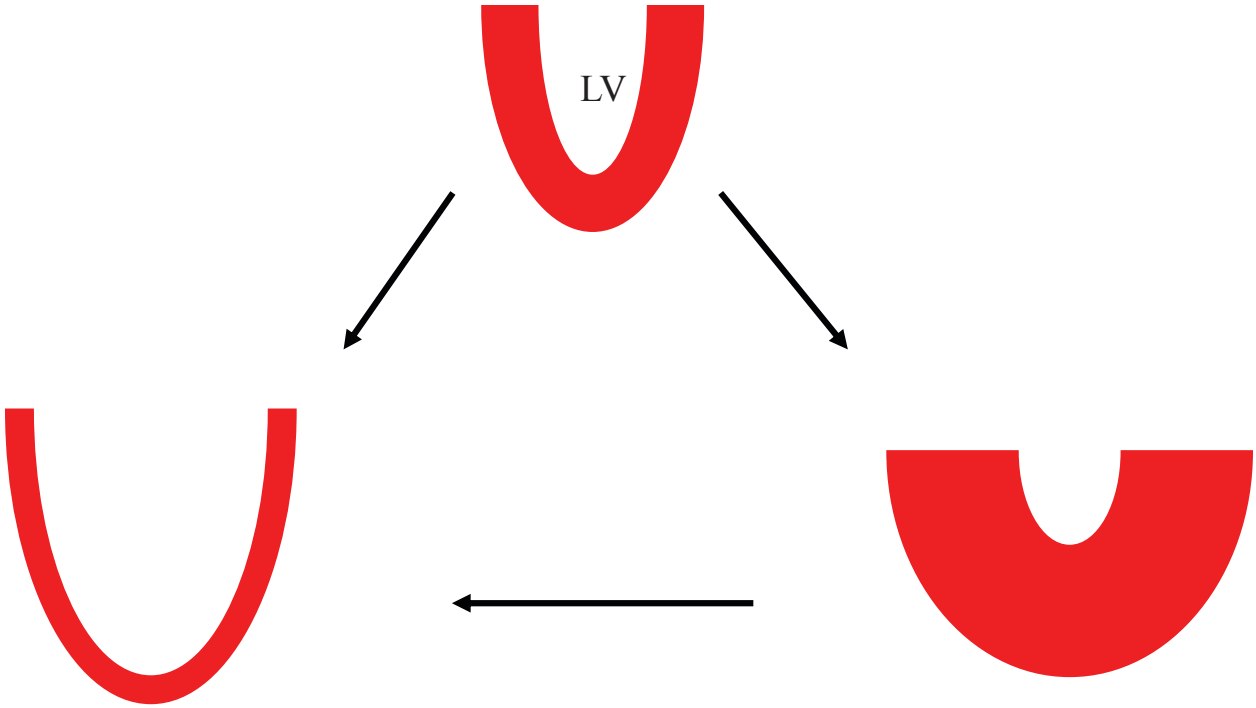

Figure 1.8 Ventricular remodeling in HF. A cartoon of left ventricle (LV) hypertrophy expected during HF. Normal hearts can exhibit a hypertrophic phenotype, where ventricular walls thicken to pump more strongly; while a dilated phenotype results from inadequate filling capacity. Severe hypertrophy can result in diastolic dysfunction that leads to ventricular dilation.

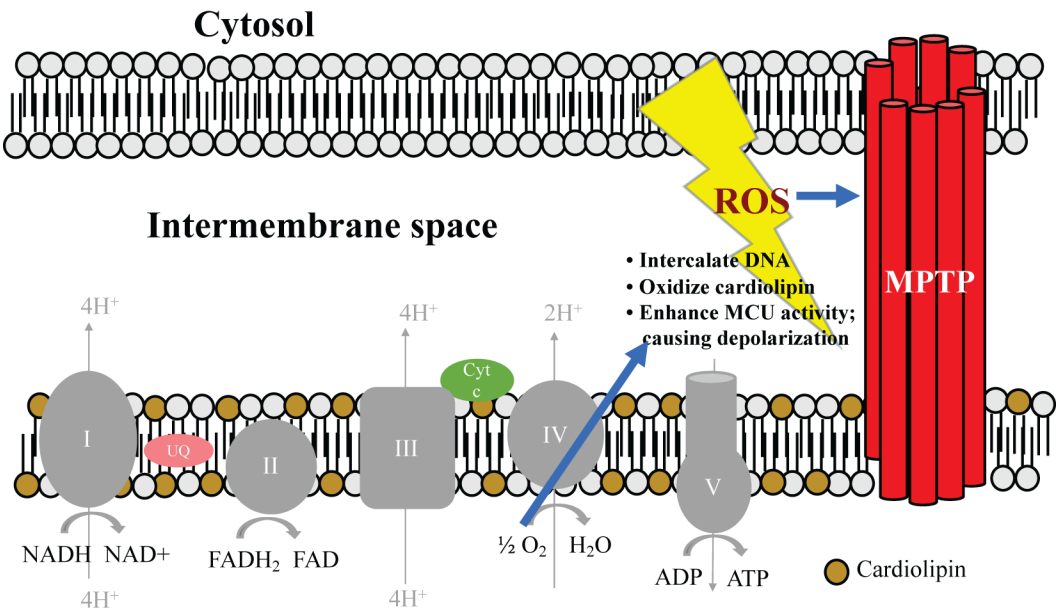

Figure 1.9 Electron transport chain (ETC). Schematic depiction of electron transport chain within the mitochondria. Complexes I-V of the ETC are represented. Primary energy carriers, NADH and $FADH_2$, are shown for complexes I and II, respectively. Coenzyme Q accepts electrons from complexes I and II, and becomes ubiquinone (UQ) which can carry electrons to complex III. Cytochrome C carries single electrons to complex IV where molecular oxygen is reduced to water. Meanwhile, protons are pumped from complexes I, II, and IV into the intermembrane space, creating an electrochemical gradient for ATP generation at complex V. If molecular oxygen is not efficiently reduces to water, it can be released as superoxide or reactive oxygen species (ROS), which can intercalate into DNA, oxidize fatty acids within the membrane, and enhance the activity of the mitochondrial Ca^{2+} uniporter, which can cause depolarization of the mitochondria. The mitochondrial permeability transition pore (MPTP) is shown in the membrane as a channel which opens during mitochondria depolarization.

Mouse Model	Replacement %	Type of Model	*In vitro*	*In vivo*	Pitfall
cTnI S23/24D ($cTnI_{PP}$)	100%	Transgenic	• No change in basal MgATPase activity • Decrease in PKC-stimulated MgATPase activity • Basal and PKC-stimulated Ca^{2+} sensitivity decreased	Micromanometry (hemodynamic assessment) • Heart rate: increase • Systolic Pressure: increase • Diastolic pressure: no change • dP/dt_{max} increase • dP/dt_{min} decrease • dP/dt_{40} no change • Peak LVP no change	100 % phosphorylation is not physiological; adult mice
cTnI S23/24A (cTnI Ala_2^{nb})	100%	Knock-out cTnI, knock-in alanine substitutions	• No change in basal MgATPase activity • Decreased PKC-activated MgATPase activity • No change in force production	No data provided	Adult mice
cTnI S23/24D + S43/45D + T144D ($cTnI_{All\text{-}P}$)	100%	Transgenic	• Basal and PKC-stimulated MgATPase activity decreased • Basal and PKC-stimulated Ca^{2+} sensitivity decreased	Micromanometry Heart rate: increase systolic pressure: no change dp/dt_{max} decreased dP/dt_{min} no change dP/dt_{40} decreased	100 % phosphorylation is not physiological; adult mice; lack of functional change may be due to compensations
cTnI S23/24A + S43/45A + T144A (cTnI Ala_5^{nb})	100%	Knock-out cTnI, knock-in alanine substitutions	• No change in basal or PKC-activated MgATPase activity	No data provided	100 % phosphorylation is not physiological Alanine causes *in vitro* functional

			• Ca^{2+} sensitivity decreased • No change in basal shortening		changes; adult mice
cTnI S23A/S24D + S43/45D	23%	Transgenic	• No change in maximal force production • PKA-activated Ca^{2+} sensitivity decreased • Increase in p-PLB/PLB ratio • Decrease in SERCA/Actin expression	<u>Echocardiography</u> • LVED increase • LVES increase • FS% decrease • LV wall dimension decreased <u>Micromanometry</u> dP/dt_{max} decreased dP/dtIP decreased	Adult mice
cTnI S43/45E + T144E ($cTnI_{PKC-P}$)	7%	Transgenic	• Basal MgATPase activity decreased • No change in basal Ca^{2+} sensitivity • Maximum basal Ca^{2+}-activated force decreased	<u>Isolated perfused heart</u> dP/dt_{max}: decreased dP/dt_{min} decreaed Peak LVP: decreased	Adult mice; questions arise about how replacement impacts phenotype since 7% replacement produces a drastic phenotype while 100% replacement (PP and All-P) mice produced minimal changes comparatively
cTnI S43/45A	50%	Transgenic	• No change in basal MgATPase activity • Basal Ca^{2+} sensitivity decreased	<u>Isolated perfused heart</u> • Diastolic pressure no change • Systolic pressure no change • dP/dt_{max} no change • dP/dt_{min} no change	Alanine causes changes *in vitro* and lack of functional changes *in vivo* are likely due to compensations; adult mice

Table 1.1 Existing phospho-mimetic and phospho-null mouse models.

A detailed summary of existing mouse models for the study of cTnI phosphorylation. *In vitro* information provided in this table was derived from animal models, rather than from reconstituted myofilament studies, or from studies with viral transduction of phospho-mutant cTnI constructs. Important abbreviations: dP/dt_{max}, rate of pressure development; dP/dt_{min}, rate of relaxation; dP/dt_{40}, a measure of contractility; dP/dtIP, normalized for instantaneous pressure, LVP, left ventricular (LV) pressure; LVED, LV end diastolic dimension; LVES, LV end systolic dimension; FS%, fractional shortening%; PLB, phospholamban; p-PLB, phosphorylated phospholamban.

Chapter 2

Cardiac Contractile Dysfunction and Protein Kinase C-Mediated Myofilament Phosphorylation in Disease and Aging

Vani S. Ravichandran, Himanshu J. Patel, Francis D. Pagani, and Margaret V. Westfall

SUMMARY

Cardiac troponin I Ser44 is a downstream target for protein kinase C. The current studies show heightened phosphorylation develops during contractile dysfunction in failing human myocardium and in rat models of pressure overload and aging with contractile dysfunction.

NOTE: While the following manuscript contains data from humans, the nomenclature for rodent cTnI S43/45 is used.

Abstract

Increases in protein kinase C (PKC) are associated with diminished cardiac function, but the contribution of downstream myofilament phosphorylation is debated in human and animal models of heart failure. The current experiments evaluated PKC isoform expression, downstream cardiac troponin I (cTnI) S45 phosphorylation (p-S45), and contractile function in failing (F) human myocardium, and in rat models of cardiac dysfunction caused by pressure overload and aging. In F human myocardium, elevated PKCα expression and cTnI p-S45 developed prior to ventricular assist device implantation. Circulatory support partially reduced PKCα expression and cTnI p-S45 levels and improved cellular contractile function. Gene transfer of dominant negative PKCα (PKCαDN) into F human cardiomyocytes also improved contractile function and reduced cTnI p-S45. Heightened cTnI phosphorylation of the analogous residue also accompanied reduced cardiomyocyte contractile function in a rat model of pressure overload and in aged F344 x BN F1 rats (≥26 mos). Together, these results indicate PKC-targeted cTnI p-S45 accompanies cardiac cellular dysfunction in human and animal models. Interfering with PKCα activity reduces downstream cTnI p-S45 levels and partially restores function, suggesting cTnI p-S45 may be a useful target to improve contractile function in the future.

Introduction

More than 26 million people worldwide have heart failure (HF) and the associated increased mortality and morbidity risk [135]. Clinical treatment of human HF by mechanical circulatory support with ventricular assist devices (VADs) continues to increase [136], though long-term improvement in cardiac function and VAD removal remain limited for most patients [137]. However, VAD therapy produces some reverse remodeling [138], and changes which may help in risk stratification for patients [139, 140]. Further work is needed to identify underlying cellular and molecular targets which improve cardiac function in addition to mechanical unloading.

Elevated expression and activity of protein kinase C (PKC) is consistently linked to HF in humans [68, 141, 142]. PKC activation modulates cardiac performance via a variety of downstream pathways and targets to influence hypertrophy [92], Ca^{2+} cycling [92, 143, 144], and metabolism [145]. The promiscuous expression and diverse targets of PKC suggests it functions as a central node for processing and modulating cardiac structure and function. In the sarcomere, which is the functional unit of striated muscle, there is growing evidence that PKC phosphorylation of the molecular switch protein, cTnI, reduces contractile function [111, 112]. Other signaling pathways respond to mechanical loading [146], but the relationship between PKC upregulation, downstream cTnI phosphorylation, contractile function during HF, and the response to VAD therapy remain to be investigated.

Work in cardiomyocytes is needed to investigate the relationship between PKC, downstream myofilament phosphorylation, and contractile function. Several investigators demonstrated the feasibility of isolating adult ventricular cardiomyocytes from explanted human hearts for contractile function studies [147-149]. Cardiomyocytes from non-failing (NF) human

hearts demonstrate a positive force-frequency relationship, while F human hearts develop a negative staircase response [150]. Partial reversal of the negative staircase response is reported in cardiomyocytes from HF patients after VAD support [150]. In addition, alterations in Ca^{2+} cycling proteins are associated with the negative frequency response [148], and VAD improves both Ca^{2+} handling and the stimulation frequency response in isolated cardiomyocytes.

Few studies have examined whether chronic post-translational modifications within the myofilament contribute to contractile dysfunction. Earlier work indicates increased PKC expression and activity are linked to human HF [68, 142], but the role played by its downstream myofilament targets in dysfunction is not clear. The present study shows PKC-targeted human cTnI p-S45 is associated with contractile dysfunction, by analyzing human F myocardium collected before and after VAD treatment, and hearts from pressure overloaded and aging rat myocardium.

Materials and Methods

Human cardiac tissue collection

Cardiac tissue collected from F and NF hearts was approved by the Internal Review Board at the University of Michigan, and the consent and protocol for collecting non-matched, NF hearts was approved by Gift of Life-Michigan, as described in detail earlier [141, 147]. Briefly the criteria for F hearts was a left ventricular ejection fraction (EF) $\leq$25% in F hearts, while structurally normal hearts with an EF $\geq$50% was required for the NF group [147]. Supplemental Table 1 provides information for the human myocardial tissue. Myocardium not designated for cell isolation was immediately flash frozen in liquid N_2 upon removal of the heart and stored at -80^{o}C. Pre- and post-VAD F and NF myocardium were analyzed for protein expression, and contractile function was compared in cardiomyocytes from pre- and post-VAD tissue and post-VAD cardiomyocytes after gene transfer of PKCα, PKCαDN are compared to non-treated (NT) cells, as described below.

Animal model studies

Studies performed in rat models were approved by the University of Michigan Institutional Animal Care and Use Committee and followed the PHS policy on Humane Care and Use of Laboratory animals.

Pressure overload (PO) rat model. The procedures for surgery, post-operative care, cardiac tissue and isolated Ca^{2+} tolerant cardiomyocytes were prepared at 18-20 wks after sham or PO surgery in Sprague-Dawley rats, when the ejection fraction begins to decrease [141].

Cardiomyocytes from sham- and PO-treated rats were analyzed for protein expression, immunolabeling of PKCα in cryosections, and cellular contractile function, as described below.

Aging rat model (Fischer 344 x Brown Norway F1 rats). Female Fisher 344 x Brown Norway F1 (F344BN) rats were obtained from the National Institute on Aging colony as described earlier [151]. Rats were maintained on a 12 hr light:dark cycle and fed normal chow for 2-4 months (mos) prior to harvesting hearts from 6, 18, 26, and 34 mos old rats. For studies with these rats, protein expression and cardiomyocyte contractile function were analyzed after adenoviral-mediated gene transfer of PKCα, PKCαDN, or green fluorescence protein (GFP) and compared to time-matched, NT cardiomyocytes. In preliminary studies, there were no differences in contractile function after GFP gene transfer compared to NT cardiomyocytes from 6-18 or 34 month old rats (Supp. Fig. 2.1).

Cardiomyocyte Isolation and Culture Conditions

Human cardiomyocytes. The isolation and culture conditions for Ca^{2+}-tolerant cardiomyocytes from HF and NF human hearts is described earlier [147]. Briefly, hearts were flushed with ice-cold cardioplegia prior to explant, and ventricles immediately transported to the lab to be minced into 5-10 mm pieces in ice-cold stock buffer (100 mM NaCl, 5.4 mM KCl, 1.5 mM $MgSO_4$, 10 mM NaOAc, 1.5 mM NaH_2PO_4, 15 mM glucose, 10 mM taurine, 10 mM HEPES; pH 7.40) supplemented with 2,3-butanedione monoxime (BDM, 15 mM) and nitrilotriacetic acid (5 mM). Then, protease type XXIV (4 U/ml), type II collagenase (400 U/ml), hyaluronidase (200 U/ml), and 1.25 mM $CaCl_2$ were sequentially added at 37°C to digest myocardium. Isolated cardiomyocytes were briefly centrifuged, re-suspended in stock buffer containing 2% bovine

serum albumin plus 10 mM BDM, and 5% fetal bovine serum (FBS) and then equal aliquots of $CaCl_2$ added back every 10 min over 1 hr to reach a final concentration of 1.8 mM. Then, 40,000 rod-shaped cells were plated on laminin-coated 22 mm coverslips in minimum essential culture media (MEM; Gibco) containing 5% FBS, 20 mM BDM, 40 mM HEPES, 50 U/ml penicillin plus 50 μg/ml streptomycin (P/S) for 2 hrs (MEM+). For gene transfer, media was replaced with media (NT), or adenovirus (Ad) containing GFP (AdGFP), PKCα (AdPKCα) or PKCαDN (AdPKCαDN) diluted in MEM+ or in MEM+ alone for 1 hr, followed by the addition of MEM containing 5 mM BDM, 40 mM HEPES, 2 mM glutamine, 24 mM $NaHCO_3$ and P/S. Media was changed daily and then cells were analyzed 24-36 hrs post-gene transfer.

Adult rat cardiomyocytes. The isolation and culture of Ca^{2+} tolerant cardiomyocytes from each rat heart followed the protocol described earlier [4, 5]. Briefly, Ca^{2+}- tolerant adult Sprague-Dawley rats or F344BN rat cardiomyocytes were isolated from collagenase-treated hearts [4, 5]. Rod-shaped cardiomyocytes were plated on laminin-coated coverslips in Dulbecco's Modified Eagle Medium (DMEM) supplemented with 5% FBS plus P/S at 37°C for 2 hrs [4, 5], and then replaced by serum-free DMEM plus P/S media containing recombinant AdGFP, AdPKCα or AdPKCαDN or media alone (NT). After an additional hour, M199 supplemented with 10 mM HEPES, 0.2 mg/ml BSA, 10 mM glutathione plus P/S (M199+) was added to each coverslip. For contractile function studies rat cardiomyocytes were paced starting the day after isolation, with media exchanged every 12 hrs. Media was also changed daily for cardiomyocytes used in protein expression work.

Protein expression and localization

Myocardial tissue and isolated cardiomyocytes. Human myocardium was pulverized to a fine powder in liquid N_2, homogenized in ice cold sample buffer supplemented with proteolysis and phosphatase inhibitors (Roche), and assayed for protein concentration [69, 141]. For Western analysis after gene transfer experiments using human or rat cardiomyocytes, cells were scraped from coverslips into the same ice-cold sample buffer and stored at 80^{o}C prior to protein separation [4, 5]. Homogenate samples or isolated cardiomyocyte proteins were separated by sodium dodecylsulfate polyacrylamide gel electrophoreses (SDS-PAGE; 12%), transferred to polyvinylidene difluoride (PVDF) membrane, and probed with primary Abs followed by an appropriate horseradish peroxidase (HRP)-conjugated goat anti-mouse (GAM) or goat anti-rabbit (GAR) secondary antibody (Ab), as described previously (Kim et al., 2016). Previously published Western protocols using primary Ab for PKCα (Santa Cruz Biotech sc-208), phosphorylated PKCα T638 (p-T638; Cell Signaling Technologies 9375), δ (Cell Signaling Tech 9616) , ε (Cell Signaling Tech 2683), phosphorylated human cTnI S45 (p-S44; PhosphoSolutions p2010-43), phosphorylated S23/24 (p-S23/24; Cell Signaling Tech 4004), and total cTnI (EMD Millipore MAB1691; 1:2000) were used to detect proteins in human homogenates and isolated human and rat cardiomyocytes (Hwang et al., 2012; Lang et al., 2015; Lang et al., 2017). Phosphorylation of S45 (p-S45) in rat cTnI is equivalent to human cTnI p-S45, while p-S23/24 is the same in cTnI from both species based on the UniProtKB TNNI3 human (P19429) and rat (P23693) sequences. In addition, phospholamban (PLB; EMD Millipore A1), plus phosphorylated phospholamban (p-PLB; Ser16; EMD Millipore 07-052) were probed in human myocardium and rat cardiomyocytes, as well as phosphorylated cTnI T144 (p-T144; Abcam ab58546) in rat cardiomyocytes. Unless otherwise noted, a titer of 1:1000

was used for each primary antibody (Ab). Protein expression was then detected by enhanced chemiluminescence (ECL) using a BioRad ChemiDoc MP imager (BioRad, Hercules, CA) or HyBlot CL film. A portion of each SDS-PAGE gel also was silver (Ag)-stained, and expression on Western blots and the silver (Ag)-stained gel quantified with Quantity One™ software (BioRad, Hercules, CA).

In most cases, protein expression detected by Western blot is expressed relative to a Ag-stained band on the gel to account for protein loading. These values are then normalized to the expression of the respective protein in non-failing (human), sham (rat) or NT (human or rat) samples on the same blot to determine fold changes in expression. For PKC isoform detection in human myocardium, these normalized values also were used to determine the ratio of pre- versus post-VAD expression in human myocardium. For phosphorylation studies, the ratio of phosphorylated to total protein is determined and compared for the quantitative analysis unless otherwise specified.

Localization in adult cardiomyocytes. Images for GFP and brightfield microscopy were collected from live human cardiomyocytes 1-2 days after gene transfer. To determine the PKCα cellular distribution in rat cardiomyocytes, paraformaldehyde fixed cardiomyocytes isolated 18-20 wks after sham and PO surgery were immunostained with PKCα (Santa Cruz) and TR-conjugated GAM Abs, as described earlier [141, 152]. Images were collected with a Nikon Ti-U inverted fluorescence microscope and DS-Fi1 5 megapixel digital imaging using identical exposure times for each sample.

Contractile function studies

Basal sarcomere shortening measurements. Sarcomere shortening and re-lengthening were analyzed in signal averaged traces collected from intact cardiomyocytes 24-36 hours after isolation and gene transfer using a high intensity video-based detection system (Ionoptix; Beverly, MA) [4, 5]. Cells were washed twice with M199+ and equilibrated for 20 min prior to measuring contractile function in human cardiomyocytes. Resting sarcomere length, peak shortening amplitude, shortening rate, re-lengthening rate, time to 50% re-lengthening ($TTR_{50\%}$) were measured in cardiomyocytes perfused with M199+ at 37^{o}C and field stimulated at 0.2 Hertz (Hz).

Frequency-dependent changes in steady state contractile function. Field stimulated human and rat cardiomyocytes paced at 0.2 (basal), 0.5, 1 and/or 2 Hz were monitored for contractile shortening. Contractile function was measured after reaching steady state contraction at each frequency and signal averaged traces were collected as described above for basal shortening measurements. Responses at 0.5-2 Hz were analyzed relative to the results obtained for basal stimulation (0.2 Hz), and then expressed as a percent change from this baseline measurement (% change = ((x Hz – 0.2 Hz)/0.2 Hz) x 100) [147]. Relative shortening in human cardiomyocytes is determined by normalizing contractile function to the functional range obtained at 2 Hz in NF cardiomyocytes.

Statistical analysis

Samples were compared using an unpaired Student's t-test, one- or two-way analysis of variance (ANOVA) and appropriate post-hoc tests with statistical significance set at $p<0.05$. The specific statistical test used for each group of data are described in the figure legends.

Results

PKC isoform expression and contractile function was initially studied in human samples from NF donors and F tissue collected before or after VAD therapy. PKCα expression levels were elevated in pre-VAD F myocardium compared to NF myocardium, and there were no significant changes in PKC δ or ε levels pre- or post-VAD (Fig. 2.1A,B, Supp Fig 2.2A), which agrees with earlier results [68, 142]. In post-VAD myocardium, PKCα expression was reduced by 34% compared to pre-VAD levels (Fig 3.1B), although expression still remained higher than in NF hearts (Supp Fig. 2.2A). The slowed $TTR_{50\%}$ observed in F cardiomyocytes at a low stimulation frequency is significantly improved by device support (Fig. 2.1C, D). The reduced frequency-dependent amplitude of contraction, and rates of shortening and re-lengthening observed in pre-VAD cardiomyocytes are also improved in post-VAD cardiomyocytes (Fig 2.1E, Supp Table 2.2), which is consistent with earlier studies [148].

In pre-VAD tissue, PKC-targeted cTnI p-S45 levels were elevated compared to NF hearts, while post-VAD levels were not significantly different from either NF or pre-VAD levels (Fig. 2.1F). This intermediate post-VAD cTnI p-S45 is between NF and pre-VAD expression and agrees with the partial reduction of PKCα levels in post- versus pre-VAD samples (Supp Fig. 2.2A). Together, the post-VAD cTnI p-S45 and reduced p-S23/24 (Fig. 2.1F; [153]) help to explain the incomplete restoration of the positive frequency response observed in NF cardiomyocytes (Fig. 2.1C). In addition, PKC phosphorylates cTnI S42 (p-S42; [104, 154] which could also be elevated during HF. However, this site was not examined here due to the lack of specific p-S42 phospho-Abs, and difficulties distinguishing between p-S42 and p-S45 by mass spectrometry [69]. Another target of PKCα is protein phosphatase I and the downstream reduction in sarcoplasmic reticulum p-

PLB [92]. As with cTnI p-S45, p-PLB levels were not a significantly different in post- versus pre-VAD myocardium, although post-VAD levels tended to improve (Supp Fig. 2.2B, C).

In additional studies, contractile function was measured in F human cardiomyocytes after gene transfer of PKCα or PKCαDN into F cardiomyocytes and compared to time-matched, NT controls (Fig. 2.2). Initially, AdGFP gene transfer was utilized to show the feasibility of successful gene transfer in human cardiomyocytes (Fig. 2.2A). Within 24 hours after gene transfer, Western analysis detected increased PKCα or PKCαDN protein expression (Fig. 2.2B). Parallel measurements of contractile function showed that PKCαDN improved the frequency-dependent responses compared to NT cardiomyocytes (Fig. 2.2C). However, gene transfer of PKCα resulted in no shortening at any stimulation frequency, and thus, contractile function was not quantitatively analyzed in these cardiomyocytes. In agreement with these functional changes, increased cTnI p-S45 levels were detected by Western analysis after PKCα but not PKCαDN gene transfer (Fig. 2.2B).

Due to a limited number of cardiomyocytes available from each human heart preparation, the relationship between PKCα, cTnI p-S45 (e.g. analogous to human cTnI S45) and function was further explored in rat models with cardiac dysfunction. Increased PKC expression or enhanced PKC-mediated cTnI p-S45 developed in earlier PO animal models [10, 155] but PKCα, cTnI p-S45 and cellular function have not been analyzed in one model. Here, analysis of myocardium from an established rat model of PO [141] showed increased PKCα and PKCα p-T638 levels in PO versus sham rat cardiomyocytes (Fig. 2.3A). Increased PKCα signaling was previously linked to elevated p-T638 levels in earlier studies on human heart failure [156]. Immuno-labeling showed PKCα primarily localized to the intercalated disks in sham myocardium but developed a more striated distribution in PO cardiomyocytes (Fig. 2.3B; Supp. Fig. 2.3). A slight increase in PKCδ

and decrease in PKCε expression observed in this rat PO model (Fig. 2.3C) also are consistent with the changes reported in earlier PO models [10, 155]. In functional studies, PO caused a significant reduction in basal shortening amplitude at 0.2 Hz (Fig. 2.3D) along with diminished frequency-dependent amplitude and rates of shortening and re-lengthening (Fig. 2.3E) compared to cardiomyocytes from sham rats. Heightened cTnI p-S45 (Fig. 2.3F) levels accompanied the PO-induced increase in PKCα levels and diminished function, while there was no significant change in cTnI p-T144 (Fig. 2.3G) or basal cTnI p-S23/24 levels (Fig. 2.3H), which are also targets for PKC [104, 154].

In addition to PKC, β-adrenergic receptor (β-AR) activation of protein kinase A (PKA) phosphorylates cTnI S23/24. More severe PO-induced cardiac dysfunction increases cTnI p-S23/24 [157], while β-AR downregulation also develops with hypertension [158]. Thus, p-S23/24 responses to increasing doses of isoproterenol (ISO) were evaluated and the β-AR-mediated cTnI p-S23/24 levels are attenuated in PO compared to sham cardiomyocytes (Figs. 2.3H). Overall, these data are consistent with increased p-S45 contributing to basal and frequency-dependent systolic and diastolic dysfunction during PO (Fig. 2.3D-F), and the attenuated ISO-induced p-S23/24 working with p-S45 to further slow relaxation in the PO cardiomyocytes (Fig. 2.3H).

The F344BN rat has a significantly longer life span than many other rat strains but also develops cardiomyocyte dysfunction with age [151, 159, 160]. Isolated cardiomyocytes from F344BN rats were studied at 6, 18, 26, and 34 mos of age to determine whether alterations in PKC and/or downstream p-S45 phosphorylation are linked with age-dependent contractile dysfunction. In support of this idea, peak shortening as well as shortening and re-lengthening rates were each significantly reduced in older 26-34 mos compared to 6 mos old rat cardiomyocytes (Fig. 2.4B). Although there were no significant changes in basal PKC α, δ, or ε expression detected by

quantitative Western analysis in older rats (Fig. 2.4A), enhanced downstream cTnI p-S45 accompanied cellular contractile dysfunction in these cardiomyocytes (Fig. 2.4C). Representative Westerns showing basal PKC isoform expression and phosphorylated cTnI in 6 and 26 mos old NT cardiomyocytes are provided in Fig. 2.5, panels A, B, E, and F.

Gene transfer of PKCα and PKCαDN into 6-18 and ≥26 mos old F344BN rat cardiomyocytes also was analyzed after gene transfer of AdGFP, AdPKCα and AdPKCαDN to time-matched, NT cardiomyocytes to gain further insight into the relationship between PKC and aging-related contractile dysfunction. PKC isoform expression in either young or old cardiomyocytes did not change after AdGFP gene transfer (Fig. 2.5A), and similar increases in PKCα/PKCαDN expression levels developed in both young and old cardiomyocytes after AdPKCα/AdPKCαDN gene transfer (Fig. 2.5A-C). Age did not change the level of increased PKCαDN (Fig. 2.5C, left panel) or PKCα expression after gene transfer. In addition, the increases in PKCα and PKCαDN were similar (Fig. 2.5C, right panel). Thus, any functional differences are not caused by age-related differences in PKCαDN expression after gene transfer or to a difference in PKCαDN versus PKCα expression after gene transfer. In functional studies, the shortening and re-lengthening rates in cardiomyocytes from young rats (6-18 mos) were consistent with earlier results after gene transfer of PKCα and PKCαDN [92] (Fig. 2.5D). However, there were interesting age-related differences in the functional response of older cardiomyocytes (≥26 mos) after gene transfer. Specifically, the increased peak shortening amplitude observed after AdPKCαDN gene transfer into younger cardiomyocytes was absent in cardiomyocytes from ≥26 mos old rats, and in fact further decreased compared to younger cardiomyocytes (Fig. 2.5D). The enhanced p-PLB/PLB produced by PKCαDN gene transfer is comparable for both age groups (Fig. 2.5E), but there is a sustained elevation in cTnI p-S45 levels in cardiomyocytes from older rats regardless of gene transfer group

(Fig. 2.5F). This age-related elevation in cTnI p-S45 levels is consistent with the inability of PKCαDN to improve peak shortening in the older rat cardiomyocytes.

Discussion

The current results show that elevated cTnI p-S45 levels accompany chronic contractile dysfunction in cardiomyocytes from F human hearts and the equivalent p-S45 in a PO rat model, when there is up-regulation of PKC (Figs. 2.1A, 2.3A). Previously, the contribution of PKC-targeted cTnI p-S42/44 (rat pS-43/45) to progressive contractile dysfunction has received little attention even though rodent cTnI S43/45 is a known target for PKC [104, 154], and phospho-mimetic cTnI S43 and/or S45 substitutions significantly reduce cardiomyocyte contractile function [4, 5]. The improved cellular function and reduced cTnI p-S45 after gene transfer of PKCαDN into F human cardiomyocytes (Fig. 2.2) further supports the idea that this cTnI phosphorylation site contributes significantly to chronic cardiac dysfunction associated with elevated PKC levels. Chronic PKC up-regulation and impaired cardiac function have been more often linked to changes in other cellular functions not directly responsible for contractile function [92, 143, 161-163]. The current studies suggest chronic cTnI p-S45 in human myocardium contributes to progressive dysfunction and thus, therapeutically targeting this site may improve cardiac performance in HF.

Relationship between PKC expression and contractile dysfunction. The increased PKCα levels observed in F human hearts and in a rat model of PO (Figs. 2.1A, 2.3A) are consistent with earlier work showing that chronic PKC activity is associated with up-regulation and produces contractile dysfunction [65, 68, 142, 164]. Improved contractile function in post-VAD hearts with reduced PKCα expression (Fig. 2.1B-E) and after PKCαDN gene transfer in F human cardiomyocytes (Fig. 2.2C) also agree with the cardiac phenotype in genetically targeted PKCα knockout mice [92]. However, in aging rat cardiomyocytes, contractile dysfunction and increased cTnI p-S45 developed even though PKC isoform expression did not change (Fig.

2.4A-C). The PO-related re-distribution of PKCα in rat cardiomyocytes (Fig. 2.3B) suggests spatiotemporal localization of cardiac PKC could produce diverse responses by targeting different patterns of downstream proteins [165]. This possibility could also help to explain age-associated increases in cTnI p-S45 and contractile dysfunction in F344xBN rats (Fig. 2.4B,C), especially given that there is no significant age-related change in basal p-S23/24 observed here and in previous work (Fig. 2.4C) [166]. The potential for changes in downstream targeting patterns also indicates that in addition to monitoring PKC, there is a need to identify downstream proteins in the PKC pathway and their contribution to chronic cardiac dysfunction.

PKC and downstream cTnI phosphorylation. Sarcomere proteins play a pivotal role in cardiac pressure development and relaxation [167, 168]. Thus, myofilament signaling targets such as cTnI are especially important to investigate in the context of understanding pump dysfunction. Our results show chronic cardiac contractile dysfunction is consistently associated with increased PKC-targeted rat cTnI p-S45 levels (Figs. 2.3, 2.4). PKC preferentially phosphorylates rat cTnI S23, S24, S43, S45, and T144 [154]. The best understood site on cTnI is S23/24, which is phosphorylated by PKA, PKC and other kinases [169] to accelerate *in vivo* cardiac relaxation by increasing Ca^{2+} dissociation from cTnC and reducing myofilament Ca^{2+} sensitivity [65, 170, 171]. In contrast, cTnI p-S43/45 reduces maximum actomyosin ATPase, force, and shortening in addition to decreasing myofilament calcium sensitivity [3, 70, 104, 170]. Thus, this cluster is expected to diminish *in vivo* function.

Endogenous cTnI has been replaced with cTnI containing phospho-mimetic S43/45 combined with other PKC-targeted residues (e.g. S23/24, T144) in genetic mouse models to determine the impact of PKC phosphorylation on cTnI and myofilament function. However,

phenotypes in these mice range from minimal to severe cardiac dysfunction [66, 111, 112]. These findings are not easily explained by the other modified residue and/or cTnI replacement levels, which has led to ambiguity in the role cTnIS43/45 plays in modulating *in vivo* contractile performance. There is no published genetic animal model expressing cardiac-specific phospho-mimetic cTnI S43/45 alone, but work in isolated cardiomyocytes provides some insight [169]. Specifically, gene transfer and replacement of endogenous cTnI with phospho-mimetic cTnI-S43D, -S45D or -S43/45D reduces cardiomyocyte contraction and relaxation [5], which is consistent with the enhanced cTnI p-S45/p-S45 and contractile dysfunction observed in human hearts and in PO and aging rat cardiomyocytes (Figs. 2.1, 2.3, 2.4). The enhanced cTnI p-S45 linked to dysfunction in older F344BN cardiomyocytes and the inability of PKCαDN gene transfer to improve shortening amplitude and reduce p-S45 levels in older cardiomyocytes (Figs. 2.4, 2.5) further supports a significant role for cTnI p-S45 in chronic cardiac dysfunction. Cellular studies also showed that secondary phosphorylation develops at other myofilament protein sites over time and coincides with a partial attenuation of cardiomyocyte dysfunction [4]. This adaptive mechanism may contribute to the partial improvement in post-VAD cardiomyocyte contractile function, when there were no significant improvements in pre- versus post-VAD cTnI p-S45 and p-PLB (Fig. 2.1F, Supp Fig. 2.1C). Most importantly, the current set of studies show that elevated cTnI p-S45 is consistently observed during contractile dysfunction (Figs. 2.1, 2.3, 2.4). Future work is needed to determine if there is a similar relationship between human cTnI p-S42 and chronic *in vivo* cardiac dysfunction, and to better understand the intricate modulatory nature of the myofilament.

Our results also show that elevated cTnI p-S45 is present in addition to the well-documented reduction in cTnI p-S23/24 during cardiac dysfunction and end-stage human HF

[172-174] (Fig. 1). Heightened rat cTnI p-S45 develops under circumstances when there is chronic contractile dysfunction without decreases in basal p-S23/24 levels (Figs. 2.3F and H, 2.4C). As a result, data from both human and rat models support the idea that cTnI p-S45 significantly contributes to chronic cardiac dysfunction.

Therapeutically targeting downstream PKC sites in the myofilament. Recent clinical trials tested whether molecular inotropes targeted to myofilament myosin can improve cardiac performance [175]. The elevated PKC-targeted cTnI p-S45/p-S45 which accompanies cardiomyocyte dysfunction (Figs. 2.1, 2.3, 2.4) indicates reduced human cTnI p-S45 may be functionally beneficial. Thus, this site should be considered as an additional myofilament target for therapeutically treating cardiac dysfunction. Therapeutic strategies designed to broadly modify multiple post-translational sites and thus, target the rheostat-like function of cTn may optimize improvements in both systolic and diastolic function, and potentially increase the relatively small improvement observed in cardiac performance during VAD support [176, 177].

Limitations. The current cardiomyocyte studies do not include measurement of Ca^{2+} transients, and the peak amplitude and rate of Ca^{2+} decay does improve and contributes to the functional improvement in F human cardiomyocytes after VAD therapy [148]. However, there is also earlier work showing contractile dysfunction can develop independent of changes in Ca^{2+}. For example, no significant changes in diastolic Ca^{2+} or the peak Ca^{2+} transient were detected at a point when peak shortening was impaired in a rat hypertensive model with a comparable duration of suprarenal aortic banding as the cardiomyocytes in Fig. 3.3 [178]. Significant reductions in peak shortening and the rates of shortening and re-lengthening also were

accompanied by higher peak Ca^{2+} transients in rat cardiomyocytes after aortic banding [179]. There were also no significant changes in the Ca^{2+} transient in the same aging rodent model used here [151] and a similar outcome was reported in Wistar rats [180]. Although these findings collectively suggest elevated human cTnI p-S45 (or rat p-S45) contributes to chronic reductions in contractile function, future work is needed to test the impact of cTnI p-S43/45 alone on *in vivo* contractile performance.

Acknowledgements

We gratefully acknowledge the technical contributions of Michelle Tracy. This work was supported by National Institutes of Health Grant R01-HL-067254 (MVW) and NIGMS T32 GM007315 (VR).

Author Contributions

Vani Ravichandran, Himanshu Patel and Margaret Westfall collected and analyzed data. Himanshu Patel and Francis Pagani provided human tissue. Vani Ravichandran wrote the original draft and edited the manuscript with Margaret Westfall.

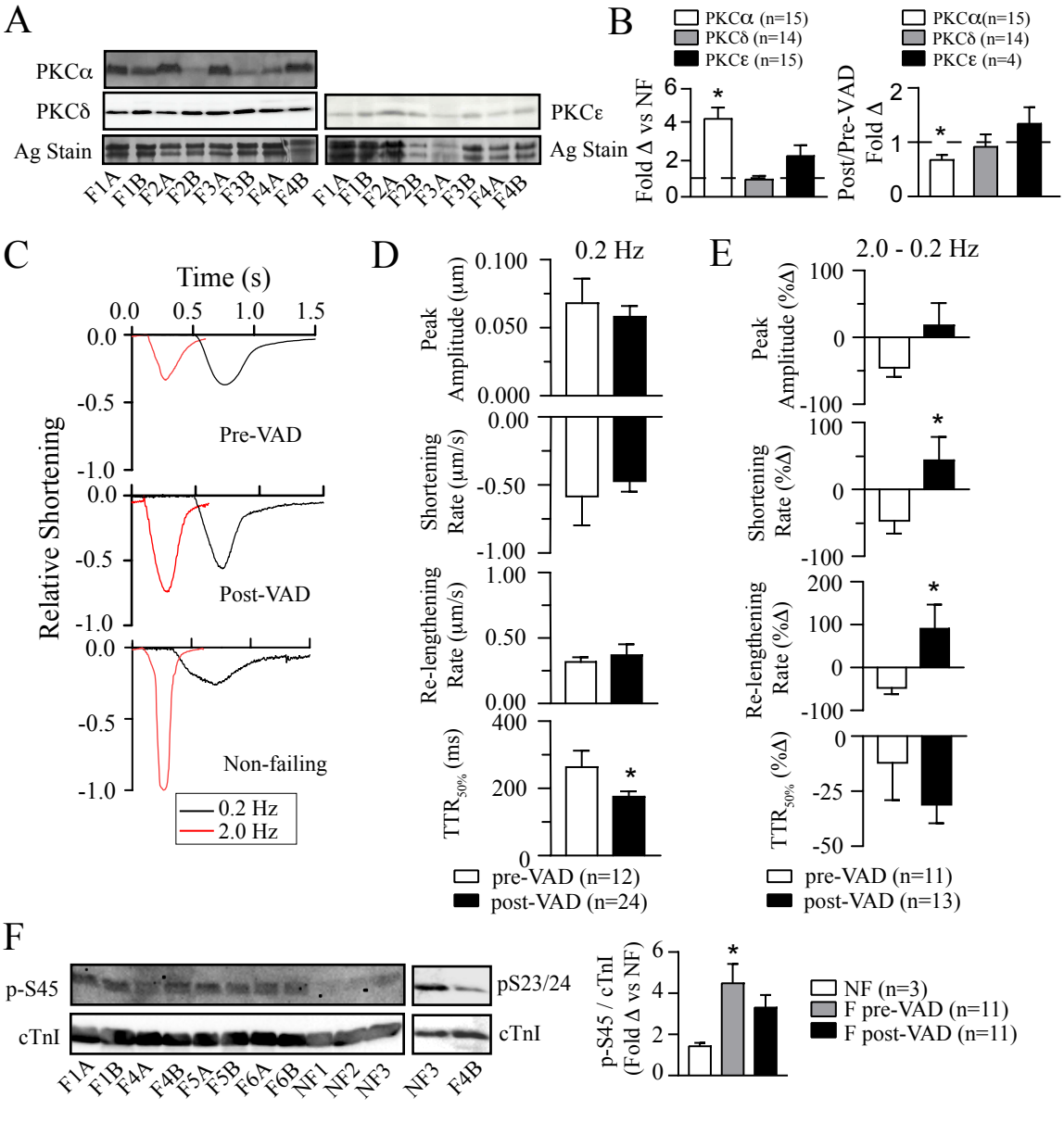
A
PKCα
PKCδ
Ag Stain
PKCε
Ag Stain
F1A F1B F2A F2B F3A F3B F4A F4B
B
PKCα (n=15)
PKCδ (n=14)
PKCε (n=15)
Fold Δ vs NF
PKCα(n=15)
PKCδ (n=14)
PKCε (n=4)
Post/Pre-VAD Fold Δ
C
Time (s)
Relative Shortening
Pre-VAD
Post-VAD
Non-failing
0.2 Hz
2.0 Hz
D
0.2 Hz
Peak Amplitude (μm)
Shortening Rate (μm/s)
Re-lengthening Rate (μm/s)
TTR50% (ms)
pre-VAD (n=12)
post-VAD (n=24)
E
2.0 - 0.2 Hz
Peak Amplitude (%Δ)
Shortening Rate (%Δ)
Re-lengthening Rate (%Δ)
TTR50% (%Δ)
pre-VAD (n=11)
post-VAD (n=13)
F
p-S45
cTnI
pS23/24
cTnI
F1A F1B F4A F4B F5A F5B F6A F6B NF1 NF2 NF3 NF3 F4B
p-S45 / cTnI (Fold Δ vs NF)
NF (n=3)
F pre-VAD (n=11)
F post-VAD (n=11)

Figure 2.1 PKC expression, contractile function and PKC-targeted cTnI - phosphorylation in human myocardium before and after VAD support.A. Representative Western blots for PKCα, PKCδ, PKCε expression in F human heart tissue collected pre- vs post-VAD treatment along with a silver-stained (Ag stain) portion of the SDS-PAGE gel to indicate protein loading. "A" indicates pre-VAD while "B" indicates post-VAD samples for the labels shown below the blot. **B.** Quantitative analysis of the fold change (Δ) in PKCα, δ, and ε protein expression in F compared to NF myocardial tissue (NF; left panel) and the fold change in the ratio of post-/pre-VAD isoform expression (right panel). Results are expressed as mean±SEM for quantitative data shown in panels B, and D-F. An unpaired Student's t-test was used to compare F versus NF samples and post- versus pre-VAD levels, with $p<0.05$ (*) considered statistically significant (n= number of hearts in each group for panels B and F. **C.** Representative shortening traces collected from F cardiomyocytes before VAD (upper panel), or after VAD (middle panel) implantation compared to NF (lower panel) cardiomyocytes. Individual traces are shown at stimulation frequencies of 0.2 (black) and 2.0 (red) Hz to illustrate the negative frequency response in cardiomyocytes from F human hearts prior to VAD (Goldberg et al., 2000) and partial restoration after VAD therapy. **D.** Quantitative analysis of contractile function stimulated at 0.2 Hz in cardiomyocytes collected from 6 pre- versus 7 post-VAD hearts (n=number of cells for panels D and E). **E.** Analysis of the percent change (%Δ) in the shortening amplitude, rates of shortening and re-lengthening, plus $TTR_{50\%}$ measured at 2.0 versus 0.2 Hz. **F.** Representative Western blots show cTnI phosphorylation at residue p-S45 relative to total cTnI expression in pre- and post-VAD samples (left panel), and the previously established decrease in p-S23/24 levels in F hearts (middle panel; Messer et al., 2007). Quantitative analysis of cTnI p-S45 shows significantly higher levels before VAD therapy compared to NF tissue using a one-way ANOVA and post-hoc Tukey statistical comparison (right panel; *$p<0.05$). After VAD support, cTnI p-S45 levels are not significantly different from NF or pre-VAD F levels.

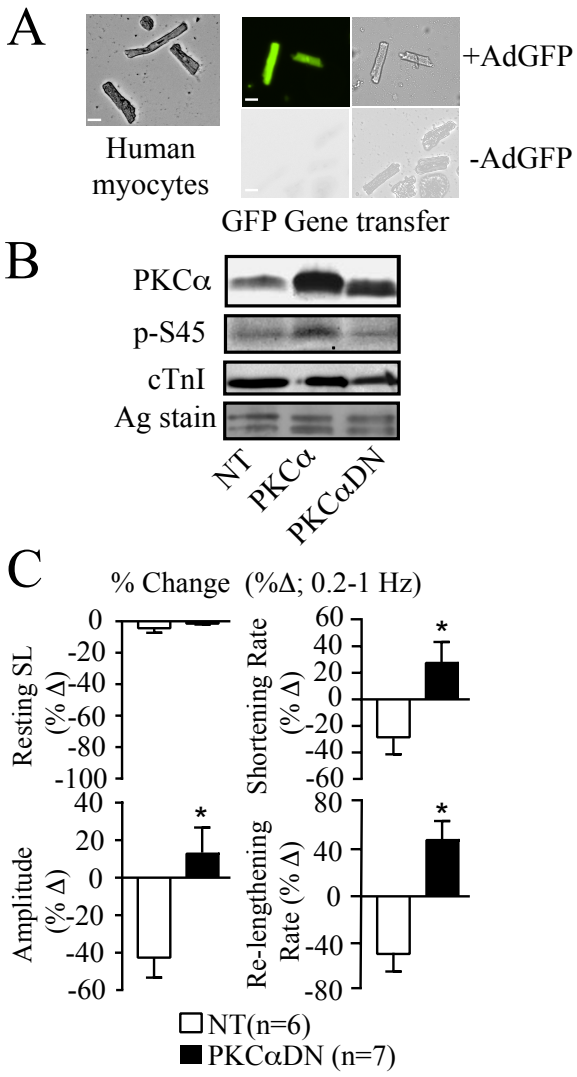
A
+AdGFP
-AdGFP
Human myocytes
GFP Gene transfer
B
PKCα
p-S45
cTnI
Ag stain
NT
PKCα
PKCαDN
C
% Change (%Δ; 0.2-1 Hz)
Resting SL (% Δ)
Shortening Rate (% Δ)
Amplitude (% Δ)
Re-lengthening Rate (% Δ)
NT(n=6)
PKCαDN (n=7)

Figure 2.2 Protein expression and the contractile function frequency response after gene transfer in human cardiomyocytes. A. Representative bright field (left, far right panels) and fluorescence (middle panel) images of F human cardiomyocytes with AdGFP gene transfer (upper panels) compared to NT cardiomyocytes (lower panels). Scale bars = 25 μm. **B.** Representative Western analysis showing PKCα/PKCαDN, cTnI p-S45, and cTnI expression in isolated F cardiomyocytes after AdPKCα or AdPKCαDN gene transfer compared to NT cardiomyocytes. The Ag-stained gel is included to show protein loading in each lane. The limited number of cardiomyocytes available for Westerns in each prep did not allow for quantitative analysis of multiple Western blots. **C.** Cardiomyocyte function after gene transfer of PKCαDN into F cardiomyocytes compared to NT cardiomyocytes. Results are expressed as the percent change (%Δ) in the amplitude, shortening and re-lengthening rates collected at 1 versus 0.2 Hz (n= number of cells from 3 separate hearts in each group). Data is presented as mean ± SEM, with a Student's unpaired t-test used for statistical comparisons (*$p<0.05$ vs. control). Cells no longer contracted after gene transfer of AdPKCα into F cardiomyocytes and therefore, this group was not included in the quantitative analysis.

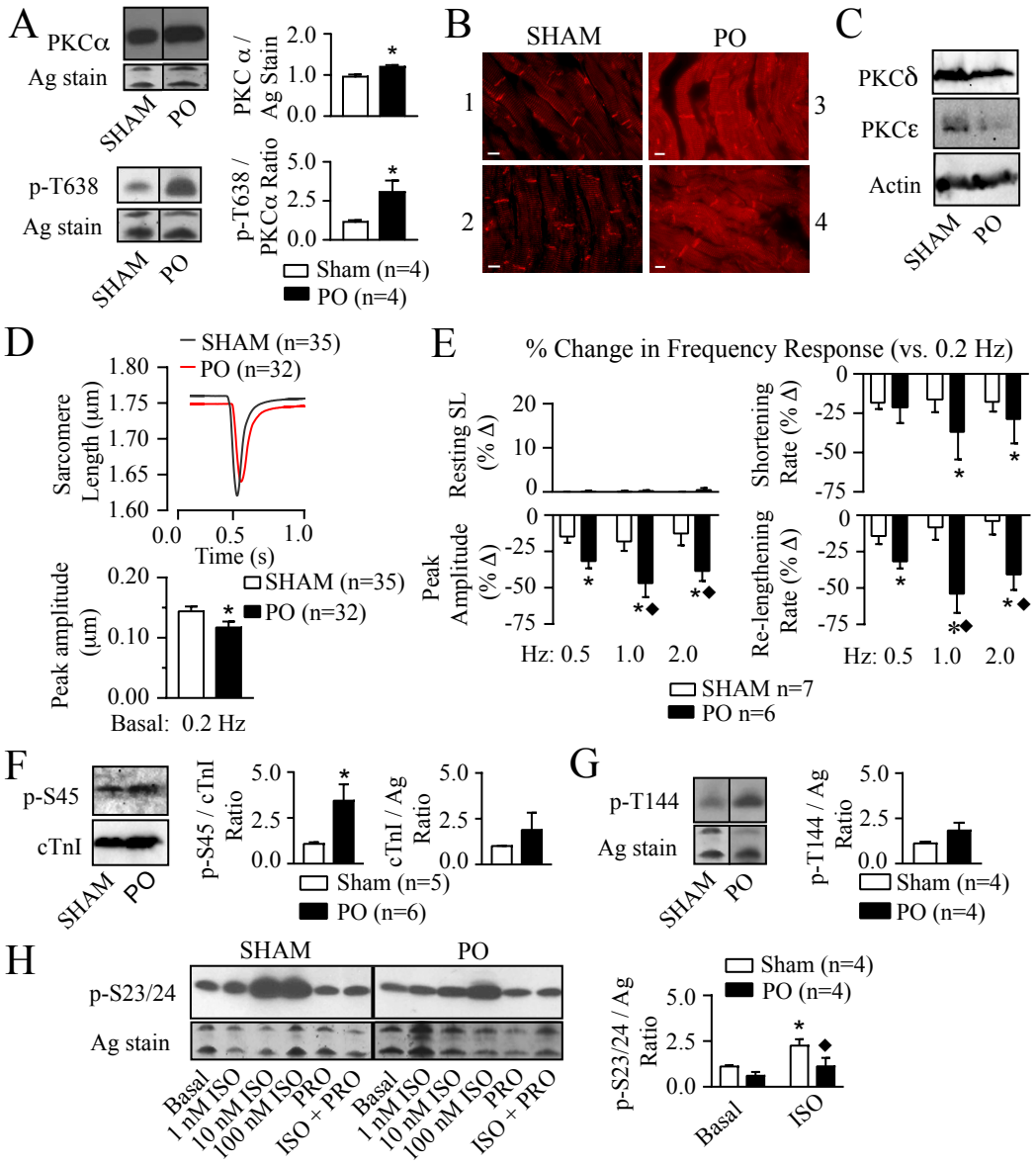
A
PKCα
Ag stain
SHAM
PO
PKC α / Ag Stain
p-T638
Ag stain
p-T638 / PKCα Ratio
Sham (n=4)
PO (n=4)
B
SHAM
PO
1
2
3
4
C
PKCδ
PKCε
Actin
SHAM
PO
D
SHAM (n=35)
PO (n=32)
Sarcomere Length (μm)
Time (s)
Peak amplitude (μm)
Basal: 0.2 Hz
E
% Change in Frequency Response (vs. 0.2 Hz)
Resting SL (% Δ)
Peak Amplitude (% Δ)
Shortening Rate (% Δ)
Re-lengthening Rate (% Δ)
Hz: 0.5 1.0 2.0
SHAM n=7
PO n=6
F
p-S45
cTnI
p-S45 / cTnI Ratio
cTnI / Ag Ratio
Sham (n=5)
PO (n=6)
G
p-T144
Ag stain
p-T144 / Ag Ratio
Sham (n=4)
PO (n=4)
H
SHAM
PO
p-S23/24
Ag stain
Basal
1 nM ISO
10 nM ISO
100 nM ISO
PRO
ISO + PRO
p-S23/24 / Ag Ratio
Sham (n=4)
PO (n=4)
Basal
ISO

Figure 2.3 Comparison of PKC expression and localization, contractile function and cTnI phosphorylation in hearts from PO- versus sham-treated rats. A. Representative Western for PKCα (upper left panel), phosphorylated PKCα T638 (PKCα p-T638; lower left panel) in PO compared to sham rat hearts. An Ag-stained portion of the gel also is shown as a loading control. The quantitative analyses of PKCα, and phosphorylated PKCα p-T638 are shown in the upper and lower right panels, respectively. There were increases in the ratio of PKCα p-S657/total PKCα in 2 samples from PO (1.42, 2.64) when normalized to the sham control ratio (1.00, 1.00). Quantitative data presented in panels A and D-H are expressed as mean±SEM. The n values in panels A and F-H equal the number of rat samples. Statistical analysis in panels A, D, F, and G utilized an unpaired Student's t-test (*$p<0.05$). **B.** Fluorescence images collected with comparable exposure times after immunostaining for PKCα show the re-distribution of PKCα in 2 sham (panels 1,2) compared to 2 PO (panels 3,4) rat hearts. Scale bars = 10 μm. **C.** Representative Westerns show PKCδ and PKCε expression in PO compared to sham-treated rat hearts. Actin immunostaining is shown as a loading control for each lane. **D.** Composite shortening traces collected from sham (black) and PO (red) cardiomyocytes at 0.2 Hz (upper panel) and the quantitative analysis of traces showed PO produced a significant reduction in shortening amplitude vs. sham cardiomyocytes (lower panel; *$p<0.05$; n = number of cardiomyocytes in panels D-E). No significant changes were detected in resting sarcomere length or the rates of shortening and re-lengthening (results not shown). **E.** The percent change (%Δ) in resting sarcomere length, peak shortening amplitude, and the rates of shortening and re-lengthening at 0.5, 1 and 2 Hz were compared to the response at 0.2 Hz in sham and PO cardiomyocytes. Results are analyzed with a 2-way ANOVA and Tukey's post-hoc tests, with significance set to $p<0.05$ (* vs. 0.2 Hz response; ◆vs sham at the same frequency). PO and stimulation frequency each caused significant effects in the peak amplitude, shortening and re-lengthening rates, and there were interaction effects for peak amplitude and re-lengthening rate. Overall, shortening amplitude and re-lengthening rate are significantly more impaired at higher frequencies in PO compared to sham cardiomyocytes. **F.** Representative cTnI p-S45 and cTnI Westerns (left panels) and the quantitative analysis of expression (middle, right panels) show that PO increases cTnI p-S43 without a change in total cTnI compared to sham rat cardiomyocytes. The cTnI expression is normalized to an Ag-stained band in each gel. **G.** Representative Western for cTnI p-T144 and an Ag-stained portion of the gel, which is used as a loading control (left panels) and quantitative analysis of cTnI p-T144/Ag ratio (right panel) show there are no significant differences in cTnI p-T144 levels for PO compared to sham rat cardiomyocytes. **H.** Representative Westerns for cTnI p-S23/24 and an Ag-stained portion of the gel (left panels) and quantitative analysis of cTnI p-S23/24 levels (right panel) in sham and PO rat cardiomyocytes under basal conditions and in response to 1, 10 and 100 nM of the β-adrenergic receptor agonist isoproterenol (ISO), and/or the β-antagonist, propranolol (PRO; 10 μM). Results are analyzed with a 2-way ANOVA and post-hoc Tukey's test. The quantitative analysis shows that 10 nM ISO produced a significant increase in p-S23/24 above basal levels in sham cardiomyocytes (*$p<0.05$ vs basal sham), but not PO cardiomyocytes ($p>0.05$ vs basal PO), and this ISO response is reduced in PO compared to sham cardiomyocytes (◆$p<0.05$ vs sham+ISO).

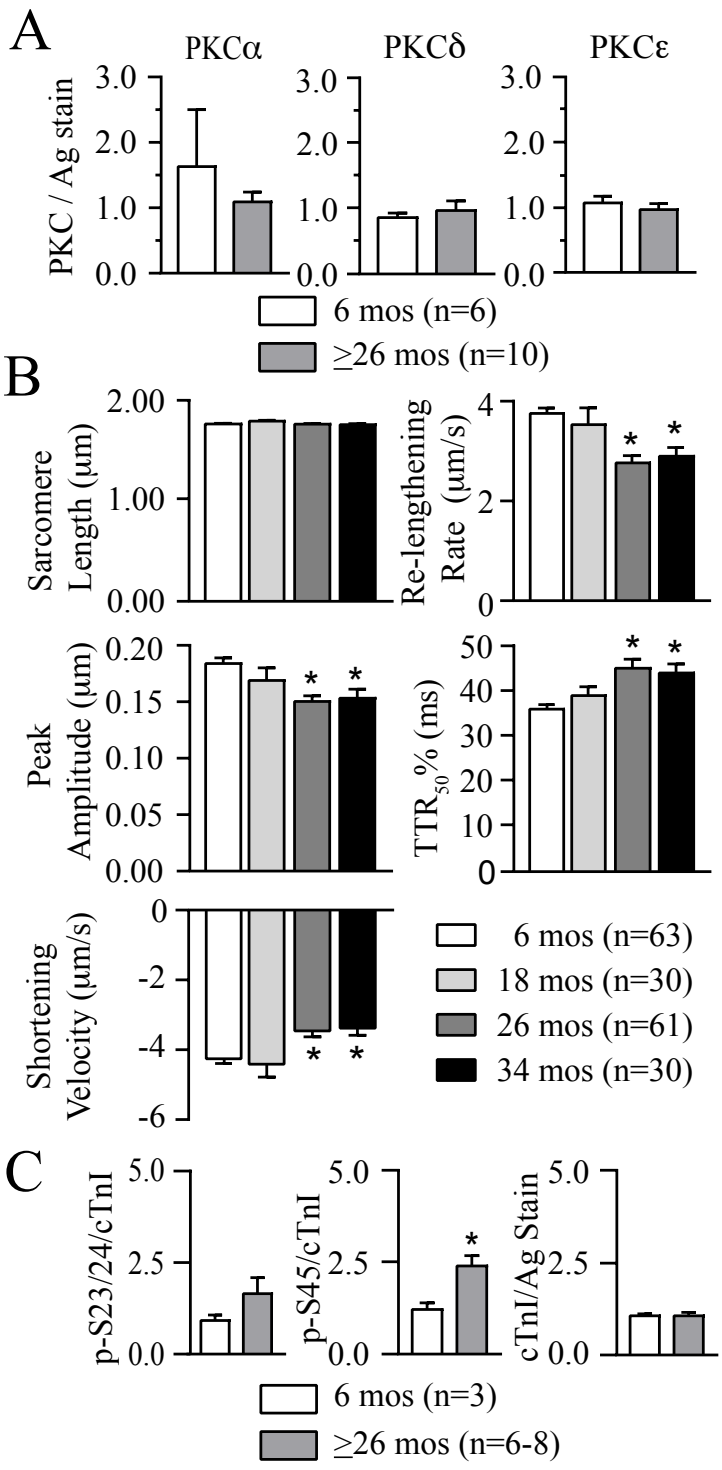
A
PKCα
PKCδ
PKCε
PKC / Ag stain
3.0
2.0
1.0
0.0
6 mos (n=6)
≥26 mos (n=10)
B
Sarcomere Length (μm)
2.00
1.00
0.00
Re-lengthening Rate (μm/s)
4
2
0
Peak Amplitude (μm)
0.20
0.15
0.10
0.05
0.00
TTR50% (ms)
50
40
30
20
10
0
Shortening Velocity (μm/s)
0
-2
-4
-6
*
6 mos (n=63)
18 mos (n=30)
26 mos (n=61)
34 mos (n=30)
C
p-S23/24/cTnI
p-S45/cTnI
cTnI/Ag Stain
5.0
2.5
0.0
6 mos (n=3)
≥26 mos (n=6-8)

Figure 2.4 PKC isoform expression, basal contractile function and cTnI phosphorylation in young compared to older F344 x Brown Norway rat hearts. A. Quantitative analysis showed no significant change in basal expression of PKCα, δ and ε protein levels in cardiomyocytes from young adult (6 mos) versus older (26, 34 mos = ≥26 mos) rats. PKC isoform expression is normalized to a portion of the Ag stained gel. Quantitative results in each panel are expressed as mean±SEM (n = number of rat samples in panels A and C). Statistical comparisons in panels A and C utilized an unpaired Student's t-test (*$p<0.05$). **B.** Analysis of composite cardiomyocyte contractile function in 6, 18, 26, and 34 mos old rat cardiomyocytes paced at 0.2 Hz (n = number of cardiomyocytes from ≥ 4 different rats). Resting sarcomere length, peak shortening amplitude, the rates of shortening and re-lengthening and the $TTR_{50\%}$ were analyzed with a 1-way ANOVA and post-hoc Dunnett's tests (*$p<0.05$ vs 6 mos). **C.** Quantitative analysis of cTnI phosphorylation at cTnI p-S23/24, p-S45 and total cTnI expression in 6 versus ≥26 mos old rat hearts. Total cTnI levels are normalized to a portion of the Ag stained gel. The p-S45 levels are significantly elevated in rat hearts from ≥26 mos compared to 6 mos olds (middle panel), while there were no differences in cTnI p-S23/24 (left panel) or total cTnI (right panel) expression. Note that representative Western blots for panel A are shown in Figure 3.5A, B, E and the representative Western results for basal cTnI p-S23/24, p-S45 and cTnI are shown in Figure 3.5F.

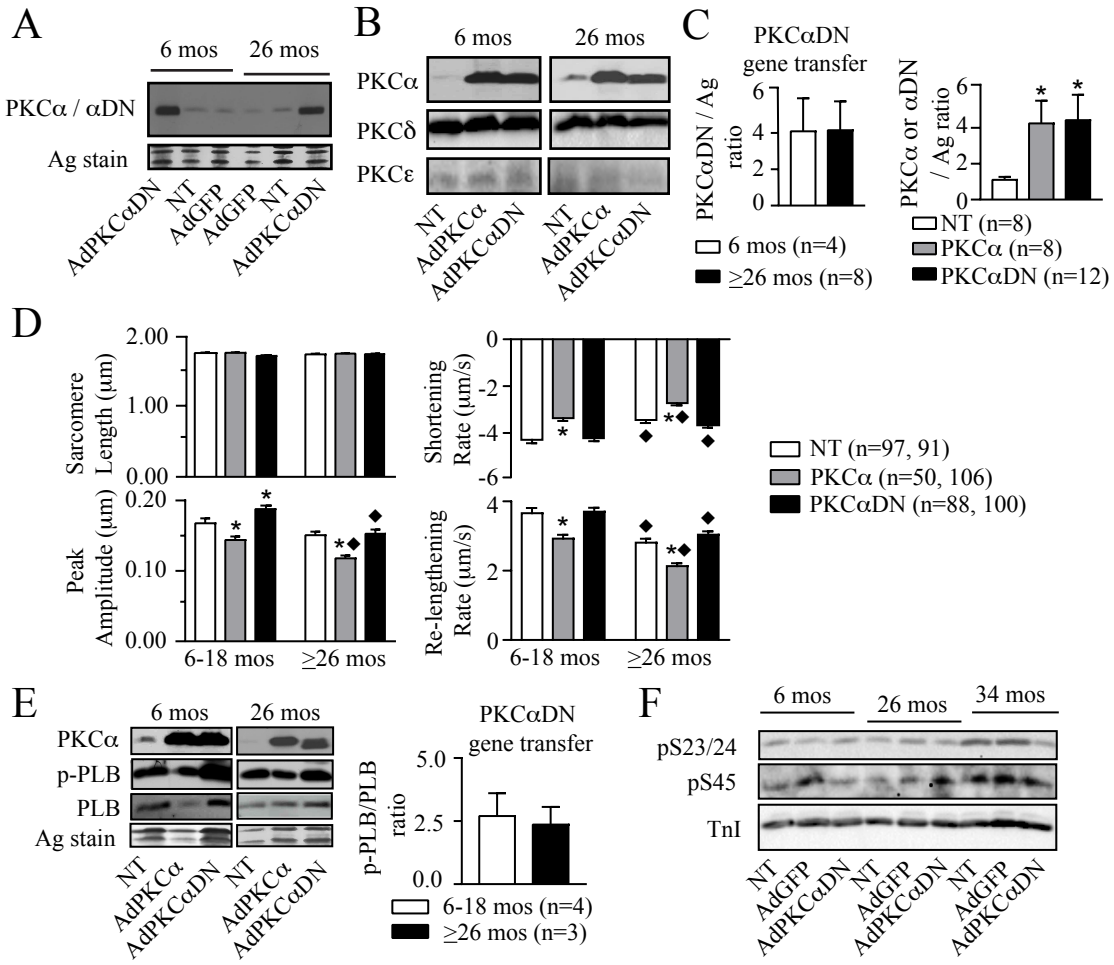
A
6 mos
26 mos
PKCα / αDN
Ag stain
AdPKCαDN
NT
AdGFP
AdGFP
NT
AdPKCαDN
B
6 mos
26 mos
PKCα
PKCδ
PKCε
NT
AdPKCα
AdPKCαDN
NT
AdPKCα
AdPKCαDN
C
PKCαDN
gene transfer
PKCαDN / Ag
ratio
6 mos (n=4)
≥26 mos (n=8)
PKCα or αDN
/ Ag ratio
NT (n=8)
PKCα (n=8)
PKCαDN (n=12)
D
Sarcomere
Length (μm)
Peak
Amplitude (μm)
Shortening
Rate (μm/s)
Re-lengthening
Rate (μm/s)
6-18 mos
≥26 mos
NT (n=97, 91)
PKCα (n=50, 106)
PKCαDN (n=88, 100)
E
6 mos
26 mos
PKCα
p-PLB
PLB
Ag stain
NT
AdPKCα
AdPKCαDN
NT
AdPKCα
AdPKCαDN
PKCαDN
gene transfer
p-PLB/PLB
ratio
6-18 mos (n=4)
≥26 mos (n=3)
F
6 mos
26 mos
34 mos
pS23/24
pS45
TnI
NT
AdGFP
AdPKCαDN
NT
AdGFP
AdPKCαDN
NT
AdGFP
AdPKCαDN

Figure 2.5 PKC expression, contractile function, and phosphorylation in young and aging F344 x Brown Norway rats after gene transfer. A. Representative Western detecting PKCα in NT cardiomyocytes and after AdGFP gene transfer along with PKCαDN after AdPKCαDN gene transfer in cardiomyocytes from 6 and 26 mos old rats. A portion of Ag-stained gel also is included as a loading control. **B.** Representative Westerns showing gene transfer of AdPKCα or AdPKCαDN increases PKCα or PKCαDN expression, respectively, compared to NT cardiomyocytes. These representative blots also illustrate that gene transfer produces similar increases in PKCαDN expression in 6 (left panel) versus 26 (right panel) mos old rat cardiomyocytes. As shown here and in panel E, the levels of PKCα expression after gene transfer of AdPKCα also were similar in 6 and >26 mos old cardiomyocytes. These Westerns also were re-probed for PKCδ and ε expression in 6 and ≥26 mos old cardiomyocytes. **C.** Quantitative analysis of PKCαDN/PKCα protein expression after gene transfer. In the left panel, PKCαDN protein expression after gene transfer is normalized to an Ag-stained gel band from young (6 mos) and older (≥26 mos) samples. Results are expressed as mean+SEM, and n= number of rat hearts in panels B and **D**. PKCαDN expression is similar in cardiomyocytes from the 2 age groups when compared using an unpaired Student's t-test ($p>0.05$). Gene transfer also produced similar increases in PKCα expression in cardiomyocytes from 6 and ≥26 mos old rats (results not shown). Thus, expression in the 2 age groups were pooled to quantitatively compare the level of PKCα versus PKCαDN expression levels after gene transfer and relative to NT cardiomyocytes (NT) using 1-way ANOVA and post-hoc Dunnett's tests (*$p<0.05$ versus NT; right panel). This comparison shows gene transfer results in comparable increases in PKCα and PKCαDN expression in adult cardiomyocytes. **D.** Sarcomere length, peak shortening amplitude, and the rates of shortening and re-lengthening in NT cardiomyocytes and after gene transfer of AdPKCα or AdPKCαDN for 6-18 versus ≥26 mos old rats (n= number of cardiomyocytes). A 2-way ANOVA (PKC, age) and post-hoc Tukey's tests was used for the statistical comparison (*$p<0.05$ versus NT for PKC effect; ◆ $p<0.05$ versus 6-18 mos old cardiomyocytes for age effect). **E.** Representative Western analysis of PKCα, p-PLB, and PLB expression plus an Ag-stained portion of the gel in 6 and 26 mos old rat cardiomyocytes after AdPKCα, AdPKCαDN gene transfer compared to NT cardiomyocytes (left, middle panel). Quantitative analysis of p-PLB/PLB ratio in 6-18 versus ≥26 old rat cardiomyocytes (right panel) after PKCαDN gene transfer is compared using a Student's unpaired t-test ($p>0.05$; right panel). **F.** Representative Westerns show cTnI p-S23/24, p-S45, and total cTnI expression in 6, 26 and 34 mos old rat cardiomyocytes after AdGFP or AdPKCαDN gene transfer compared to time-matched NT cardiomyocytes.

Supplementary Figures

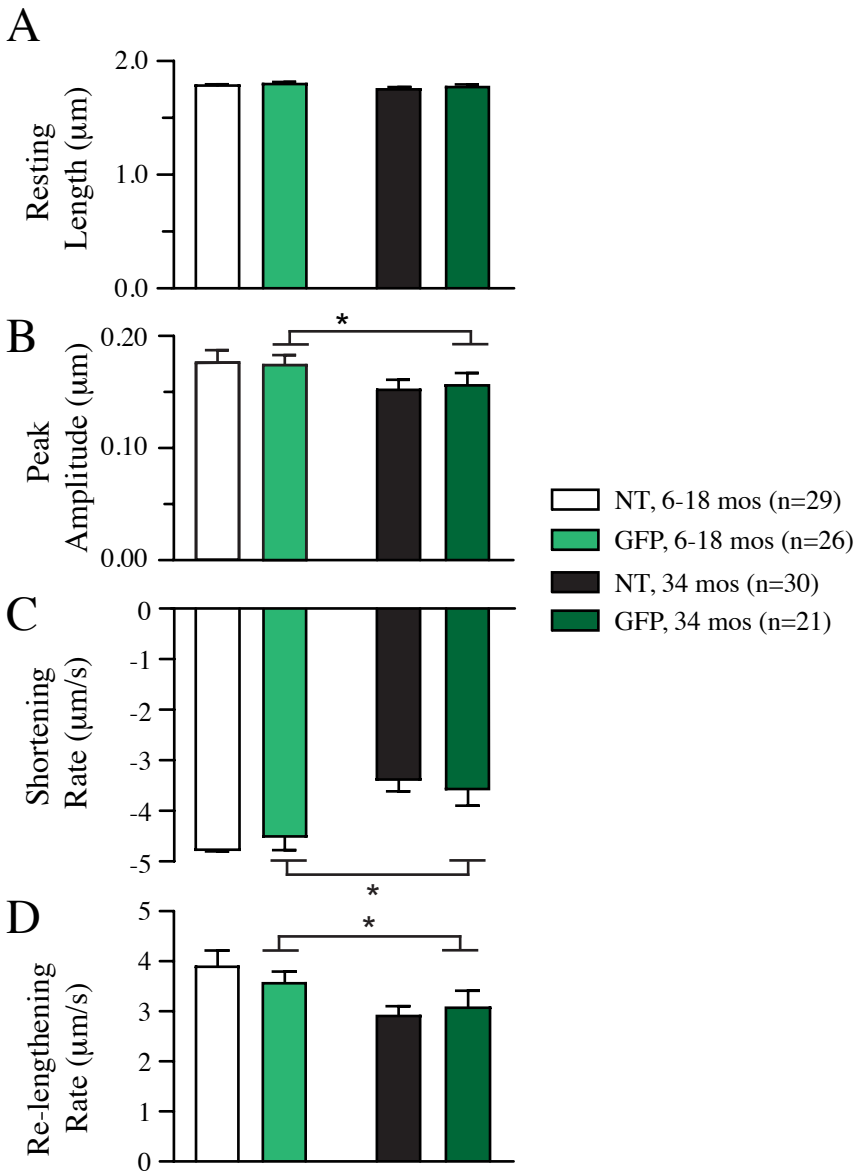

Supplemental Figure 2.1 Analysis of contractile function in non-treated (NT) and GFP-treated cardiomyocytes. Comparison of (**A**) resting sarcomere length, (**B**) peak shortening amplitude, plus shortening and re-lengthening rates (**C, D**) in NT and GFP- treated cardiomyocytes isolated from 6-18 and 34 mos old rats. Results are expressed as mean+SEM (n = number of cardiomyocytes from >2 rats) compared using a 2-way ANOVA with statistical significance set at $p<0.05$ (* indicates significant age-related changes). There were no significant changes due to GFP treatment or interaction effects.

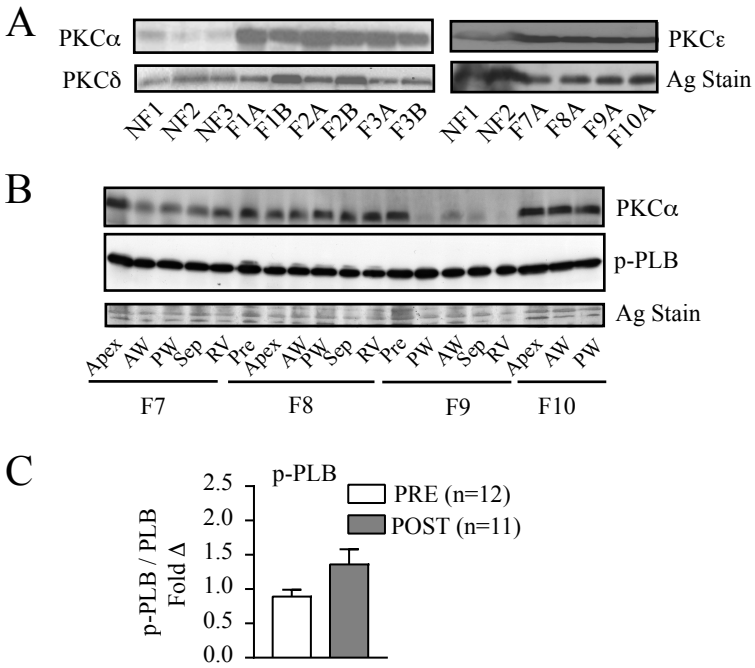

Supplemental Figure 2.2 PKC isoform and p-PLB expression in human myocardium.

A. Representative PKCα, δ, and ε isoform expression in NF and F human myocardium collected before (A) and after (B) VAD therapy. **B.** Representative Western analysis of regional PKCα and S16 phosphorylated PLB (p-PLB) and a section of Ag stained gel to indicate protein loading in F human heart tissue. Samples collected from the apex before VAD are labelled pre, while samples collected at the time of transplantation include the apex, anterior wall (AW), posterior wall (PW), septum, and right ventricle (RV). The F8 and F9 samples also include pre-VAD samples for comparison to regional post-VAD expression. **C.** Quantitative analysis of the p-PLB/PLB ratio in pre- and post-VAD myocardium to compare the impact of VAD on another downstream target for PKCα, which is known to activate protein phosphatase I and reduce p-PLB/PLB ratios (n=number of hearts). The trend for improvement in the p-PLB/PLB ratio after VAD support did not reach statistical significance using a Student's t-test (p=0.058).

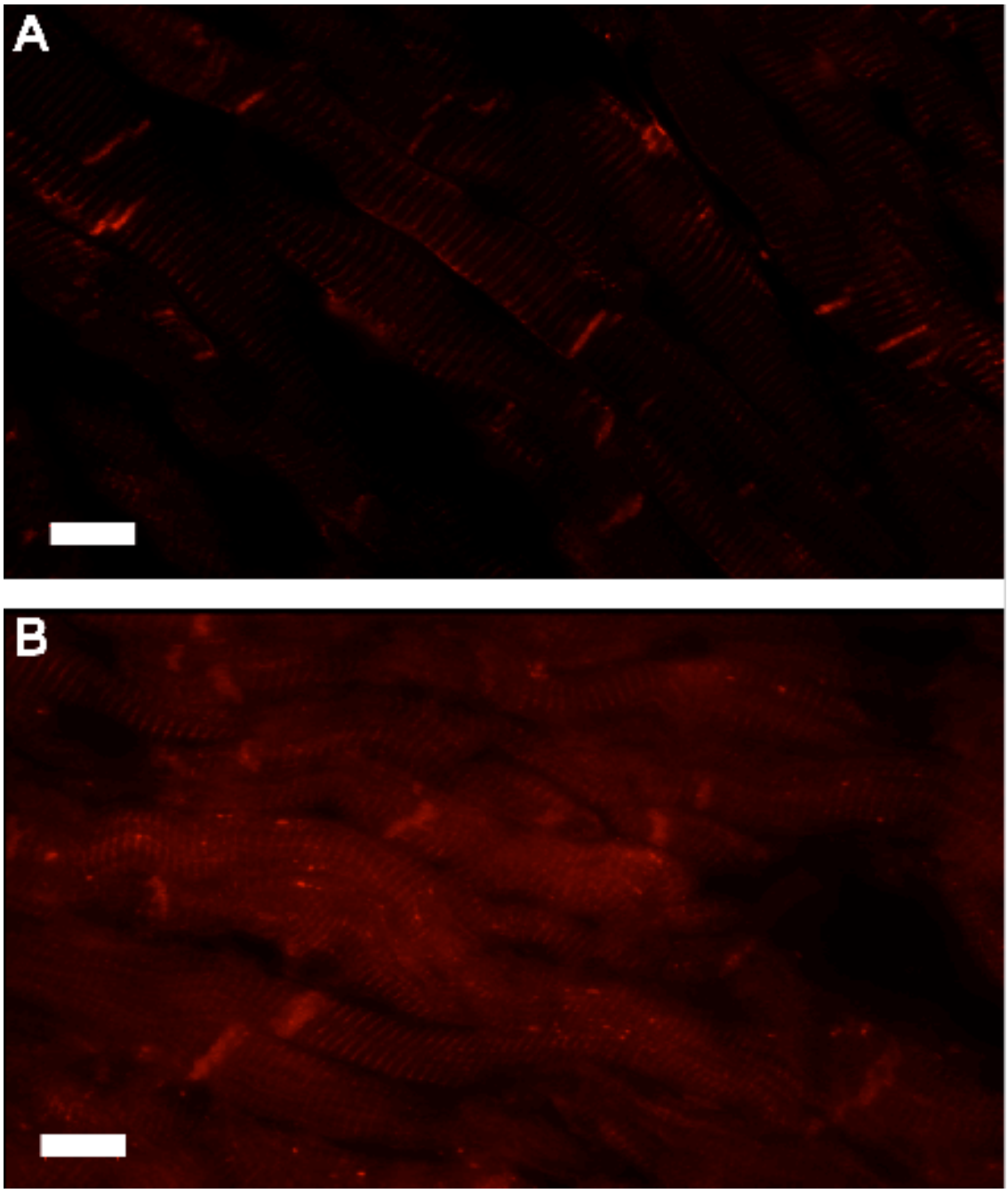

Supplemental Figure 2.3 Enlarged immunohistochemical stained images for PKCα in cryosections from sham and pressure overload-treated rats. Smaller, lower resolution images are shown in Figure 2.3B. **A.** Enlarged image #1 from sham rat myocardium shows strong localization of PKCα in the intercalated disc and a less intense striated distribution. B. Enlarged image #4 is from pressure overload-treated rats. A wider band of PKCα is detected in the intercalated disc and there is a more intense staining of striations. Scale bar = 10 μm in each image.

Group	Total n	Diagnosis	Time from Diagnosis to VAD (years)	Duration of VAD support (Days)	Gender	Age	EF
F	21	I: n=3 NI: n=18	2.5 ± 0.8	135 ± 29	16M, 5F	41 ± 3	12 ± 1
NF	3	--	--	--	1M, 2F	57 ± 6	58 ± 1

Supplemental Table 2.1Failing (F) and Non-failing (NF) Human Heart Composite Data I = ischemic; NI = non-ischemic; All F patients were treated with beta-blockers and/or angiotensin converting enzyme inhibitors.

	0.2 Hz			2 Hz		
Group	Resting SL (μm)	Peak shortening (μm)	n	Resting SL (μm)	Peak shortening (μm)	n
F-pre VAD	1.769±0.035	0.053±0.012	12	1.732±0.026	0.033±0.007	11
F-post VAD	1.766±0.021	0.058±0.008	24	1.747±0.029	0.054±0.009	13

Supplemental Table 2.2 Resting sarcomere length and the peak shortening amplitude in cardiomyocytes from F-pre-VAD and F-post-VAD myocardium stimulated at 0.2 and 2 Hz.

Chapter 3

Mouse Cardiomyocyte Isolation and Gene Transfer

Vani S. Ravichandran and Margaret V. Westfall

Abstract

Viral-mediated gene transfer is efficient for introducing exogenous cDNA into terminally differentiated primary cell cultures, such as adult cardiomyocytes. Vector-based strategies overcome the often toxic and inefficient transfer of DNA produced by traditional techniques. In our work, viral gene transfer into adult cardiomyocytes has provided important insights into myofilament modulation of the cardiac contractile response. This chapter provides detailed protocols for mouse cardiomyocyte isolation, recombinant adenoviral gene transfer, and cell culture. These techniques enable the study of contractile function after gene transfer, as vector-based expression of the exogenous protein replaces endogenous contractile proteins.

Introduction

Introduction of cDNA into primary cell culture is often necessary for identifying the structural and/or functional role of a protein [181]. Genetic models and gene transfer approaches are essential for understanding cardiac pump performance. While amenable to typical transfection approaches for gene transfer such as lipofectamine, immortalized cells lines such as HL-1 or inducible pluripotent stem cells (iPSCs) differentiated into cardiac cells do not fully recapitulate adult cardiomyocyte architecture and contractile performance, primarily because of isoform transitions in key contractile proteins are not completed during cardiac muscle cell maturation in these cells [182, 183]. Primary cell culture in terminally differentiated adult cardiomyocytes is a powerful tool to bridge the gap between biochemical/molecular experiments, and provide insight into the complexity of cardiac performance in animal models [181, 184, 185]. Therefore, isolated adult cardiomyocytes are a beneficial model for investigating cardiomyocyte contractile function.

Work in adult cardiomyocytes has contributed to our understanding of Ca^{2+} handling, kinetics and mechanics of contraction, and changes that occur in subcellular organelles during development and with disease pathology [91, 184, 186-188]. Studies in adult cardiomyocytes are efficient and cost-effective for achieving protein expression, as well as studying short-term responses to stress or drug treatments [91, 109, 184, 186, 188]. In contrast to immortalized cell lines, conventional transfection methods are often toxic to adult cardiomyocytes [188, 189]. Other methods, such as poly-L-orinthine, have proven to be less toxic but are inefficient and produce inadequate protein expression [188]. Recombinant virus is an alternative approach for efficient and non-toxic gene transfer into cardiomyocytes.

Many types of viruses are used for gene transfer, including integrative and non-integrative vectors [188-194]. Single-stranded vectors integrate into the host genome and result in germline transmission [190, 191, 195, 196]. While integration is stochastic, lentiviral constructs can be effective in various cell types and can produce persistent global or tissue-specific transgene expression [197-200]. Efficient, long-term expression is also achieved with adeno-associated virus (AAV), which contains single-stranded DNA and is more commonly used for gene therapy [201]. Part of the AAV genome integrates on chromosome 19 and as episomal genomes. Recombinant AAV vectors can also be constructed to target specific genes via homologous recombination [202, 203]. However, protein production for both lentiviral and AAV vector-mediated gene transfer is preceded by a latent or lag phase due to viral integration [201, 204]. This latency can be disadvantageous in short-term cellular studies. Thus, the specific characteristics of each vector are important to consider for optimal *in* vivo and *in vitro* studies. Studies with isolated adult cardiomyocytes are typically performed within a week of isolation, as these cells are cultured in serum-free media to maintain their rod-shaped morphology.

Adenovirus is an ideal vector for cellular studies because it produces rapid, efficient gene expression in a variety of cell types, including the adult cardiomyocyte. Gene transfer using the adenovirus has provided substantial insight into cardiac cellular function, including myofilament function. Importantly, adenoviral gene transfer does not independently affect sarcomere stoichiometry, myofilament integrity, or contractile function, thus serving as a reliable tool to study contractile performance [31, 35, 184, 188, 205-208].

This chapter delineates how to isolate, plate, and culture Ca^{2+}-tolerant, adult mouse cardiomyocytes in serum-free medium. The chapter additionally provides details on adenoviral

gene transfer methodology in adult cardiomyocytes. The protocol was adapted from a previously-established protocol for rat cardiomyocyte isolation [209, 210].

Materials

All solutions should be prepared with purified, deionized water (dH_2O; 18Ω).

2.1 Reagents and materials for rodent anesthesia and adult cardiomyocyte isolation

1. Perfusion setup: A Baker apparatus (Harvard "Baker" perfusion set #50-8382) with a double-barrel warming coil and an upper changeover stopcock is used to regulate flow from two 50-mL syringes containing perfusion buffers (syringe #1: Cardiomyocyte Buffer in Subheading 2.1, #22; syringe #2: Collagenase Solution, Subheading 2.1, #23), which are attached to the coils via Tygon tubing. The syringes are positioned 70 cm above the bottom of the Baker apparatus. A second set of tubing is attached above the warming coils with the opened ends extending to the same height as the syringes, serving as bubble traps. Two additional pieces of tubing are connected to the bottom of each coil and capped with stopcocks on one end. Stopcocks are only opened to remove bubbles and drain buffers prior to cell isolation. A piece of tubing also is inserted into the bottom of the Baker apparatus warming chamber and connected via a stopcock to perfuse the cannulated heart. Finally, the coils of the Baker apparatus are warmed via tubing from a circulating water bath to maintain the temperature of the perfused heart at 37°C. A piece of PE-20 tubing connected to Tygon tubing is used to re-circulate the effluent from the heart using a peristaltic pump when the heart is perfused by syringe #2 during the digestion phase of the perfusion (see subheading 3.1.1, step 4).
2. The sterile surgical tools for this procedure include: One pair each of Mayo-Stille scissors, curved Halsted-Mosquito hemostats (Fine Science Tools or FST 13009-

12), standard pattern forceps, curved scissors (FST14091-09), fine Iris scissors (FST14060-10), and two pairs of Dumont #3 forceps. Tools are autoclaved before use and sterility should be maintained during the cell isolation procedure.

3. A 1.25 mm, 22-gauge straight gavage needle (Cadence Scientific #7901) also is sterilized with the surgical tools.
4. Size 3 braided, non-absorbable silk suture is cut into ~2-3 centimeter lengths and each length loosely tied in a surgical knot.
5. The following beakers are needed to prepare stock solutions and buffers in steps 7-24 below: 12 x 1L, 1 x 250 mL, 1 x 100 mL, 1 x 50 mL. The following sterile bottles are needed to store stock solutions and reagents: 12 x 1L, 1 x 250 mL, 1 x 100 mL. Three additional sterile 50 mL conical tubes also are needed.
6. Two silanized trituration pipets (one large and one smaller bore) are prepared by marking a Pasteur pipet with a diamond knife, cleanly breaking the step, and fire polishing the glass prior to the first use. Pipets are first washed in 7x soap, rinsed thoroughly with distilled water, silanized in Sigmacote and air dried. Pipets are autoclaved before each use.
7. 3-4 L sterile (autoclaved) distilled water (dH_2O) stored in 1 L bottles.
8. Heparin Sodium (1000 USP units/mL) for injection.
9. Nembutal: Pentobarbital sodium (50 mg/mL).
10. 0.9% saline (NaCl): dissolve 0.45 g NaCl in 50 mL dH_2O and filter sterilize into a 50 mL conical tube. (see note 1)
11. 70% ethyl alcohol: Dilute 700 mL ethyl alcohol (200 proof) to a final volume of 1 L in dH_2O.

12. 1 M NaCl: Dissolve 58.44 g NaCl in a final volume of 1 L dH_2O.
13. 0.5 M KCl: Dissolve 37.27g KCl in a final volume of 1 L dH_2O.
14. 0.5 M KH_2PO_4: Dissolve 68.05 g KH_2PO_4 in a final volume of 1 L dH_2O.
15. 0.5 M NaH_2PO_4: Dissolve 59.98 g NaH_2PO_4 in a final volume of 1 L dH_2O.
16. 0.1 M $MgSO_4*7H_2O$: Dissolve 24.65 g $MgSO_4*7H_2O$ in a final volume of 1 L dH_2O.
17. 0.10 M $CaCl_2*2H_2O$: Dissolve 14.70 g $CaCl_2*2H_2O$ in a final volume of 1 L dH_2O.
18. Collagenase, Type 2: 254 U/mg; Store lyophilized collagenase in a sealed and desiccated container at 4°C.
19. DNAse I grade 2 (Sigma 104159 powder); store dessicated at -20°C.
20. Protease XIV (Sigma P5147); store dessicated at -20°C.
21. Fraction V, Fatty Acid-free Bovine Serum Albumin (Roche 0311705700): Store lyophilized powder at 4°C.
22. Cardiomyocyte Buffer: Prepare 1 L of buffer with the following final concentrations using the stock solutions listed above (see Subheading 2.1, #12-16 and note 1).
    - 113 mM NaCl
    - 4.7 mM KCl
    - 1.2 mM $MgSO_4*7H_2O$
    - 0.6 mM KH_2PO_4
    - 0.6 mM NaH_2PO_4

Add the following reagents:

- 10 mM HEPES (Sigma H7006; MW 260.29 g/mol)
- 10 mM Butanedione Monoxime (Sigma B0753; MW 101.10 g/mol)
- 1.6 mM $NaHCO_3$ (Sigma S8875;MW 84.01 g/mol)
- 30 mM Taurine (Sigma T8691; 125.15 g/mol)
- 20 mM D-(+)-Glucose (Sigma G7528; MW 180.16 g/mol)

Bring the cardiomyocyte buffer to a final pH of 7.4 with HCl, and filter-sterilize. See note 1.

23. Collagenase Solution: Combine reagents from #18-21 in a final volume of 75 ml cardiomyocyte buffer (Subheading 2.1, #22) and filter-sterilize into a sterile 100mL bottle. The final concentrations of each components are: Collagenase, 436U/mL; DNAse I grade 2, 0.015 mg/mL; Protease XIV, 0.104 U/mL.
24. Collagenase Stopping Buffer: Add $CaCl_2$ (final concentration = 0.1 mM; subheading 2.1 #17) and BSA (final concentration = 25 mg/ ml; subheading 2.1, #21) to 30 mL aliquot of cardiomyocyte buffer (pH 7.4; subheading 2.1 #22). Filter sterilize in a 50 mL conical tube. See note 2.

2.2 Reagents and materials for gene transfer – all reagents should be filter-sterilized and warmed to 37°C before use. Reagents can be stored at 4°C as long as they remain uncontaminated.

1. Culture plates: Sterile Falcon 6 well (Corning #353046)

2. 2 Culture dishes: 100 mm culture dish (Fisher FB0875713). Sylgard is placed and cured in the center of one culture dish in a bowl shape to keep the heart in place during cannulation.
3. Glass coverslips: Glass coverslips 22 x 22mm (Fisher 12-542-B).
4. Two 15 mL sterile conical tubes and a sterile 15 mL beaker.
5. Laminin: Laminin (Invitrogen 23017-5) is thawed on ice, diluted to 40 μg/mL in 1X phosphate buffer saline (PBS), aliquoted into one-use prechilled microfuge tubes, and stored at -80°C. The microfuge tubes with diluted laminin are thawed on ice just prior to coating coverslips.
6. Minimum Essential Medium (MEM 11575-032)
7. Insulin Transferrin Selenium (ITS; Gibco 51500-056); 0.55 μg/mL.
8. 50 U/mL Penicillin + 50 μg/mL Streptomycin (P/S; Gibco 15070-063): Store in 5 mL, 1 use aliquots at -20°C.
9. 1 M HEPES (Gibco 1563008); store at 4°C.
10. S-(-)-Blebbistatin (Toronto Research Chemicals, B592500): Blebbistatin is prepared as a 100 mM stock in DMSO (Sigma D2650) See note 3. This stock solution is diluted to 10 mM in DMSO just before use.
11. Fetal Bovine Serum (FBS; Atlanta Biologicals, S11550)
12. M199 culture media (Sigma M3769): Mix 10 g M199 with 3.073 g L-glutathione, 200 mg BSA (subheading 2.1, #21), 2.2 g NaH_2CO_3, and 2.6 g HEPES buffer. Adjust the pH to 7.4 (NaOH), bring volume to 1 L and filter sterilize into two 500 mL sterilized bottles using Steri-top filters.

13. Basic Culture Media: Combine 150 mL MEM (subheading 2.2, #6) with reagents #7-9 (subheading 2.2) to achieve a final concentration of 0.5 ng/mL ITS, 0.5 U/ml and 0.5 μg/ml P/S, plus 10 mM HEPES. Add 0.2% BSA (subheading 2.1 #21), mix thoroughly and filter-sterilize using a 250 mL Steri-top filter.

14. Culture Media: Add blebbistatin (subheading 2.2, #10) at a final concentration of 25 μM to basal culture media (subheading 2.2, #13). Filter-sterilize in 250 mL bottle with Steri-top filter.

15. Plating Media: Prepare 5% FBS culture media by combining 45 ml basal culture media (subheading 2.2, #13) with 5 ml thawed FBS (subheading 2.2, #11). Filter sterilize in a 50 mL conical tube with Steri-top filter. See note 4.

Methods

3.1 Isolation of cardiomyocytes from adult mouse hearts

3.1.1 Preparation for cardiomyocyte isolation

1. All "open" tubing on the Baker apparatus should be covered tightly with Parafilm between each cell isolation. Just prior to each isolation, remove Parafilm from all openings. The perfusion apparatus should contain 70% ethyl alcohol in all tubing, syringes, and in the manifold between each isolation.
2. Heat the Baker perfusion manifold to 37^{o}C by turning on the circulating water bath. Drain the perfusion system of ethyl alcohol. Thoroughly wash the perfusion apparatus, both syringes, and all tubing with 3-4 L sterile dH_2O.
3. Add some cardiomyocyte buffer (subheading 2.1, #22) to one 50 mL syringe (syringe #1) to flush the coils using the lower and side stopcocks to ensure there are no bubbles trapped in the perfusion coils. Place an oxygenator tube in the syringe to bubble the perfusion solution with 100% O_2 during perfusion.
4. Add collagenase solution (subheading 2.1, #23) to the 2nd 50 mL syringe (syringe #2). Flush some collagenase solution through the system (syringe #2, as described in subheading 3.1.1 #3).
5. In the biosafety cabinet, transfer 1 glass coverslip into each well of the culture plate (subheading 2.2, #3 and 1, respectively).
6. Place culture plate under the UV light for 10 min to minimize contamination.
7. Fill an ice bucket to the rim with ice, put on fresh gloves and open all sterile surgical tools in autoclave bags.

8. Place two halves of a culture dish (subheading 2.2, #2) on the ice in the bucket and fill each dish halfway with cardiomyocyte buffer.
9. Fill a 10 mL syringe with cardiomyocyte buffer. Place a gavage needle (subheading 2.1, #3) on the tip of the syringe, ensuring all bubbles are removed from the syringe and gavage needle. Place two tied sutures (subheading 2.1, #4) on the stem of the needle. Ensure no bubbles are in the syringe. Angle the needle so that the tip sits just below the surface of the cardiomyocyte buffer in one half of the culture dish on ice (about 45^{o}).

3.1.2 Surgical removal of mouse heart

1. Inject an adult mouse (25-30 g) with an intraperitoneal (IP) injection of heparin (1500U/kg body weight; subheading 2.1, #8). Wait 20 minutes for adequate heparinization, and then anesthetize the animal with an injection of 150-200 mg/kg body weight Nembutal (subheading 2.1, #9) (see note 5). Prepare the collagenase solution during this time (subheading 2.1, #23, see note 6).
2. When the mouse does not respond to a foot pinch, sterilize the mouse abdomen with 70% ethanol (subheading 2.1, #11). Use Mayo-Stille scissors and standard forceps to cut open the thorax on either side and cut through the diaphragm. Clip the cut thorax away with curved Halsted Mosquito Hemostats.
3. Hold the lungs with standard forceps and use curved scissors to cut behind the lungs, keeping the thymus intact. Place the heart and all surrounding tissue in

the half of the culture dish on ice which contains cardiomyocyte buffer but no gavage needle.

4. Use standard forceps and dissection scissors to remove lung tissue from the heart.
5. Transfer the heart to the culture dish with the cardiomyocyte buffer plus the gavage needle. Keeping the heart submerged in cardiomyocyte buffer, pull apart the two lobes of the intact thymus with Dumont #3 forceps and locate the aorta. Use fine Iris scissors and Dumont #3 forceps to cut just above the ascending aorta and below the brachiocephalic artery.
6. Using Dumont #3 forceps, place the aorta on the bulbed-tip of the gavage needle without introducing bubbles into the heart or aorta. Tie the aorta in place with one of the sutures on the needle. See note 7.
7. Gently flushing the heart with cardiomyocyte buffer from the syringe. Coronary arteries should flush, and the heart will enlarge slightly while remaining attached to the gavage needle. Secure the aorta to the needle with the second suture.

3.1.3 Retrograde perfusion of the heart

1. Open the lower stopcock on the perfusion system to allow free flow of cardiomyocyte buffer from syringe #1. Gently pushing cardiomyocyte buffer through the syringe during removal of the heart, quickly transfer the heart from the syringe to perfusion system (see note 8).

2. After 4 min, place a 15 mL beaker on a wire mesh mounted to a ring stand (subheading 2.1, #5; see note 9) and position under the heart. Transfer oxygenater to syringe #2 which contains the collagenase solution.
3. After 5 additional minutes of perfusion with cardiomyocyte buffer, turn the lower stopcock to perfuse from syringe #2 containing collagenase solution.
4. After perfusing with collagenase solution for 2 min, add 0.1M $CaCl_2$ (subheading 2.1, #7) to the solution in syringe #2, to a final concentration of 50 μM, and perfuse the heart or another 8-12 minutes, or until the flow rate through the heart speeds up significantly. See note 10.
5. Close the lower stopcock and turn off the oxygenator. Remove the heart from the perfusion system and place it in sterile culture dish (subheading 2.2, #2) along with ~5 mL of collagenase buffer from syringe #2. Aliquots of 5 mL collagenase buffer are used to further digest the tissue pieces.

3.1.4 Cardiomyocyte isolation

1. Using fine iris scissors, cut heart into approximately 4 pieces.
2. Using Dumont #3 forceps, gently pull apart the tissue to liberate cells into the collagenase (See note 11).
3. Transfer the tissue-collagenase mixture to a 15 mL sterile conical tube (tube 1; subheading 2.2, #4), triturate gently with a glass-polished Pasteur pipette (see notes 12 and 13), and place in 37°C CO_2-incubator for 5 min.

4. Add 5 mL of stopping buffer (subheading 2.1, #24) to tube 1 containing tissue pieces, triturate gently, and place in the incubator for an additional 2 min or until the tissue has settled.
5. Transfer "supernatant" to 15 mL sterile conical tube (tube 2; subheading 2.2, #4) and add 10 mL of stopping buffer (subheading 2.1, #24) to remaining tissue in tube 1. Triturate tube 1 containing tissue pieces again, with the 10 mL of stopping buffer just placed the tube. Place this tube in the incubator to let tissue settle.
6. Centrifuge tube 2 at ~1000 x g for 30 seconds. Discard supernatant and replace with stopping buffer containing tissue pieces from tube 1. Gently re-suspend the cell pellet in stopping buffer.
7. Gently add 10 μL of 100 mM $CaCl_2$ (subheading 2.1, #17) 4 times in 5 minute intervals to bring final Ca^{2+} concentration to 500 μM (see note 14). Gently invert to mix. Place tube 2 in incubator during each 5-minute incubation after each Ca^{2+} addition.
8. Repeat centrifugation step (subheading 3.1.4, #6).

3.1.5 Initial cardiomyocyte culture

1. Remove supernatant from tube 2 in the biosafety cabinet. Re-suspend pellet with 2-4 mL of plating media and place in 37ºC CO_2 incubator until plated.
2. Pipet 100 μL of laminin onto glass coverslips in 6-well dish (subheading 2.2, #1; see note 10), making sure to place a small amount of laminin under the

coverslip to adhere the coverslip to the plate. Let laminin coat the glass for 10 minutes under UV light, ensuring laminin does not evaporate.

3. During laminin coating, count cells with hemocytometer. Aspirate laminin from glass coverslips and plate cells at a density of 20,000 rod-shaped cardiomyocytes per coverslip.
4. Allow cells to adhere to laminin-coated coverslips for 2 hours at 37°C in a CO_2-equilibrated incubator (see note 15).
5. After 2 hours, plated cardiomyocytes are ready for gene transfer.

3.2 Gene transfer

3.2.1 Work with recombinant adenovirus requires BL2 approval. Viral vectors should be handled in a biosafety cabinet that has been treated with 60% Lysol followed by 70% ethyl alcohol with each entry and exit from the cabinet. Personnel handling vectors should wear safety goggles, gloves, and a lab coat. The biosafety cabinet should be equipped with a vacuum system containing tandem Erlenmeyer flasks attached to a 0.1 μm approved vacuum filter. The Erlenmeyer used for direct collection of media and a 2 L beaker should have adequate amounts of 10% bleach to treat all virus for at least 20 minutes prior to discarding excess media. All plastic and glassware should also be treated with 10% bleach for 20 minutes and then disposed of in a biocontainment bag.

1. During the 2 hr adherence period discussed in step 5 of 3.1.5, dilute adenoviral stocks in sterile microfuge tubes to the desired multiplicity of

infection (MOI) with culture media (subheading 2.2, #14). Place in incubator for ~ 5 min prior to starting gene transfer step. (see note 16 and 17).

2. Aspirate media after 2-hour adherence period (see note 15)
3. Add 200 μL of adenovirus diluted in media to each well and place in incubator for 1 hour.

3.3. Mouse cardiomyocyte cultures

1. One hour after the addition of virus, add 2 mL culture media (see note 17).
2. Replace culture media after 24 hours and change media every day for up to 3 days post-gene transfer.

NOTE: While this chapter discusses adenoviral transduction of cardiomyocytes, the studies presented in this dissertation work do not use adenoviral transduction.

Notes

1. Stock solutions listed in subheading 2.1 #10-27 can be stored at room temperature for up to 1 month, while buffers in subheading 2.1 #22-24 are stored at 4ºC for up to 2 weeks.
2. Stopping buffer can be re-used provided it is filter-sterilized before each prep.
3. Blebbistatin powder should be stored at -20ºC, and a 100 mM stock made with DMSO, to use as a 1-or-2-use aliquot.
4. FBS and P/S are sterile and should only be opened and added to media in a biosafety cabinet.
5. A small volume of Nembutal (subheading 2.1, #9; <0.1 cc) can be added to the heparin (subheading 2.1, #8) syringe. For injections, bring the volume up to 0.5-1cc using 0.9% saline solution (subheading 2.1, #10).
6. This protocol is optimized for collagenase, type 2 containing 254 U/mg collagenase, lyophilized powder (Worthington lot #47D9570).
7. While cannulating, tie the aorta just past the bulb of the cannula. The heart will not be adequately perfused if the cannula is placed too deep into the aorta.
8. A flow rate of <3 mL/min is optimal for perfusion.
9. During collagenase perfusion, collect collagenase flow-through in a 15 mL beaker such that the heart is submerged. Shine a light on the beaker as well to keep the heart warm.
10. Thaw laminin on ice during Ca^{2+} addition step.
11. Cut and minced pieces of heart should come apart without resistance for optimal isolation of cardiomyocytes.
12. Do not force tissue into trituration pipet.
13. Only use p1000 tips to transfer cardiomyocytes to conical tubes.

14. Slowly add Ca^{2+} along the sides of the conical tube during each Ca^{2+} addition. Rotate the tube horizontally. Then gently invert to re-suspend the cell pellet.
15. Leaving cardiomyocytes in serum-containing media for >2.5 hours can lead to cardiomyocyte de-differentiation [184, 188].
16. This gene transfer protocol is optimized for high-titer recombinant adenovirus. High titer preparations contain ~1 x 10^{12} viral particles/mL and 10^{10} plaque forming units (pfu)/mL of virus. Prior to gene transfer, virus is diluted to a specific multiplicity of infection (MOI) or pfu/cardiomyocyte. For sarcomeric proteins, 200 MOI is sufficient for replacement using adenoviral-mediated gene transfer driven by a mouse cytomegalovirus (CMV) promoter[116, 184, 188]. For recombinant adenoviral-mediated gene transfer of non-sarcomeric proteins, 10 MOI achieves $\geq$80% cardiomyocyte transduction [152]. Control cells are incubated with the same volume of culture media (subheading 2.2, #14) in the absence of virus during the gene transfer step.

Viral aliquots are stored at -80^{o} C and thawed on ice prior to dilution. Single-use aliquots of the virus are recommended, as multiple freeze-thaw cycles reduce the number of pfu/m.

Chapter 4

Phospho-mimetic cTnI S43/45D Causes Cardiac Dysfunction and Heart Failure in Mice via Early Mitochondrial Dysfunction

Vani S. Ravichandran, Tabea M. Schatz, Emily A. Lavey, Scott Soleimanpour, Margaret V. Westfall

Abstract

Cardiac dysfunction leads to heart failure (HF), a leading cause of death in the United States. Elevated protein kinase C (PKC) activity and downstream phosphorylation of the thin filament switch protein, cardiac troponin I (cTnI) at S43/45 (p-S43/45) are linked with cardiac dysfunction in animal models and human HF, but it is not known if chronic p-S43/45 causes HF. Transgenic mice with phospho-mimetic cTnIS43/45D (cTnISD) replacement of endogenous cTnI in the thin filament were generated to test whether cTnI S43/45 modification alone produces chronic, dose-dependent and progressive *in vivo* cardiac dysfunction and end-stage heart failure. Mice were categorized into high (HE-), moderate (ME-), and low (LE-) expressing cTnISD (SD) based on cTnI protein expression in each mouse line using tandem mass spectroscopy (MS/MS) with established AQUA peptides. Cardiac dysfunction developed within 2 mos in the HE-SD line, followed by 100% mortality by 4 mos of age. The ME-SD line also developed a moderate, sustained dysfunction by 2 mos, but only progressed to end-stage HF on or after 1 year of age. These findings suggest chronic cTnISD not only causes direct cardiac

dysfunction, but also initiates progressive structural and functional remodeling to produce end-stage HF. The results additionally suggest that the level of phosphorylation of cTnI S43/45 directly correlates to the temporal development of HF. Further studies to gain mechanistic insight into the progressive HF in this model tested the idea that early sarcomere communication with mitochondria significantly contributes to progressive cardiac dysfunction. Detailed analysis of mitochondrial alterations in 2-3 mos old ME-SD mice prior to the development of extensive and irreversible cardiac remodeling demonstrate an early onset of increased oxidative stress, along with alterations in mitochondrial structure and function. A second generation derivative of elamipritide, which targets mitochondrial cardiolipin to reduce oxidative stress, improved contractile function in cardiomyocytes from ME-SD mice. Collectively, this work supports the conclusion that chronic cTnI phosphorylation by PKC induces *early* mitochondrial dysfunction which may drive the progressive structural and functional deterioration that leads to end-stage HF.

Introduction

Cardiac dysfunction and the progression to heart failure (HF) is a leading cause of death in the United States affecting >6 million Americans annually [88]. HF is defined by dysfunction in the filling and/or ejection of blood by the heart. In response to the initial cardiac dysfunction, there can also be maladaptive changes in heart structure and function which lead to further progressive dysfunction. These changes include cellular and molecular alterations such as extracellular matrix alterations, apoptosis, abnormal Ca^{2+} handling and myocyte hypertrophy. In turn, these alterations lead to organ level fibrosis, abnormal electrical conduction, myocardial infarction, and cardiac remodeling. However, HF is ultimately defined by abnormal pump function, and the myofilaments are directly responsible for pump function [211]. The sarcomere (the functional unit of contractile machinery) is comprised of thick and thin filaments organized to produce contractile function. Specifically, thick filament myosin binds to thin filament actin to induce thin filament sliding during contraction or systole, while myosin and actin dissociate during relaxation, or diastole. The heterotrimeric cardiac troponin (cTn) complex, comprised of Ca^{2+}-binding cardiac troponin C (cTnC), tropomyosin-binding cardiac troponin T (cTnT), and inhibitory cardiac troponin I (cTnI), is critical for regulating this cycle of contraction and relaxation. Among the Tn subunits, cTnI plays a key role in regulating contractile function by acting as a molecular switch. In the absence of Ca^{2+}, cTnI strongly associates with actin to inhibit the interaction between myosin and actin. The release of sarcoplasmic reticulum (SR) Ca^{2+} increases cytosolic Ca^{2+} which binds to cTnC, causing cTnI to dissociate from actin and interact more strongly with cTnC. This initiates thin filament conformational changes so the myosin crossbridge can form a strong-force generating interaction with actin [212].

Post-translational modification (PTMs) within the cTn complex modulates systole and diastole, and therefore, cardiac performance. Within cTnI, the most well-characterized PTM is phosphorylation at S23/24. This cluster is typically phosphorylated by protein kinase A during the sympathetic response, and improves heart performance by accelerating relaxation [64, 213]. During HF, PKA-phosphorylation of cTnI is reduced, in large part due to a reduction in β-adrenergic signaling and receptor abundance [172, 174, 214-216]. Conversely, a related AGC kinase, protein kinase C (PKC) is often associated with decreased cardiac function [68, 90]. PKC also targets cTnI, and can phosphorylate multiple residues, including cTnI S43/45 (p-S43/45). The p-S43/45 cluster is important because its level of phosphorylation along with PKC activity are elevated in human end-stage HF [69]. The S43/45 cluster reduces contractile function when tested *in vitro* at the cellular and myofilament level [3-5], but the *in vivo* impact of p-S43/45 has only been studied in combination with other PKC-targeted sites on cTnI, namely S23/24 and T144. As a result, the *in vivo* impact of p-S43/45 alone on cardiac function is unclear [66, 111, 112].

Transgenic (tg) animal models are a useful tool in the study of sarcomere phosphorylation because sarcomere transgenesis results in *replacement* rather than in overexpression of exogenous protein[109]. This characteristic of the sarcomere enables the study of different physiological levels of phosphorylation using phospho-mimetic substitutions. However, to date, no group has taken advantage of this unique tool to investigate p-S43/45 alone. Prior studies showed that 100% replacement with phospho-mimetic cTnI S23/24D, S43/45D and T144D caused decreased Ca^{2+} sensitivity in myofilaments, but only modestly reduced *in vivo* contraction rates measured as dP/dt [66]. In contrast, mice with 23% replacement of endogenous cTnI by S23A/24D along with S43/45D developed significant slowing of both *in vivo*

contraction *and* relaxation [111]. Finally, in mice expressing 7% replacement with an alternative phospho-mimetic substitution, glutamic acid (E) at S43/45 and T144, developed reduced *in vivo* peak pressure, plus slowed contraction and relaxation rates [112].

A few interesting questions arise based on these earlier studies: 1) What is the role of S43/45 phosphorylation in modulating *in vivo* cardiac performance? 2) Does increasing replacement of endogenous cTnI with phospho-mimetic cTnI accentuate the cardiac response and/or phenotype? and 3) How do cardiac dysfunction and remodeling progress over time? The work presented here examines the *in vivo* effect of chronic cTnI p-S43/45 on myocyte and cardiac function and remodeling. Here, our lab examines the *in vivo* time- and dose-dependent cardiac structure and function in tg C57B6J mice expressing a range of phospho-mimetic cTnIS43/45D (cTnISD) replacement. Results from these mice show that chronic cTnISD replacement causes time- and dose-dependent *in vivo* cardiac, cellular, and myofilament dysfunction and remodeling. Mutations in sarcomere proteins also can cause cardiac dysfunction [217] but because of the complex etiology of HF, the mechanism(s) responsible for progression of the disease are not well understood. Due to the close proximity of the sarcomere to the mitochondria, and the heavy reliance of the sarcomere on mitochondrial ATP [124], studies presented here test the idea that the sarcomere communicates with mitochondria early following the onset of chronic cardiac dysfunction. Specifically, early accumulation of oxidative stress results in mitochondrial dysfunction to lay the foundation for progressive cardiac dysfunction. While mitochondrial dysfunction is well-documented in end-stage HF, so far, it has not been given mechanistic credit for early disease progression initiated by alterations within the sarcomere [125]. The idea that mitochondrial dysfunction occurs as an early event in the

progression of sarcomere-induced HF also suggests novel therapeutics targeting mitochondrial dysfunction could attenuate or delay early progressive contractile dysfunction.

Methods

Animals

Transgenic mouse development. Aspartic acid (D) substitutions at S43 and S45 were made in rat cardiac cTnI-encoding cDNA in a pGEM3Z plasmid, as described previously [116, 184, 218]. After subcloning into the SalI site of plasmid pSp72, the cDNA for cTnIS43/45D (SD) was then cloned into the SalI site of a custom vector containing the minimal promoter for the cardiac-specific α-myosin heavy chain (α-MHC) and human growth hormone (hGH) signaling sequence (vector provided courtesy of Jeff Robbins [219]). After nucleotide sequencing, the vector was digested with NotI and purified in preparation for injection into C57Bl/6J x SJL F2 mouse eggs and then implanted into pseudo-pregnant females. Founder mice and subsequent generations of each line were verified by PCR with custom primers (Geno2; Table 4.1) and backcrossed onto a C57BL/6 background for at least 10 generations to confer ≥98% C57BL6/J background. Copy number for each line was determined by southern blot analysis using Not-1 digested cDNA labeled with ^{32}P-dCTP using the Rediprime II random prime labeling system (Amersham) as a primer. Southern analysis showed <2 integration sites/line (results not shown) with ~35 copies for high (HE-), ~15 copies for moderate (ME-) and ~5 copies for low (LE-) SD lines. Copy number was verified by quantitative PCR (qPCR; [220]) analysis of purified cardiac DNA collected from each mouse line using a StepOne Plus real time PCR and custom Taqman primers (cTnI1Q; Table 4.1) along with the Taqman TFRC copy number reference primer set (Table 4.1).

In vivo studies

Animal handling protocols and procedures were done in accordance with institutional guidelines and were approved by the University Committee on the Use and Care of Animals at the University of Michigan.

Analysis of cardiac function. In vivo echocardiography was performed in collaboration with the University of Michigan's Physiology Phenotyping Core. Mice were anesthetized and maintained with isoflurane throughout imaging. Echocardiography analysis included M-mode, B-mode, pulse-wave and tissue Doppler analysis of dimensions and function in mice between 1 and 12 mos of age.

Analysis of cardiac morphology. Heart weight-to-body weight and heart weight-to-tibia length were collected from mice for organ level evidence of cardiac hypertrophy [221]. Lungs were also excised from tg mice and ntg littermates and dried in a 55^{o}C oven. Wet-to-dry lung weights were used as a measure of pulmonary congestion in mice [222].

In vitro tissue and cardiomyocyte studies

Structural analysis: Histology. Hearts from 1 and 4 mos old mouse hearts were fixed in formaldehyde, paraffin embedded and sectioned (4-5μm). These coronal sections were stained by hematoxylin & eosin (H&E) or picrosirius red (PR) to detect cardiomyocyte disarray and fibrosis, respectively [223, 224].

Cell isolation. The detailed cell isolation protocol used for *in vitro* structural and functional studies on cardiomyocytes is described in detail in chapter 3.

Structural analysis: Cell morphology. Rod-shaped cardiomyocytes from 1, 2, and 3 mos old mice [91] were diluted to 10,000 cardiomyocytes/ml in stopping buffer, transferred to coverslips, and the length-to-width aspect ratios were measured using a Nikon Eclipse Ti-S Phase Contrast microscope. Dimensions were determined using an Imaging Source 0.3 megapixel CCD camera and a pre-calibrated IC Measure software. Measurements were made on 30 representative cells (~10 cardiomyocytes/coverslip and 3 coverslips/heart) from 6 separate mice in each age group within a line. These cellular measurements are used as a metric for concentric versus eccentric hypertrophy in cardiomyocytes.

Analysis of cardiomyocyte contractile function and Ca^{2+} transients. Isolated intact cardiomyocytes were cultured overnight on laminin-coated coverslips in blebbistatin-containing MEM media (see chapter 3). Coverslips were transferred to a custom cell chamber and perfused with M199 buffer supplemented with 10mM glutathione, 2% BSA, 20mM HEPES and 26mM $NaHCO_3$, and paced at 0.5 Hz at 37^{o}C on an Ionoptix platform [5]. Signal-averaged traces were analyzed for resting sarcomere length (SL), peak shortening amplitude, and rates of shortening and re-lengthening, and time 50% re-lengthening as described earlier [5]. For assays with CTP-03, cardiomyocytes were incubated in blebbistatin-supplemented MEM media plus 10μM CTP-03 overnight at 37^{o}C. CTP-03 was present in media and throughout the cell function experiments. In separate coverslips, basal Ca^{2+} transients were measured in cardiomyocytes after

loading with 5 μM Fura-2AM, and perfusion of cardiomyocytes at 37°C in the same cell chamber used for cell shortening experiments [4]. Basal and peak Ca^{2+} ratios were determined from signal-averaged traces [5].

In vitro subcellular and molecular structure analysis

Myofilament replacement with cTnISD. Replacement of endogenous wildtype cTnI with cTnISD was determined in myofibrils isolated from each mouse line and compared to non-transgenic (ntg) littermates [69]. For these studies, a 50 μg aliquot of myofilament proteins was separated on 12% SDS-polyacrylamide gels (PAGE), and stained with Coomassie blue to observe individual myofilament protein bands [225]. The band just below 25 kDa was cut from each lane, extracted and trypsin-digested prior to separation by nano-liquid chromatography (nLC). Individual peptides were analyzed by MS Bioworks on a Q-Exactive tandem mass spectrometer (MS/MS) together with established absolute quantification (AQUA) peptides [69]. Synthetic peptides containing cTnISD were denoted as "heavy" in figure 1A, while native peptides derived from trypsinized fragments were denoted as "light". To determine the amount of each type of cTnI in a mouse line, mass-to-charge (*m/z*) ratios were used to quantitate and distinguish cTnI SD from wildtype cTnI.

Myofilament incorporation of cTnI. Isolated cardiomyocytes (see Chapter 3) were fixed in 3.5% paraformaldehyde, immunostained with primary antibodies (Abs) to troponin I (TnI) and α-actinin [116] followed by goat anti-mouse secondary Abs conjugated to Alexa-fluor 488 and 555 (Table 4.2) [5]. Z-plane projection images were collected with a Leica D-MIRE inverted fluorescence microscope. The localized TnI flanking the z-band stained with α-actinin rather

than diffuse cytosolic TnI staining indicates endogenous and mutant cTnI protein were incorporated into the sarcomere (Fig. 4.1).

Quantitative PCR. Q- or RT-PCR was performed using specific primers listed below.

Table 4.1 Primers for Q/RT-PCR

Protein Encoded	**Primer Sequences (5'-3') or commercial catalog #**
cTnI	Fw: ATGGCGGATGAGAGCAGCGATG Rev: CAATGTCCTCCTTCTTCACCTGCTTG
Transgene cTnI	Fw: AACCGGTGGGACATTTGAGTT Rev: TGGACCCAACGCATGAGA Probe: TTGCTTGGCACTGTC
Transferrin receptor (TFRC)	Thermofisher #4458370
β–actin	Mm00607939_s1 (Applied Biosciences)
Atrial Natriuretic Peptide (ANP)	Mm01255747_g1 (Applied Biosciences)
Mt-CO1 (Complex IV ETC)	Fw: GCTAGCCGCAGGCATTACTATAC Rev: GCGGGATCAAAGAAAGTTGTGT Probe: ACTAACAGACCGCAACCT
Rpl13a	Mm01612986_gH (Applied Biosciences)
Cytochrome b (Complex III ETC)	Fw: GCGGCCCTAGCAATCGTT Rev: GTTGGGTTGTTTGATCCTGTTTC Probe: ACCTCCTCTTCCTCC

Gene expression: QPCR analysis. Mouse left and right ventricles were separated, immersed in RNALater and stored at -20^{o}C. For preparation of RNA, samples were pulverized in liquid N_2, and RNA isolated with RNeasy fibrous tissue kit (Qiagen). RNA concentration and quality were determined on a Thermofisher Qubit fluorometer. Then, reverse transcription of RNA to cDNA was performed using a high-capacity cDNA reverse transcription kit (Thermofisher 4373966). After nanodrop determination of cDNA concentration, qPCR was used to determine gene

expression levels in each mouse line using 0.1μg cDNA and Taqman probes in a StepOne Plus real time PCR instrument (Applied Biosystems). The specific probes for qPCR are listed in table 4.1 with Rpl13a used as a reference primer.

Western Blot analysis. Information regarding antibodies and analysis of protein expression is listed in the table below.

Table 4.2 Antibodies for Western blot and immunohistochemistry.

Primary Antibody	Catalog #	Dilution	Secondary Antibody
Cardiac Troponin I (cTnI)	Sigma mAb1691 (C5 Clone)	1:1000	BDBiosciences Goat anti-mouse Ab #554002 (1:1000)
Tropomyosin (Tm)	Novus Biologicals T2780 (Clone Tm311)	1:10000	
OXPHOS (Electron Transport Chain I-V)	Life Technologies 458099	1:1000	
α-actinin	Sigma EA-53	1:500	
VDAC	Abcam Ab15895	1:1000	Goat anti-rabbit; Upstate Cell Signaling Solutions 123-48 (1:1000 or 1:2000*)
IRE-1α	Cell Signaling 3294	1:500*	
NRF2	Cell Signaling D1Z9C	1:1000*	
SOD2	Cell Signaling D3X8F	1:1000	Goat anti-rabbit; Sigma A0545 (1:1000)
Catalase	Cell Signaling D4P7B	1:1000	

Thin filament stoichiometry. Mouse hearts were pulverized in liquid N_2 after removal from pentobarbital-anesthetized mice, and stored at -80°C if not immediately processed. Whole heart lysates were prepared by homogenizing the pulverized samples in ice-cold leupeptin-supplemented Laemmli sample buffer (62.5mM Tris pH 6.8, 1% SDS, 15mM DTT, 1.1 mM leupeptin; [4]), and transferred to pre-cooled, one-use microfuge tubes stored at -80°C. Protein

concentration in each sample was determined with a BCA protein assay (Pierce 23227). For stoichiometry, 100 μg of lysate protein was separated on 12% SDS-PAGE, transblotted to a PVDF membrane, and then probed with primary Abs to TnI and tropomyosin followed by goat anti-mouse secondary Ab conjugated to horseradish peroxidase (Table 4.1) and ECL (Pierce 32106) which was detected with a BioRad GelDoc system. Individual bands were quantitated using Image Lab (BioRad).

Protein expression: Western analysis. Additional Western analysis was performed on the whole heart lysates and separated on 12% SDS-PAGE gels, as described above. The amount of protein loaded for Western analysis was 150μg for IRE1-α ; 100μg for NRF2 and OXPHOS, 50μg for SOD2, 250 μg for catalase, and. Mitochondrial fractions were isolated from a separate group of pulverized heart samples by differential centrifugation in HES buffer containing 250mM sucrose, 1mM EDTA, and 10mM HEPES [226, 227]. Proteins in the mitochondrial fraction (25 μg) were separated on 12% SDS-PAGE gels, transblotted to PVDF, and probed with OXPHOS primary and goat anti-mouse secondary antibodies (Table 4.2) as described above. For OXPHOS analysis, VDAC also was probed as a loading control (see table 4.2) after a low pH strip (Abcam). Protein bands were quantitated using Image Lab.

Sypro staining. The NRF-2 and IRE-1α blots were stained with Sypro Ruby to normalize for protein load, as described by the manufacturer (Invitrogen S11791). After staining, the membrane was washed and then imaged on a BioRad Gel Doc.

Mitochondrial Architecture

Analysis of mitochondrial/nuclear DNA ratio. Tissue was minced in lysis buffer containing 10mM EDTA, 0.6% SDS, 10mM Trizma HCl (pH 8) and 0.4 mg/mL Proteinase K. Samples were digested at 37^{o}C for 3 hours, precipitated with 1M NaCl on ice for 1 hour, and centrifuged at 4^{o}C for 1 hour at 10,000 x g. DNA in the supernatant was extracted with phenol-chloroform (1:1 volume; Invitrogen 15593031), centrifuged at 4^{o}C for 15 minutes and precipitated from the supernatant in 2 volumes of 100% ethanol and 0.1 volume of 3M sodium acetate at -20^{o}C, centrifuged for 20 minutes, washed with 100% ethanol and dried. Each pellet was resuspended in 20µL of Endotoxin-free TE buffer supplemented with RNAse A. Quantitative PCR was performed as described above, with 0.1µg DNA assayed per sample. Cytochrome b was used as the marker for mitochondrial DNA while β-actin was used as the marker for nuclear DNA using Taqman probes (Table 4.1).

Citrate synthase activity. Citrate synthase (CS) activity was assayed at 30^{o}C in mitochondria extracted from heart tissue, as previously published by Oroboros [228]. Briefly, mitochondria were extracted from quickly weighed mouse hearts immediately after removing and pulverizing hearts in liquid N_2. Tissue was homogenized in a, all-glass tissue grinder in a 10-fold volume of ice-cold 0.1M Tris (pH 7; [229]), diluted 1:15 in 0.1M Tris plus 1% Triton X-100 and incubated on ice for 30 minutes with frequent vortexing. Each homogenate was further diluted 26-fold with 0.1M Tris plus 1% Triton X-100 in triplicate. For each CS assay, 20uL aliquots were incubated with mastermix (0.3M Tris pH 8, 0.5mM oxaloacetate dissolved in triethanolamine/EDTA (0.1M/1mM), 0.101mM Ellman's Reagent (5,5-dithio-bis-(2-nitrobenzoic

acid or DTNB dissolved in Tris 1M pH 8), 0.31mM Acetyl Co-A, and 0.25% Triton X-100 heated to 30°C in visible light cuvettes and measured in a Thermofisher Evolution 300 UV-Vis Spectrophotometer (412 nm) at regular intervals over 3 minutes. CS activity was normalized to tissue weight. For cellular CS activity, Triton X-100 10% was added to cardiomyocytes in respiration buffer after Oxygraph experiments (see below), to reach 1% Triton X-100. Cells were vortexed and 200uL aliquots were brought to 1mL with 30°C mastermix and assayed as described for the mitochondrial CS assay described above.

Mitochondrial Oxidative Stress

Reactive oxygen species (ROS) measurement: Imaging in cardiomyocytes. Rod-shaped, Ca^{2+} tolerant mouse cardiomyocytes plated on laminin-coated coverslips in blebbistatin-free MEM media were stained with a cell-permeant fluorescent mitochondrial ROS-specific indicator, CellROX Green (2.5 mM; Invitrogen C10444) for 15 minutes at 37°C with or without menadione (100μM). Cells were fixed in formalin at 4°C, washed in ice-cold PBS, followed by PBS + 1% glycine, and mounted on slides using Prolong Gold for imaging using a Nikon E800 fluorescence microscope.

Reactive oxygen species (ROS) measurement: Quantification in isolated mitochondria and cardiomyocytes. Rod-shaped, Ca^{2+} tolerant mouse cardiomyocytes were permeabilized with 0.01mg/mL digitonin and loaded with CM-H_2DCFDA (5 μM; Thermofisher # C6827) for 1 hour in Tyrode's solution (140mM NaCl, 5.4mM KCl, 10mM D-Glucose, 5mM HEPES, 1mM $MgCl_2$*$6H_2O$, 1.8mM $CaCl_2$*$2H_2O$ pH 7.4) at 37°C. A 2.05mM stock solution of CM-H_2DCFDA was freshly prepared in DMSO for each experiment. For each analysis, CM-

H_2DCFDA fluorescence was measured over 20 minutes in myocytes under basal conditions. For experiments using CTP-03, a second generation elamipretide reagent (RA Ventures; provided by Dr. Scott Soleimanpour), 10μM CTP-03 was added to a Tyrode's + CM-H_2DCFDA mixture and then loaded into cardiomyocytes for 1 hour. ROS activity was measured at an excitation of 485nm and emission of 528nm in a Biotek Synergy H1 Hybrid Multi-Mode Reader (Model H1M, 5th generation) in all ROS experiments. A subset of assays in isolated mitochondria prepared as described for the CS assay, basal and H_2O_2-stimulated ROS production were analyzed over 20 min after loading them with 5μM CM-H_2DCFDA. The ability to block ROS production also was studied in these mitochondria using the non-specific ROS inhibitor, N-Acetyl Cysteine (NAC, 10mM; Thermofisher A7250).

Mitochondrial Energetics

Adenine Nucleotide Extraction. Adenine nucleotides were extracted from hearts pulverized in liquid N_2 and stored at -80^{o}C for <1 week prior to analysis. Adenine nucleotide assays were performed as described previously [229]. Briefly, 60-100 mg of pulverized hearts were homogenized in 15 x tissue weight in μL of ice cold 2N perchloric acid (PCA) and 2mM EDTA per mg tissue, and centrifuged at 15000 x g at 4^{o}C for 5 minutes. The supernatant was neutralized to pH 7.4-7.8 with a combination of 10N and 2N KOH, 40mM TES, and 300mM KCl, and centrifuged again. The supernatant was stored at -80^{o}C and adenine nucleotides were measured in UV transparent cuvettes with an Evolution spectrometer at 25^{o}C using the NADH/NADPH absorbance of 340nm.

ATP quantification. A 250µL aliquot of nucleotide extract was mixed in a total volume of 1mL in ATP assay mastermix containing 56.8mM Tris pH 7.8), 5mM $MgCl_2$ plus 0.05% w/v NADP (Calzyme) and 0.5U/µL glucose-6-phosphate dehydrogenase (Calzyme). The background absorbance was followed initially, and the increase in absorbance was measured at NAD(P)H absorbance of 340 nm over 15 minutes upon addition of 10 mM D-Glucose and 1 U/mL Hexokinase. The concentration of ATP was calculated from the change in absorbance and the extinction coefficient of NAD(P)H, then normalized to the original sample weight prior to extraction.

ADP and AMP quantification. ADP and AMP were assayed with a similar protocol using a ADP/AMP mastermix 0.1M triethanolamine, 30 mM $MgSO_4$, 110 mM KCl, 160µM phosphoenolpyruvate, and 8.25 U lactate dehydrogenase. ADP was calculated from the difference in 340 nm absorbance before and after addition of 90 µL NADH (Calzyme), and 4.7U pyruvate kinase (Sigma P1506). After complete ADP consumption, AMP was measured based on the difference before and after an addition of 20 µL NADH, 0.05 mM ATP, and 7U of myokinase. The concentration of ADP and AMP is calculated from the changes in absorbance and the extinction coefficient of NADH, then normalized to the original sample weight prior to extraction.

Oxygen Consumption Rate (OCR) measurements. Oxygen consumption rate (OCR) was measured in Ca^{2+} tolerant cardiomyocytes using an Oroboros Oxygraph-2k and a previously published method [229]. Ca^{2+}-tolerant, rod-shaped adult mouse cardiomyocytes were resuspended in respiration buffer (90 mM KCl , 2.5 mM KH_2PO_4, 50 mM MOPS, pH 7.2, 1 mM

EGTA, and 0.1% fatty acid-free BSA, 5 mM NaCl and 10 μL/mL of phosphate). Cardiomyocytes were placed in both Oxygraph chambers at a density of 20,000 cells/2mL chamber, permeabilized with digitonin (10 μg/mL) and treated sequentially with 5mM pyruvate + 0.5 mM malate, 1 mM ADP, 5 mM Succinate, and 2.5 μg/mL antimycin. Oxygraph measurements were made on myocytes treated with or without CTP-03 (10 μM) at 37^{o}C for 1 hr. Data for each step was collected when the OCR plateaued and indicate steady-state measurements.

Statistical comparisons. Data are presented as mean +/-SEM. Statistical comparisons were made using Student's t-tests, a one, or two-way analysis of variance (1 or 2-WAN) by PRISM (Graphpad version 9). The specific statistical test and appropriate post-hoc analyses used for each group of data are described in the figure legends. For each comparison, statistical significance was set at $p<0.05$.

Results

Our transgenesis strategy produced three lines of transgenic (tg) mice with different copy numbers. Replacement levels determined by absolute quantification (AQUA) and MS/MS [69] show that these copy number differences translated into 36%, 46.5%, and 56.5% replacement of endogenous cTnI by cTnISD (Fig 4.1A). Thus, these lines are grouped by replacement level into low (LE-), moderate (ME-), and high (HE-) -expressing cTnISD (SD) mouse lines, respectively. Immunohistochemical staining of cardiomyocytes from 3 month (mos)-old HE-SD mice also shows cTnI protein expression is restricted to the I-band flanking α-actinin in the z-band (Fig 4.1B). This observation confirmed that all cTnI is incorporated in a striated manner and is consistent with SD localization to the sarcomere. Western analysis also confirms that thin filament stoichiometry is preserved across the 3 lines, as the relative ratio of cTnI to tropomyosin (Tm) remains stable (Fig 4.1C) across all lines. Thus, these three lines of mice provide an effective set of models to study the functional and structural impact of S43/45 phosphorylation.

Cardiac function response in mice expressing cTnISD

Earlier results in rat myocytes showed cTnISD reduces cellular contractile function [4, 5]. Based on this observation, cTnISD is predicted to cause dose-dependent *in vivo* cardiac dysfunction and progression to end-stage HF in higher expressing cTnISD mice. Thus, *in vivo* contractile function measured by echocardiography (echo) in cTnISD mice indicates systolic function (EF%) is not significantly altered at 1 mos of age, but starts to decrease at 2 mos of age in ME- and HE-SD mice compared to ntg mice (Fig. 4.2A and Fig. S4.1). By 3 mos of age, systolic function progressively decreases in HE-SD mice (Fig. 4.2A), and all mice in this line die by 15 weeks of age. In contrast, the EF% in ME-SD (Fig. 4.2A), as well as LE-SD mice (not

shown) develop a more modest, but sustained decrease in EF% by 2-3 mos of age, which continues to deteriorate in ME-SD versus ntg mice between 6-12 mos of age (Fig. 4.2A). Diastolic dysfunction also appears to develop in HE-SD mice, although 2 of 5 mice at 2 mos of age, and all 3 mos old HE-SD mice died before completing pulse wave Doppler imaging for E/A ratio (Fig. S4.1F). As a result, statistical comparison of E/A ratios is not yet possible. In addition, the HE-SD mouse hearts are the first line to show signs of structural remodeling using echo, as indicated by the left ventricular dimensions (Fig S4.1B-C). These dimensions change over a slower time course in ME-SD (Fig. S4.1B-C), and LE-SD mice (results not shown). However, this slower progression of dysfunction and remodeling in ME-SD mice is only temporarily delayed, as all 3 (100%) ME-SD mice followed for longer time periods die by 13 mos of age. In summary, *in vivo* functional measurements show that chronic replacement of endogenous cTnI with cTnISD causes dose-dependent cardiac dysfunction, and can initiate a progressive deterioration in cardiac performance.

Progressive remodeling in response to cTnISD

Previous biochemical and cellular work predicted mice expressing cTnISD could develop cardiac dysfunction leading to heart failure [3-5] but did not provide insight as to whether this substitution activated a compensatory remodeling response to dysfunction. Morphological, gene expression and histological analysis establish a temporal progression relative to the *in vivo* dysfunction detected by echo. Hearts from HE-SD mice are visibly larger than ntg, indicating the presence of remodeling (Fig. 4.2B). Morphological analysis of heart weight-to-tibia (H/T) length ratios also indicates hypertrophy by 2 mos in HE-SD mice, which dramatically increases in 3 mos old mice (Fig. 4.2B). A similar trend develops in ME-SD mice, reaching significance in 3

mos old ME-SD versus ntg mice. Similar findings are observed for heart weight-to-body weight ratios (results not shown). Wet-to-dry (w/d) lung weight ratios are an indicator of congestive HF [222], and these values also tended to increase in 2 mos old HE-SD but remain just below the statistical threshold compared to ntg mice (HE-SD w/d =5.334+0.157; n=11; ntg w/d = 4.436+0.402; n=12; p=0.057). Lung w/d ratios also remain unchanged in 1-3 mos old LE- and ME-SD mice (Fig. S4.2).

Gene expression of NPPA verifies remodeling by 2 mos of age in HE-SD hearts (Fig. 4.2C), as this atrial natriuretic peptide (ANP) transcript increases during cardiac remodeling and correlates with cardiac hypertrophy [230]. Here, increased NPPA expression by 2 mos of age in HE-SD hearts verifies the onset and presence of remodeling (Fig. 4.2C), but is not yet significant in LE- and ME-SD mice by 3 mos of age. These findings suggest the SD substitution induces a stimulus for remodeling by 2 mos in HE-SD mice, but this remodeling develops more slowly in LE- and ME-SD mice (Fig 4.2B). Histological analysis also confirms there is an absence of significant remodeling at 1 mos of age in HE-SD mice, but extensive fibrosis, as well as myocyte and myofibrillar disarray develops in older mice, as noted after picrosirius red and H&E staining of sections, respectively (Fig. 4.2D).

Analysis of cellular dimensions provides further evidence of remodeling and hypertrophy (Fig. 4.3A). The sharp rise in L/W ratio in 2-3 mos-old HE-SD mice is consistent with a dilated phenotype in HE-SD hearts-but has not yet increased in 2-3 mos old ME- and LE-SD mice (Fig 4.2B). Cellular widths are provided for each line and age group in Fig. 4.3, to illustrate the lack of detectable concentric hypertrophy in SD myocytes.

Although the ME-SD mouse hearts show minimal evidence of remodeling by 3 mos of age, cellular contractile function corroborates the *in vivo* echo results. Specifically, the isolated

myocytes from >3 mos old ME-SD hearts show significant decreases in isolated cardiomyocyte peak amplitude and rates of contraction and re-lengthening (Fig. 4.3B). In agreement with an earlier *in vitro* approach [5], Ca^{2+} transients are preserved in myocytes from 3 mos-old mice at a timepoint when there is already contractile dysfunction in cardiomyocytes (Fig. S4.3). These findings indicate that while cTnISD causes contractile dysfunction prior to the onset of cellular hypertrophy (Fig. 4.3A) and/or alterations in Ca^{2+} handling (Fig. S4.3), this initial dysfunction also leads to significant remodeling, hypertrophy, and a progressive deterioration in cardiac function.

Organelles contributing to early remodeling and dysfunction

The temporal changes in this model indicate there may be additional cellular events responsible for initiating progressive remodeling, hypertrophy and cardiac dysfunction. Analysis of IRE-1α, an ER-resident protein contributing to the unfolded protein response, indicates sarcoplasmic reticulum stress does not play a significant early role as there are no significant changes in protein expression detected at 2 mos in HE-SD vs ntg mice (Fig. S4.4; [231]). Protein expression of the nuclear stress marker, NRF-2 also is similar in 3 mos old HE-SD and ntg mouse hearts (Fig S4.4).

Another possibility is that mitochondrial function could play a role in initiating progression of the cardiac phenotype, especially given the lack of early changes in Ca^{2+} handling and nuclear stress. The rationale for this hypothesis is based on the heavy dependence of the myosin head on mitochondrial ATP [124], with one study reporting that cardiac sarcomeres utilize >75% of ATP generated by cardiac mitochondria [124]. Thus, this set of studies analyzes whether there are early mitochondrial structural and functional changes in cTnISD mice.

Because mitochondria have their own DNA, early changes in mitochondrial DNA could develop in SD mice. Indeed, significant decreases are detected by 1 mos of age in the mitochondrial to nuclear (Mt/Nuc) DNA ratios for HE-SD compared to ntg mice (Fig. 4.4A), which precede the onset of significant cellular or whole-organ contractile dysfunction. A progressive decrease in cardiac Mt/Nuc DNA continues to develop over time in HE- and ME-SD mice. Decreases in mitochondrial biogenesis, altered mitochondrial turnover, and/or oxidative damage to mitochondrial DNA could produce this reduction in Mt/Nuc DNA [232-234]. Analysis of Mt-CO1 RNA determined whether reduced transcript levels accompany the decrease in Mt/Nuc DNA. Although significant changes are absent at 1 mos, similar decreases in this RNA transcript level develop by 2 mos of age. Citrate synthase (CS) activity is a widely accepted metric for mitochondrial number, and this activity also remains unchanged in HE-SD compared to ntg myocardium until 2 mos of age (Figure 4.4C). The concurrent decreases in CS activity and in heart function detected at ~2 mos of age indicate reduced Mt/Nuc DNA at 1 mos of age is not due to a decrease in mitochondrial number, and may instead reflect other mitochondrial alterations [232].

These early mitochondrial alterations led to a more in-depth analysis of mitochondrial structure and function. Our initial work focuses on early changes in the electron transport chain (ETC) using Western analysis of isolated mitochondria and whole heart lysates, to measure expression levels of the oxidative phosphorylation complexes. These studies focus on 3 mos old ME-SD hearts, which show modest dysfunction and little evidence of remodeling. Significant decreases in cardiac ETC complexes II and IV are present in ME-SD mice (Fig. 4.5A), and also are noted in HE-SD hearts compared to ntg (Fig. 4.5A).

Adenine nucleotide levels were evaluated to determine whether the dysregulated ETC protein levels also led to aberrant nucleotide production/availability within the mitochondria. Analysis of ATP indicates its availability decreases in 2 mos old HE-SD myocardium (Fig. 4.5B), due at least in part to reductions in the number of mitochondria (Fig. 4.4B). These decreases in ATP coincide with the compressed and accelerated progression of HF in the HE-SD mice, and suggest that a second approach, evaluating mitochondrial respiration is necessary to help explain low ATP availability. A representative experiment illustrates respiration measurements made at baseline, as well as in response to ADP (state 3), succinate (complex II substrate), rotenone (complex I inhibitor), oligomycin (complex V inhibitor), and antimycin A (complex III inhibitor) (Fig. 4.5C). While there is a tendency for decreases in ADP-stimulated (state 3) respiration in 3 mos old ME- and HE-SD compared to ntg myocytes ($p=0.083$), neither basal nor ADP-dependent respiration differences reach statistical significance in ME- and HE-SD myocytes at 3 mos (Fig 4.5D). The studies with antimycin A also suggest there is no change in "leak" for each of these SD lines and age groups. In summary, dysregulated mitochondrial protein expression, reduced mitochondrial number, and reduced ATP levels rapidly follow the early change in Mt/Nuc DNA, and precede significant reductions in respiration. The analysis of respiration also indicates the overall ability to generate energy is maintained even in the presence of these early mitochondrial changes in SD hearts.

Role for oxidative stress during early remodeling

Overall, these mitochondrial studies suggest mechanism(s) other than respiration contribute to the early reduction in mitochondrial/nuclear DNA ratio observed in cTnISD hearts. Further work examines whether oxidative stress plays an early role based on the known ability of

aberrant mitochondrial reactive oxygen species (ROS) accumulation to damage mitochondrial DNA, cause peroxidation of the lipid bilayer, and/or initiate additional pathophysiological processes [235-237]. To test whether aberrant ROS generation precedes or coincides with the early mitochondrial changes and thus lay the foundation for progressive dysfunction in SD mice, orthogonal approaches are used to analyze ROS generation in isolated adult mouse cardiomyocytes (Fig. 4.6A-C). First, basal steady state mitochondrial ROS is imaged with a fluorescent indicator, CellROX Green loaded into myocytes isolated from 1.5 mos-old HE-SD mice (Fig. 4.6A). The elevated mitochondrial ROS observed in HE-SD compared to ntg myocytes under basal conditions (Fig. 4.6A) is comparable to ntg myocytes treated with menadione, a positive control for mitochondrial ROS. Separate studies investigate the rate of basal ROS generation in mitochondria and myocytes loaded with CM-H_2DCFDA to quantitatively analyze this oxidative stress. In this assay, elevated ROS production develops in ME-SD compared to ntg mitochondria isolated from 2 mos old mice (Fig. 4.6B). This finding is intriguing as remodeling and dysfunction are absent at this age in ME-SD hearts. This ROS data suggests the onset of mitochondrial ROS and early dysfunction in cTnISD cardiomyocytes develops in parallel with compensatory mechanism(s) to limit the initial drop in cardiac contractile function. If there is elevated basal ROS in isolated mitochondria, then ROS levels should increase substantially in the intact cardiomyocyte. Indeed, the fold change in cellular ROS increases significantly in cardiomyocytes from 2 mos-old ME-SD compared to ntg mice (Fig. 4.6C). Either elevated ROS generation, and/or diminished ROS clearance could produce this result. In addition, the absence of increased ROS production in 2 mos old HE-SD cardiomyocytes (Fig. 4.6C) may indicate stimulation of oxidative stress is transient and/or ROS scavenger activation may develop earlier in this line at 2 mos of age.

Activation of cellular antioxidant defense systems also could contribute to the early phase of cardiac dysfunction. To test for this possibility, levels of the mitochondrial scavenger, SOD2 and the cytosolic scavenger, catalase were probed by Western blot analysis of cardiac tissue lysates from 3 mos-old mice. Interestingly, SOD2 expression decreases in ME- and HE-SD hearts, while catalase expression increases in the HE-SD samples (Fig. 4.6D). These alterations in ROS scavengers indicate early and dynamic changes in cellular antioxidant defense systems develop with elevated mitochondrial ROS, and the early alterations in mitochondrial function are consistent with significant oxidative stress in SD hearts. However, key antioxidant protein levels and activity require further analysis to understand their contribution during the progression of contractile and mitochondrial dysfunction.

Therapeutic targeting of mitochondria in cTnISD-induced dysfunction

Mitigating mitochondrial ROS should improve mitochondrial oxygen consumption and contractile function if mitochondria play a key role in the early stages of progressive remodeling and cardiac dysfunction caused by cTnISD (Fig. 4.7). The tetra-peptide elamipretide (D-Arg-dimethylTyr-Lys-Phe-NH_2) is postulated to target mitochondrial ROS by stabilizing cardiolipin, found exclusively in the inner membrane of the mitochondria, to improve coupling of electron transport within the ETC [238]. As a result, clinical trials tested the therapeutic potential of elamipretide for treating patients with end-stage HFrEF [239]. The next set of studies used a more recent, second generation version identified as CTP-03 to test whether targeting mitochondria improves mitochondrial and contractile dysfunction in SD cardiomyocytes. Indeed, a 1 hr incubation with CTP-03 (10 μM) reduces ROS production in 2 mos old ME-SD cardiomyocytes, (Fig 4.7A). In contrast, basal and ADP-stimulated cardiomyocyte respiration

remain similar in isolated myocytes from 3 mos old ntg, ME- and HE-SD myocytes 1 hr after CTP-03 (Fig. 4.7B). More specifically, no significant difference between ME-SD and ntg myocytes is detected in basal and ADP-induced respiration after CTP-03 (Fig. 4.7B), and respiration values in each group are comparable to results obtained in the absence of CTP-03 (Fig. 4.5D). While statistical comparisons in HE-SD myocytes are not yet possible, consistent respiration values are observed with CTP-03 (not shown) and without CTP-03 (Fig. 4.5D) in HE-SD myocytes. In summary, the results show short-term CTP-03 significantly reduces ROS in ME-SD myocytes but has no influence on cardiomyocyte respiration.

CTP-03 reduction of cardiomyocyte ROS is a first step, but it is equally important to determine whether targeting mitochondrial ROS improves contractile function. Thus, contractile function is measured in cardiomyocytes treated *overnight* with CTP-03, due in part to the lack of a respiratory response observed after 1 hr of treatment. Treatment with CTP-03 (10 μM) profoundly improves peak sarcomere shortening amplitude, along with the rates of contraction and re-lengthening in cardiomyocytes from 3 mos old mice (Fig. 4.7C), but has no significant impact on contractile function in ntg cardiomyocytes. These findings suggest cTnISD expression stimulates early production of mitochondrial ROS that eventually destabilizes electron transport and disrupts cardiac function. Most importantly, the proof-of-concept CTP-03 treatment shows that efforts to minimize these changes in mitochondria can delay and/or restore contractile function in SD cardiomyocytes.

Discussion

The phenotype in mice with cTnISD replacement indicates chronic phosphorylation of this cluster produces *in vivo* dysfunction, initiates structural remodeling, and causes a progressive deterioration in cardiac performance resulting in end-stage HF (Fig. 4.1-4.4). The rate that this progression advances is dose-dependent based on structural and function studies in mouse lines with a range of cTnISD replacement. Currently, the mechanisms by which cTnI S43/45 phosphorylation causes HF are poorly understood. In addition to defining the cardiac impact of cTnIS43/45D, the present studies indicate mitochondria play a pivotal early role in responding to sarcomeric cTnIS43/45D.

Our results demonstrate, for the first time, that chronic a cTnI S43/45 phospho-mimetic substitution causes *in vivo* heart dysfunction in mice [69]. Previous studies showed S43 and S45 phospho-mimetics reduce maximum tension and Ca^{2+} sensitivity in myofilaments [3, 5, 240]. These sites also independently and concurrently act as dominant brakes on cardiomyocyte contractile function [5], which is consistent with the myofilament data. However, until now, the *in vivo* impact of S43/45 alone on cardiac function remained a question. Here we show that chronic phospho-mimetic cTnI S43/45D causes dose-dependent cardiac dysfunction, remodeling, and HF (Fig. 4.1-4.3). This reduced *in vivo* function may be explained by previous biochemical studies showing phospho-mimetic S43/45 maintains thin filaments in an inactive state, producing a lower number of strong force-generating crossbridges [40]. However, the underlying conformation and/or mechanism for the impact of cTnISD is not known. The crystal structure indicates S43/45 occupies the start of the H1 helix (N-cap and N+2), and the first three amino acids in other α-helices significantly impact helix stability [54, 241]. Thus, it is possible that the negative and sterically bulky phosphorylation increases stability of the H1 helix, which impairs

transmission of the Ca^{2+} signal to downstream domains responsible for the switch function of cTnI. The 3-dimensional structure of cTnI supports this idea, as S43/45 is in close proximity to the flexible inhibitory peptide (IP) domain responsible for toggling from actin to cTnC in response to Ca^{2+} [212]. Thus, cTnISD and phosphorylation could interfere with or blunt the ability of Ca^{2+} to toggle the IP domain. Alternatively, cTnI S43/45 phospho-mimetics and phosphorylation could produce conformational changes to alter communication between the thin and thick filament. Future biophysical studies are needed to differentiate between these possibilities and identify the S43/45-mediated changes in sarcomere conformation responsible for reducing both systolic and diastolic function in cardiomyocytes (Fig. 4.2A).

The *in vivo* phenotype observed in the current SD mouse model (Fig. 4.1-4.3) is consistent with previous functional outcomes in myofilament studies [3-5], in contrast to earlier mouse models with phospho-mimetic substitutions at multiple PKC-targeted cTnI phosphorylation sites [66, 111, 112]. Specifically, contractile dysfunction develops at the whole-organ and cellular levels at 2 and 3 mos of age, respectively (Fig. 4.2, 4.3). The absence of cellular or organ-level functional impairments at 1 mos suggests early compensatory mechanisms masking the direct impact of cTnISD on contractile function [5]. The absence of contractile dysfunction at 1 mos could be due to compensatory phosphorylation within the sarcomere, as earlier work in cardiomyocytes shows increased phosphorylation of other contractile proteins, as well as changes in phosphatase activity in cardiomyocytes expressing cTnISD after adenoviral gene transfer [5]. In addition, the modest dysfunction reported in mice expressing phospho-mimetics at cTnIS43/45 plus other PKC-targeted cTnI sites suggests that comparable phosphorylation levels in other cTnI residues may be capable of blunting or delaying the *in vivo* dysfunction produced by cTnISD [66, 111, 112]. It remains unclear whether this

protection requires a threshold of phosphorylation at these additional residues and/or whether phosphorylation is protective when present on the same or different cTnI proteins.

Most importantly, this study also investigates and identifies potential downstream steps triggered during the early stages of chronic cardiac dysfunction in cTnISD mice. Specifically, *early* secondary changes develop in mitochondria prior to detectable cardiac dysfunction (Figs 4.4A), even in the highest expressing mouse line with a compressed progression of dysfunction and death by 4 mos of age (Fig. 4.1, 4.2, 4.4). With the onset of measurable cardiac and myocyte dysfunction at 2 mos of age in the higher expressing lines of cTnISD mice, mitochondrial ROS increases (Fig. 4.6), which is closely followed by reduced adenine nucleotide availability (Fig. 4.5), mitochondrial transcript expression, and the number of mitochondria per cardiomyocyte (Fig. 4.4). In addition, the altered protein expression of SOD2 and catalase also indicate elevated ROS may be accompanied by disruptions in antioxidant defense systems in cardiomyocytes. Imbalances between ROS production *and* scavenging may further compromise mitochondria during the early progression of cardiac disease in cTnISD mice. Collectively, these findings show that mimicking chronic cardiac cTnI S43/45 phosphorylation with cTnISD expression causes sustained changes in mitochondrial structure and function. These mitochondrial alterations are predicted to compromise cardiac mitochondrial energetics and respiration over time to lay the foundation for the progressive deterioration in cardiac performance observed in cTnISD mice.

To combat the initial stages of cardiac dysfunction that ultimately lead to HF, our next set of studies target the ROS scavenging system to stabilize mitochondria. In initial studies, addition of peroxide drastically increases the level of ROS produced in mitochondria from 3 mos-old ME-SD compared to ntg mice (Fig. S4.5). While future studies are needed to determine whether both

increased ROS production and abnormal ROS scavenging contributed to this response, the ability of the non-specific ROS inhibitor, N-Acetyl Cysteine (NAC) to return the peroxide response to baseline suggests ROS production not only increases but is more sensitive to stimulation (Fig. S4.5).

Additional studies utilize a second generation elamipritide compound known as CTP-03 [238, 239] to further investigate potential therapeutic strategies. The observed ability of CTP-03 to attenuate mitochondrial ROS production and improve contractile dysfunction in cardiomyocytes from 3 mos old ME-SD hearts (Fig. 4.7) supports the idea that early mitochondrial alterations underlie progressive deterioration in cardiac performance in cTnISD mice. Results with CTP-03 also indicate early efforts to mitigate elevated ROS may be therapeutically beneficial for reducing and/or delaying the onset of cardiac dysfunction and remodeling under conditions linked to chronic activation of the protein kinase C (PKC) responsible for cTnI S43/45 phosphorylation, such as hypertension, diabetes or myocardial infarction [9, 242, 243]. As a result, the outcomes in this study may have broad implications for understanding progressive dysfunction caused by sarcomere modifications such as chronic phosphorylation and/or inherited mutations, as well as individuals with an elevated risk for heart failure caused by chronic conditions such as hypertension and diabetes.

In addition to the protective effects produced by CTP-03, the inability of CTP-03 to improve respiration in myocytes from ME- and HE-SD and/or reduce ROS production in the HE-SD samples deserves consideration. These discrepancies are explained by differences in experimental design in each experiment. For respiration experiments, cardiomyocytes could only be treated with CTP-03 for 1 hr because these measurements need to be made on freshly isolated myocytes and require cells to be in suspension (Fig. 4.7B). Due to this protocol, ROS

studies also were performed using a 1 hr incubation with CTP-03, which was adequate to improve ROS production in the 2 mos old ME-SD myocytes. In contrast, an overnight incubation with CTP-03 is possible for contractile function studies performed the day after isolation to optimize cardiomyocyte attachment to laminin-coated coverslips. Future studies using similar incubation times can be achieved using an *in vivo* therapeutic regimen in young adult mice. The ability of CTP-03 to mitigate ROS production in the ME-SD but not HE-SD myocytes from 2 mos old mice (Fig. 4.7A), may be due to a more transient elevation in ROS production and/or differences in the scavenging response in the HE-SD mice with a more compressed phenotype. Regardless, further analysis of these mice at multiple timepoints are needed to better understand the different ROS responses. Most importantly, future studies are needed to test whether chronic treatment with CTP-03 improves *in vivo* function and/or prevents disease progression.

Conclusions

Our studies shed light on the *in vivo* functional impact of elevated cTnI S43/45 phosphorylation under conditions when PKC is chronically activated, as the *in vivo* role of this site has proven to be controversial. Here we show that chronic S43/45 phosphorylation causes progressive, and dose-dependent cardiac dysfunction leading to heart failure and death. Our studies also reveal a novel mechanism for sarcomere-induced HF, in studies showing the early onset of mitochondrial alterations including aberrant ROS generation prior to the development of HF. Moreover, targeting mitochondria also restores cardiomyocyte contractile function. These findings are interpreted to indicate chronic changes within the sarcomere trigger a stress signal, which is then communicated to the mitochondria. While the exact mechanism for activation of mitochondrial ROS generation is not known, these studies show that targeting mitochondrial ROS *early* during the onset of HF, may serve to delay disease progression. Further, these studies will prove to be insightful in development of new therapeutic targets for heart conditions known to develop elevated PKC activity, which then targets downstream cTnI phosphorylation at S43/45.

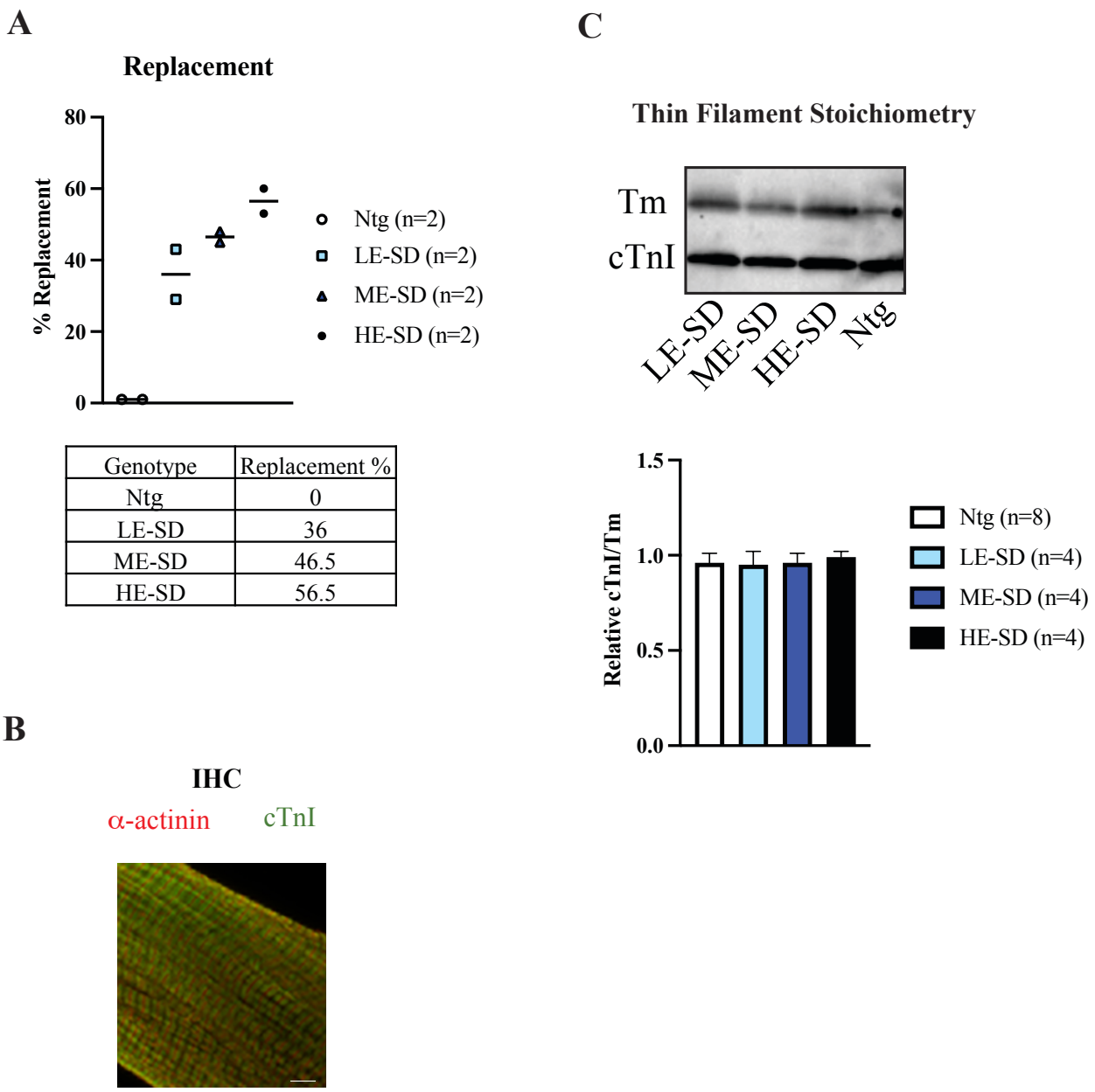

Genotype	Replacement %
Ntg	0
LE-SD	36
ME-SD	46.5
HE-SD	56.5

Figure 4.1 Replacement, sarcomere incorporation and thin filament stoichiometry in cTnIS43/45D lines. A, Tandem MS/MS with AQUA peptides were used to quantify replacement level in cTnISD mice. Three lines of mice were generated with varying levels of replacement, in low (LE-), moderate (ME-), and high (HE)-expressing SD. **B,** Representative immunohistochemistry in cardiomyocytes isolated from 3 mos-old HE-SD mice and co-immunostained for cTnI (FITC; green) and α-actinin (rhodamine, red). Scale bar = 10μm. **C,** Representative western blot and quantification of cTnI and tropomyosin (Tm) protein expression in 3 cTnISD mouse lines. A one-way analysis of variance (1-WAN) was conducted with statistical significance set to $p<0.05$ ($p>0.05$ for this analysis).

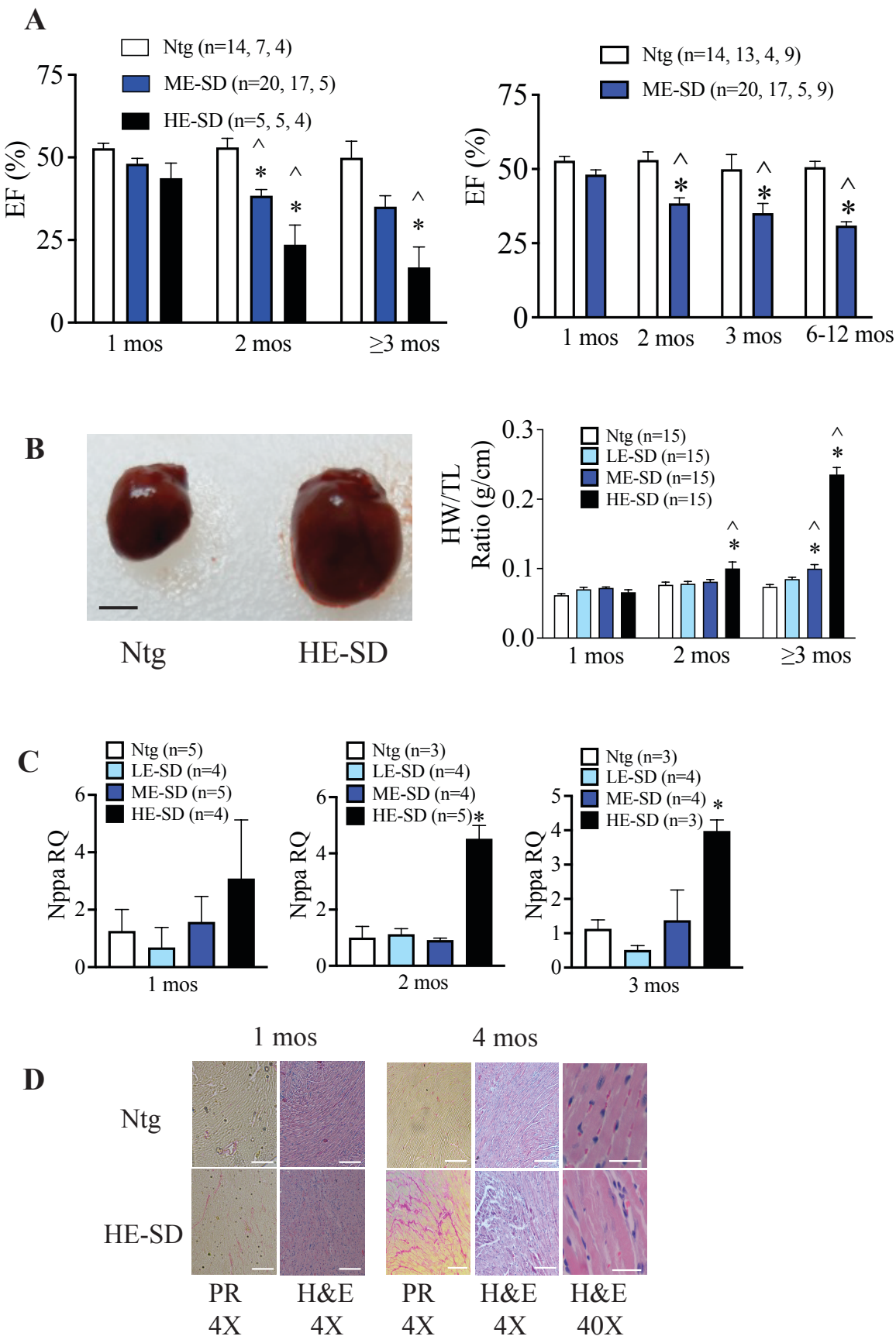
A
Ntg (n=14, 7, 4)
ME-SD (n=20, 17, 5)
HE-SD (n=5, 5, 4)
EF (%)
75
50
25
0
1 mos
2 mos
≥3 mos
Ntg (n=14, 13, 4, 9)
ME-SD (n=20, 17, 5, 9)
1 mos
2 mos
3 mos
6-12 mos
B
Ntg
HE-SD
HW/TL Ratio (g/cm)
0.3
0.2
0.1
0.0
Ntg (n=15)
LE-SD (n=15)
ME-SD (n=15)
HE-SD (n=15)
1 mos
2 mos
≥3 mos
C
Nppa RQ
Ntg (n=5)
LE-SD (n=4)
ME-SD (n=5)
HE-SD (n=4)
1 mos
Ntg (n=3)
LE-SD (n=4)
ME-SD (n=4)
HE-SD (n=5)
2 mos
Ntg (n=3)
LE-SD (n=4)
ME-SD (n=4)
HE-SD (n=3)
3 mos
D
1 mos
4 mos
Ntg
HE-SD
PR 4X
H&E 4X
PR 4X
H&E 4X
H&E 40X

Figure 4.2 Cardiac dysfunction and evidence of remodeling cTnISD-expressing mice. A, Results from 2-D echocardiography showing the onset of diminished ejection fraction (EF%) in ME- and HE-SD mice by 2 mos (left panel). The EF also was followed for up to 1 year in the ME-SD line **B,** hypertrophy in hearts from 3 mos-old ntg and HE-SD mice (left panel). Scale bar 1mm. Heart weight:tibial length ratios also indicate expression-dependent hypertrophy develops by 2-3 mos of age in the ME- and HE-SD hearts (right panel). Scale bar = 1mm **C,** NPPA transcript level is elevated in 2 and 3- mos old HE-SD mice but is not yet significantly increased in LE- and ME-SD hearts. **D,** Histological analysis reveals collagen deposition (PR panels) and cardiomyocyte disarray (H&E panels) are absent at 1 mos but develop in HE-SD mice by 4 mos. Scale bars 100μm for 4X images; 50μm for 40X images. The n for each experiment is shown in the figure panels. For **A** and **B,** 2-WAN with Tukey's post-hoc analyses were performed with statistical significance set to $p<0.05$. (*$p<0.05$ vs age-matched ntg; ^ $p<0.05$ vs 1 mos genotype-match). For **C,** 1-WAN was conducted with Dunnett's post-hoc analysis and significance set at $p<0.05$ (* vs ntg).

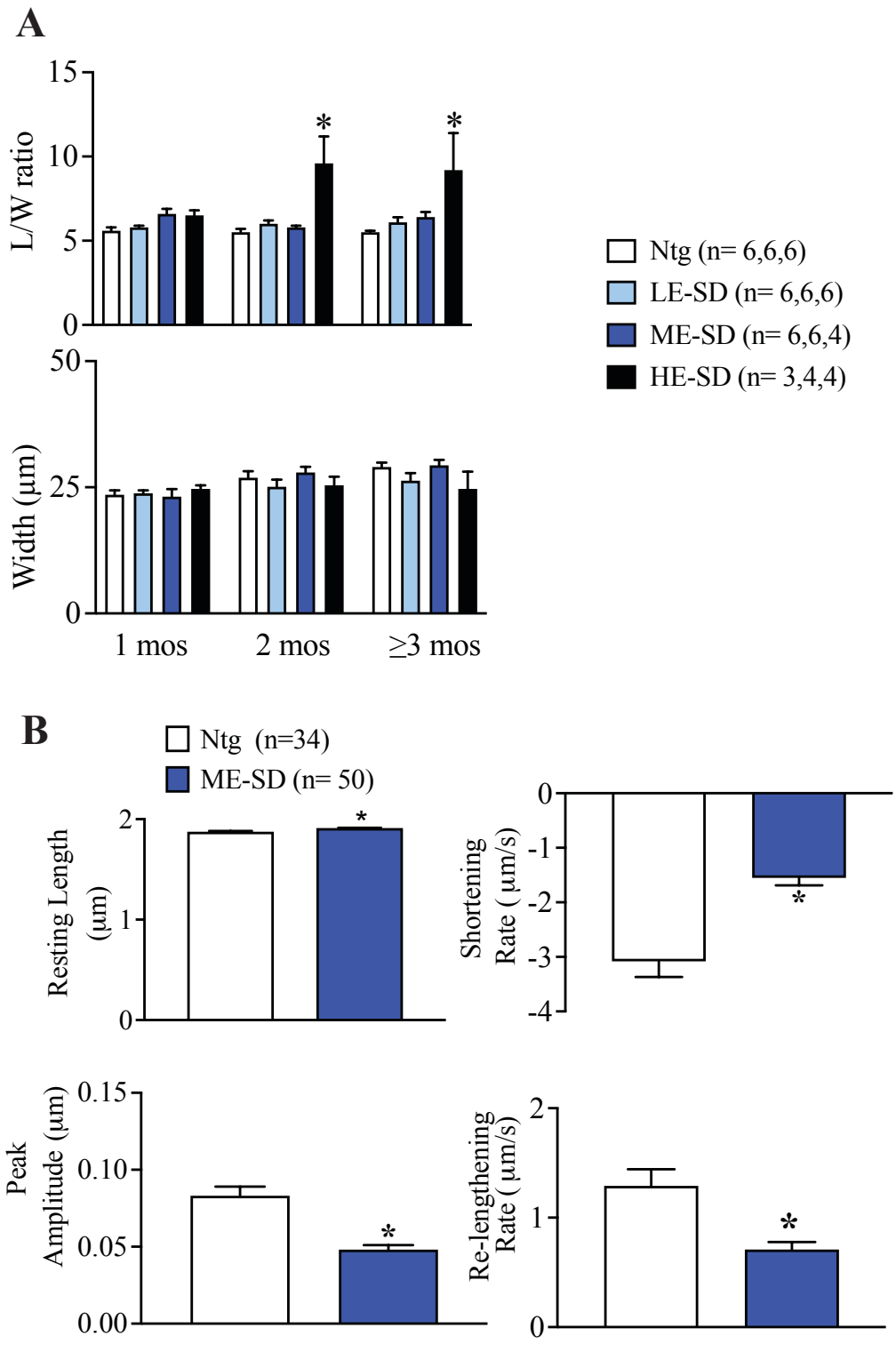
A
L/W ratio
15
10
5
0
Width (µm)
50
25
0
1 mos
2 mos
≥3 mos
Ntg (n= 6,6,6)
LE-SD (n= 6,6,6)
ME-SD (n= 6,6,4)
HE-SD (n= 3,4,4)
B
Ntg (n=34)
ME-SD (n= 50)
Resting Length (µm)
Shortening Rate (µm/s)
Peak Amplitude (µm)
Re-lengthening Rate (µm/s)

Figure 4.3 Evidence of hypertrophy and contractile dysfunction in myocytes from cTnISD hearts. A, Length-to-width aspect ratio indicates eccentric hypertrophy in cTnISD mice (upper panels), with no change in width (bottom panels). **B,** Peak amplitude of sarcomere shortening, and rates of shortening and re-lengthening in cardiomyocytes isolated from 3 mos-old ME-SD mice. The legend in panel B provides the number of cells used for shortening experiments (n=3 mice/group). For **A**, a 2-WAN with Dunnett's post-hoc analysis was conducted, with statistical significance set to $p<0.05$ (*$p<0.05$ vs age-matched ntg). For **B,** an unpaired Student's t-test was performed with statistical significance set to $p<0.05$ (* vs ntg).

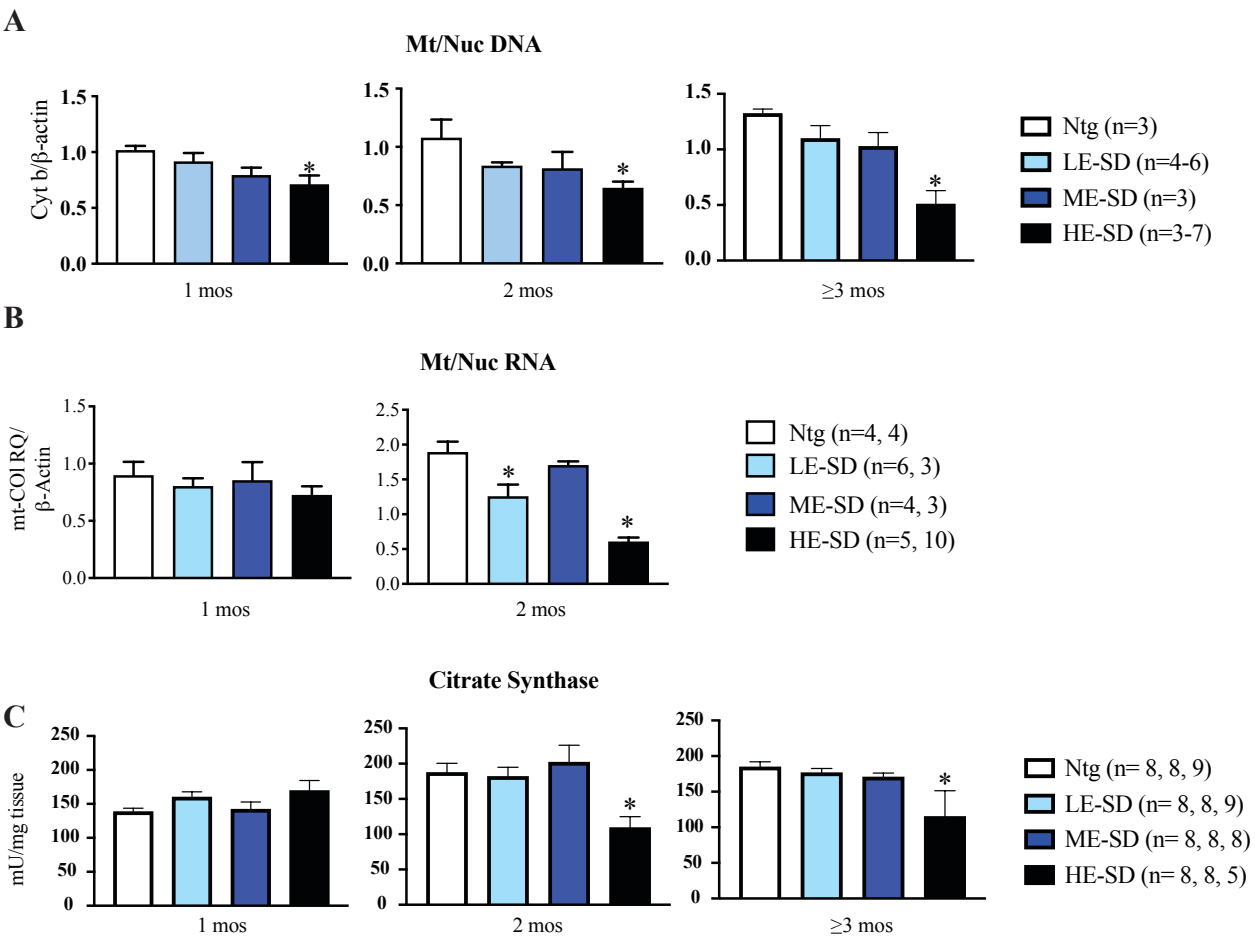

Figure 4.4 Early mitochondrial changes determined using Mt/Nuc DNA ratio, mt-CO1 RNA expression and citrate synthase activity. **A,** The qPCR-derived mitochondrial-to-nuclear (Mt/Nuc) DNA ratio in all 3 cTnISD mouse hearts from 1 to 3 month old mice. **B,** Transcript levels of electron transport chain (ETC) complex 4 Mt-CO1 quantified by qPCR. **C,** Citrate synthase activity measured spectrophotometrically to monitor the rate of DTNB conversion at 412nm in hearts from the 3 lines of cTnISD compared to ntg mice between 1 and 3 mos of age. For **A-C**, 1-WAN with Dunnett's post-hoc analyses were performed with statistical significance set to $p<0.05$ (* vs. age-matched ntg).

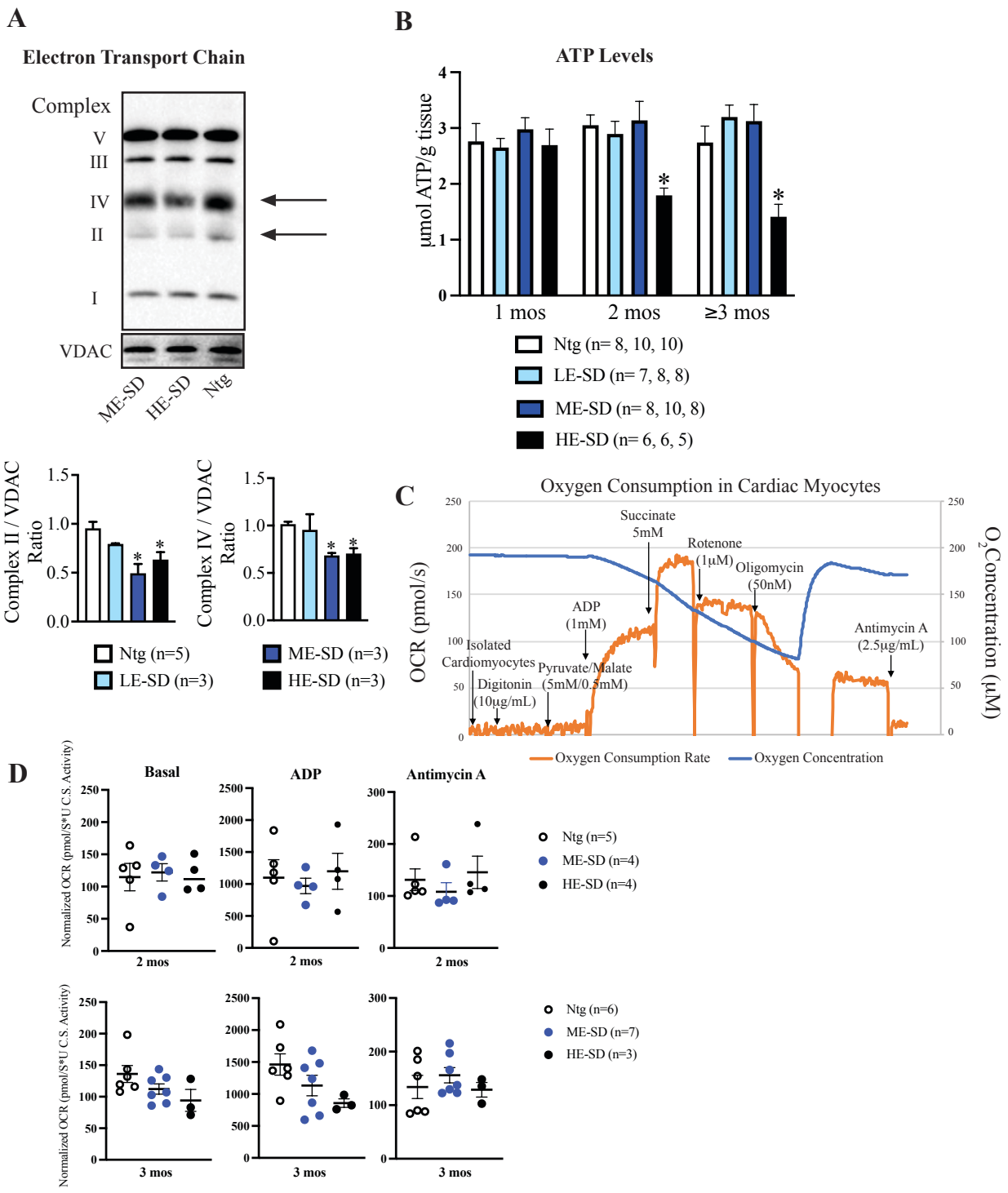
A
Electron Transport Chain
Complex
V
III
IV
II
I
VDAC
ME-SD
HE-SD
Ntg
B
ATP Levels
µmol ATP/g tissue
1 mos
2 mos
≥3 mos
Ntg (n= 8, 10, 10)
LE-SD (n= 7, 8, 8)
ME-SD (n= 8, 10, 8)
HE-SD (n= 6, 6, 5)
Complex II / VDAC Ratio
Complex IV / VDAC Ratio
Ntg (n=5)
LE-SD (n=3)
ME-SD (n=3)
HE-SD (n=3)
C
Oxygen Consumption in Cardiac Myocytes
OCR (pmol/s)
O2 Concentration (µM)
Succinate 5mM
Rotenone (1µM)
Oligomycin (50nM)
ADP (1mM)
Antimycin A (2.5µg/mL)
Isolated Cardiomyocytes
Digitonin (10µg/mL)
Pyruvate/Malate (5mM/0.5mM)
Oxygen Consumption Rate
Oxygen Concentration
D
Basal
ADP
Antimycin A
Normalized OCR (pmol/S*U C.S. Activity)
2 mos
3 mos
Ntg (n=5)
ME-SD (n=4)
HE-SD (n=4)
Ntg (n=6)
ME-SD (n=7)
HE-SD (n=3)

Figure 4.5 Electron transport chain protein expression, ATP levels and respiration in hearts from cTnISD mice. A, Western blot analysis of electron transport chain (ETC) complexes in cardiac whole cell lysates isolated just before mice reached 2 months of age (upper panel). VDAC is probed as a loading control and complexes II and IV expression are quantitatively normalized to VDAC expression in the lower panel. **B,** ATP quantification in cardiac tissue in the 3 lines of cTnISD mice between 1 and 3 mos of age. **C,** Representative trace of oxygen consumption in cardiomyocytes measured by Oroboros Oxygraph O2k showing the oxygen consumption rate (OCR; orange) and oxygen concentration (blue) in response to 10μg/mL digitonin, followed by basal respiration in 5mM / 0.5mMmalate, 1mM ADP, 5mM succinate, 1μM rotenone, 50nM oligomycin, and 2.5μg/mL antimycin A . **D,** Oxygen consumption rate (OCR) in igitonin-permeabilized cTnISD cardiomyocytes at 2 (upper panel) and 3 months (lower panel). Basal respiration was measured in cardiomyocytes respiring on 5mM Pyruvate and 0.5mM malate. ADP (state 3) respiration was measured in response to 1mM K-ADP, and complex 3 was inhibited using 2.5μg/mL antimycin A. The number (n) of hearts is provided in each figure panel. For **A**, a 1-WAN with Dunnett's multiple comparisons were conducted with $p<0.05$ (*vs ntg). For **B**, a 2-WAN with Tukey's post-hoc analysis was performed (*$p<0.05$ vs age-matched ntg; ^$p<0.05$ vs 1 mos genotype matched), and for **D**, a 1-WAN with Dunnett's post-hoc analysis was conducted with statistical significance set to $p<0.05$ (*vs ntg) for all statistical comparisons. For 3 mos ADP-stimulated respiration, $p=0.258$ in ntg vs ME-SD, and $p=0.083$ in ntg vs HE-SD.

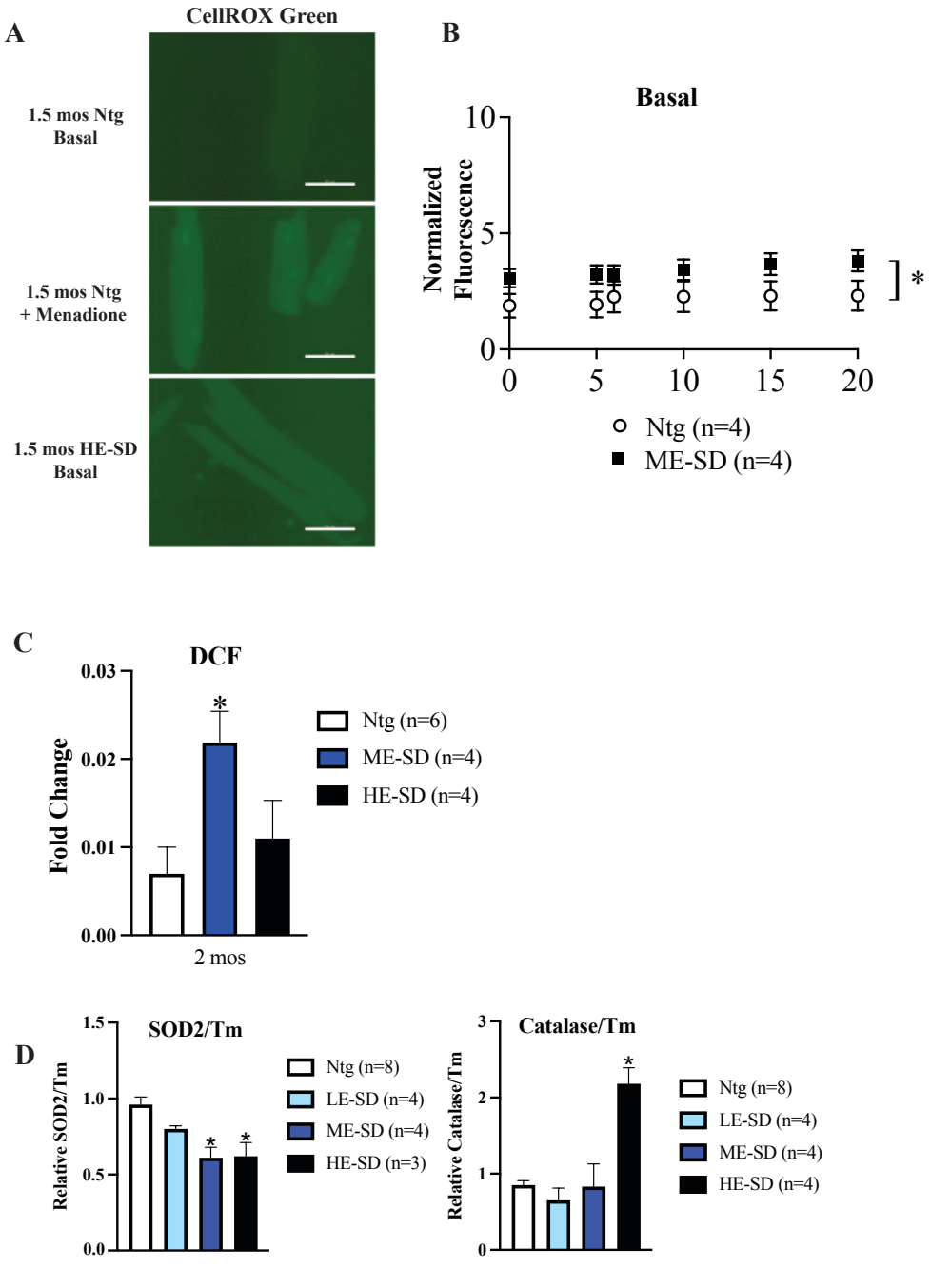
A
CellROX Green
1.5 mos Ntg
Basal
1.5 mos Ntg
+ Menadione
1.5 mos HE-SD
Basal
B
Basal
Normalized
Fluorescence
10
5
0
0
5
10
15
20
*
Ntg (n=4)
ME-SD (n=4)
C
DCF
Fold Change
0.03
0.02
0.01
0.00
*
2 mos
Ntg (n=6)
ME-SD (n=4)
HE-SD (n=4)
D
SOD2/Tm
Relative SOD2/Tm
1.5
1.0
0.5
0.0
*
*
Ntg (n=8)
LE-SD (n=4)
ME-SD (n=4)
HE-SD (n=3)
Catalase/Tm
Relative Catalase/Tm
3
2
1
0
*
Ntg (n=8)
LE-SD (n=4)
ME-SD (n=4)
HE-SD (n=4)

Figure 4.6 Evidence for early accumulation of aberrant mitochondrial reactive oxygen species (ROS) in cTnISD cardiomyocytes. A, CellROX green stain in ntg and HE-SD cardiomyocytes isolated from 3 mos-old animals. The ntg cardiomyocytes also were treated with a positive control, menadione (40μM) to show the change in fluorescence after ROS stimulation. Scale bars =50μm **B,** Baseline CM-H_2DCFDA (DCF) fluorescence was measured over 20 minutes to quantify ROS production in isolated mitochondria from ME-SD compared to ntg mice at 3 mos of age. **C,** DCF experiments also were conducted in digitonin-permeabilized cardiomyocytes and the fold change in the linear regressions over 20 minutes are shown. **D,** Western analysis of SOD2 and catalase expression in cardiac whole cell lysates from 3 mos-old mice. The n for each experiment is listed in the figure panel. For **B,** a 2-WAN with Dunnett's post-hoc analysis was conducted with statistical significance set to $p<0.05$ (* vs ntg). Statistics show a significant effect of cTnISD, without time or interaction effects. For **C-D**, a 1-WAN with Dunnett's post-hoc analysis was conducted with significance set to $p<0.05$ (*vs ntg). For **E**, 1-WAN with Dunnett's post-hoc analyses were conducted with statistical significance set to $p<0.05$ (*vs ntg).

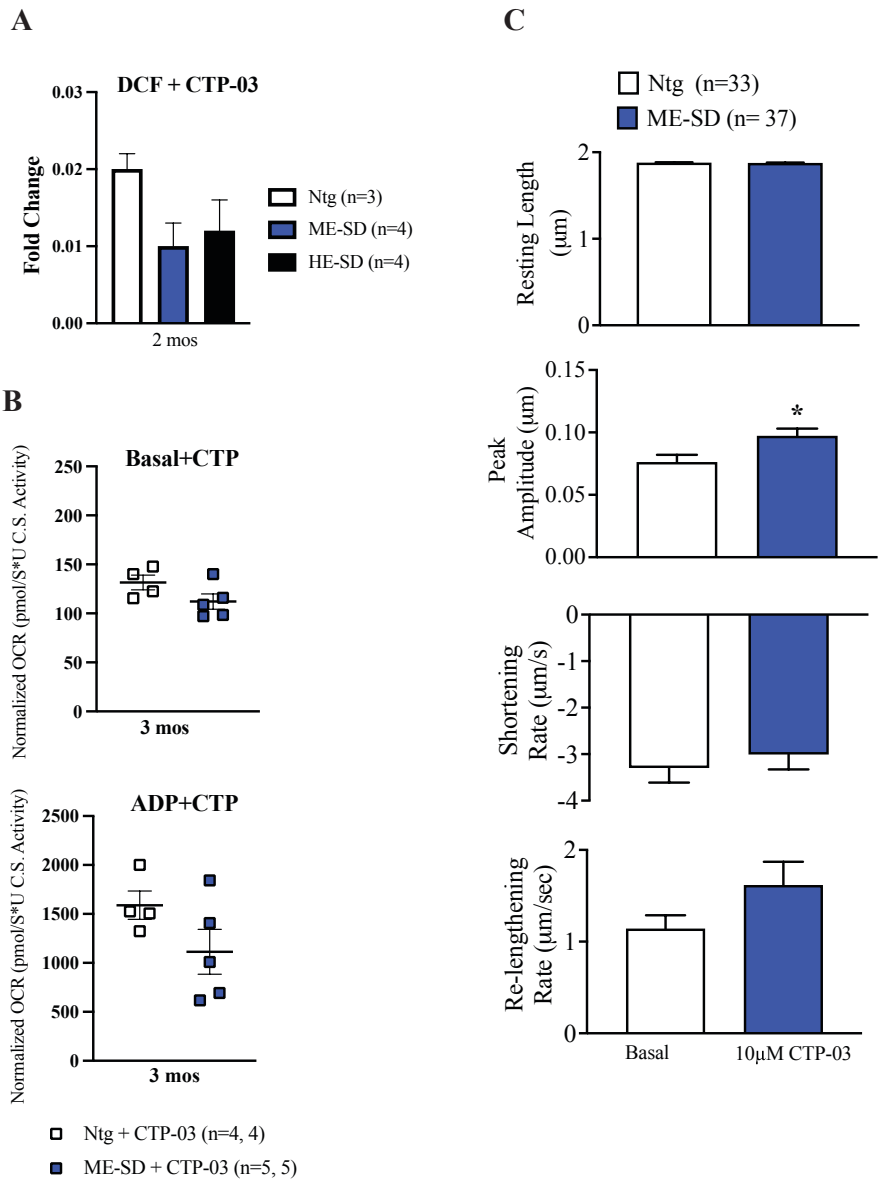
A
DCF + CTP-03
Fold Change
0.03
0.02
0.01
0.00
2 mos
Ntg (n=3)
ME-SD (n=4)
HE-SD (n=4)
B
Basal+CTP
Normalized OCR (pmol/S*U C.S. Activity)
250
200
150
100
50
0
3 mos
ADP+CTP
Normalized OCR (pmol/S*U C.S. Activity)
2500
2000
1500
1000
500
0
3 mos
Ntg + CTP-03 (n=4, 4)
ME-SD + CTP-03 (n=5, 5)
C
Ntg (n=33)
ME-SD (n= 37)
Resting Length (μm)
2
1
0
Peak Amplitude (μm)
0.15
0.10
0.05
0.00
*
Shortening Rate (μm/s)
0
-1
-2
-3
-4
Re-lengthening Rate (μm/sec)
2
1
0
Basal
10μM CTP-03

Figure 4.7 CTP-03 reduces ROS and improves contractile function in cardiomyocytes isolated from cTnISD hearts. A, CM-H_2DCFDA fluorescence was monitored over 20 minutes in cardiomyocytes treated with 10μM CTP-03 for 1 hr, and the fold change in the linear regressions are compared between cTnI ME- and HE-SD versus ntg results. **B,** Oxygen consumption rate (OCR) was measured in digitonin-permeabilized ntg and ME-SD cardiomyocytes treated with 10μM CTP-03 for 1 hr at 37^{o}C cTnI ME-SD compared to ntg results. **C,** Sarcomere shortening was measured in ME-SD and ntg cardiomyocytes from 3-mos old mice, incubated with 10μM CTP-03 overnight. The n for each experiment is listed in the figure panels. For **A,** statistical analysis was conducted by 1-WAN with statistical significance set to $p<0.05$ (*vs ntg). For **B-C,** statistical analysis was conducted by a Students unpaired t-test, with statistical significance set to $p<0.05$ (*vs ntg).

SUPPLEMENTARY FIGURES

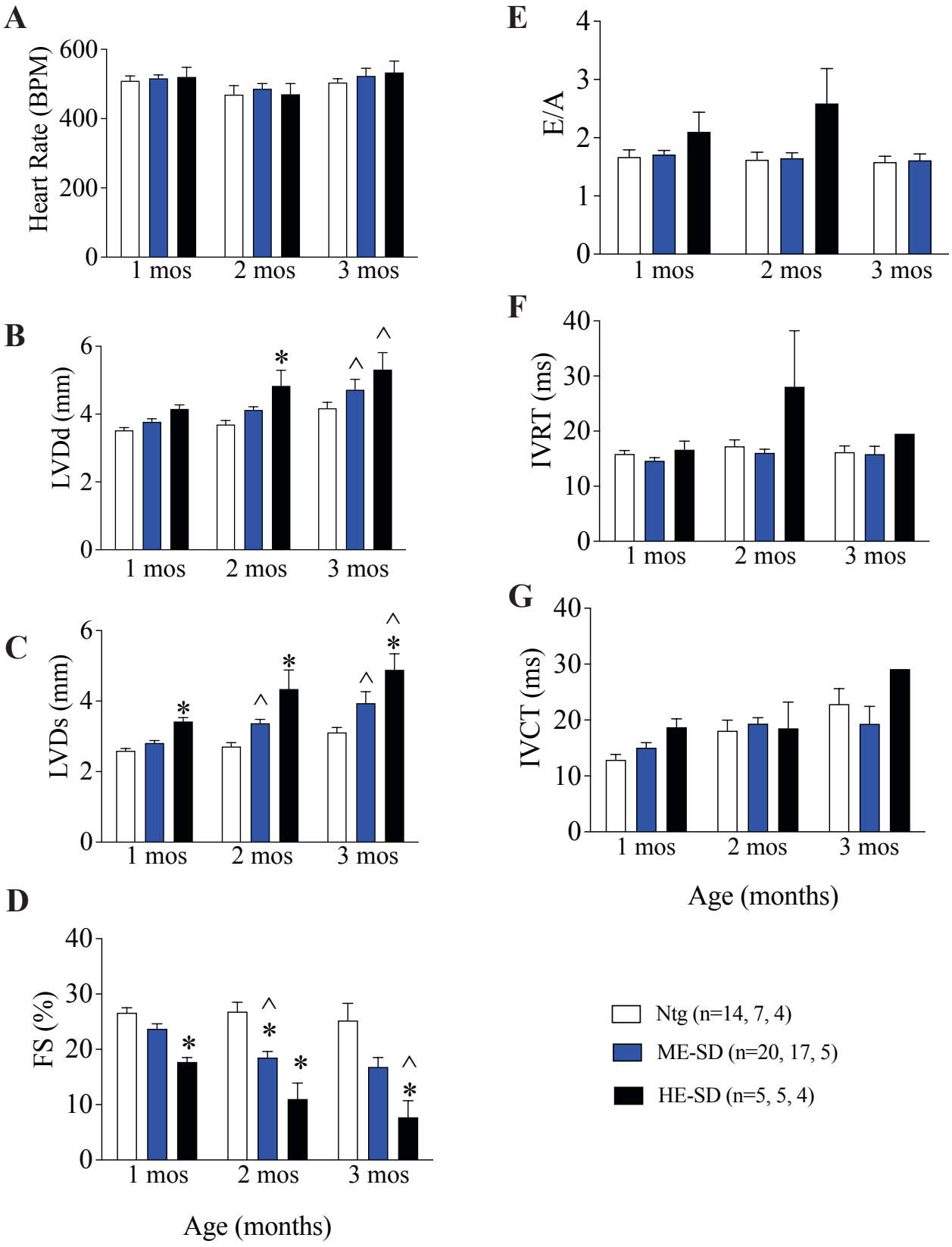

Supplemental Figure 4.1 2-dimensional echocardiography and pulse-wave doppler measurements. A, Echocardiography analysis shows that cTnISD mice maintain heart rate, while ventricular dimensions at end diastole and end systole (LVDd and LVDs) show hypertrophy in cTnISD mice **(B-C)**. **D,** fractional shortening (FS) decreases in cTnISD mice, and Pulse-Wave Doppler imaging measures diastolic function based on E/A ratio **(E)**. **F-G,** isovolumic relaxation and contraction times (IVRT and IVCT) are measured in cTnISD mice. For **E-G,** due to a severe phenotype and/or death in the HE-SD line, this group could not be used for statistical comparison. Statistical analysis was conducted for HR, FS%, LVDd, and LVDs by 2-WAN and Tukey's post-hoc test, with statistical significance set to $p<0.05$. (*$p<0.05$ vs age-matched ntg; ^ $p<0.05$ vs age-matched tg).

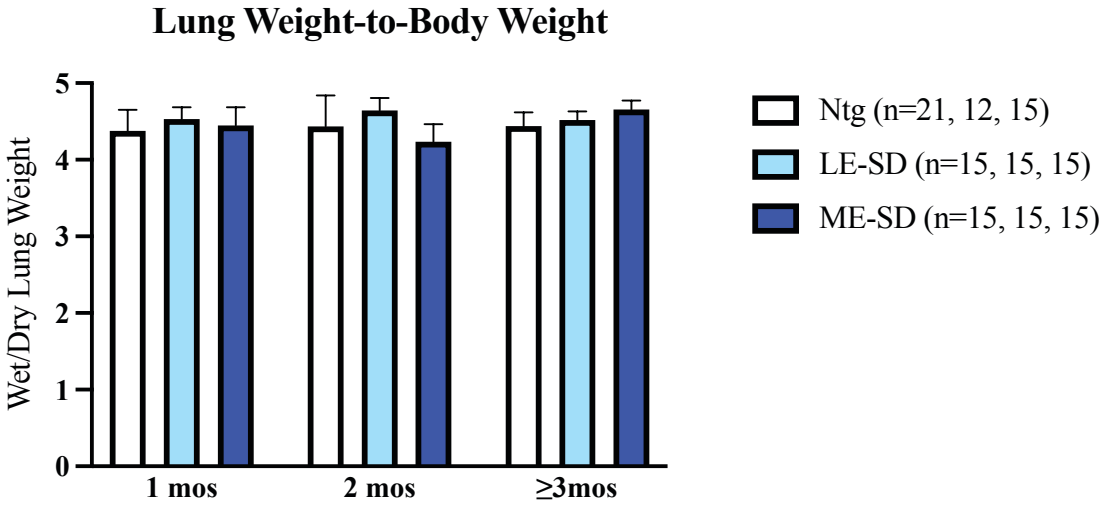

Supplemental Figure 4.2 Pulmonary congestion evaluated using wet/dry wt ratio in ntg and cTnISD mice. Lung weights were recorded in LE- and ME-SD vs ntg mice between 1-3 mos of age. The n for each group is listed in the graph legend. Statistical analysis was conducted by 2-WAN and Dunnett's post-hoc test, with statistical significance set to $p<0.05$ ($p>0.05$ vs for all comparisons).

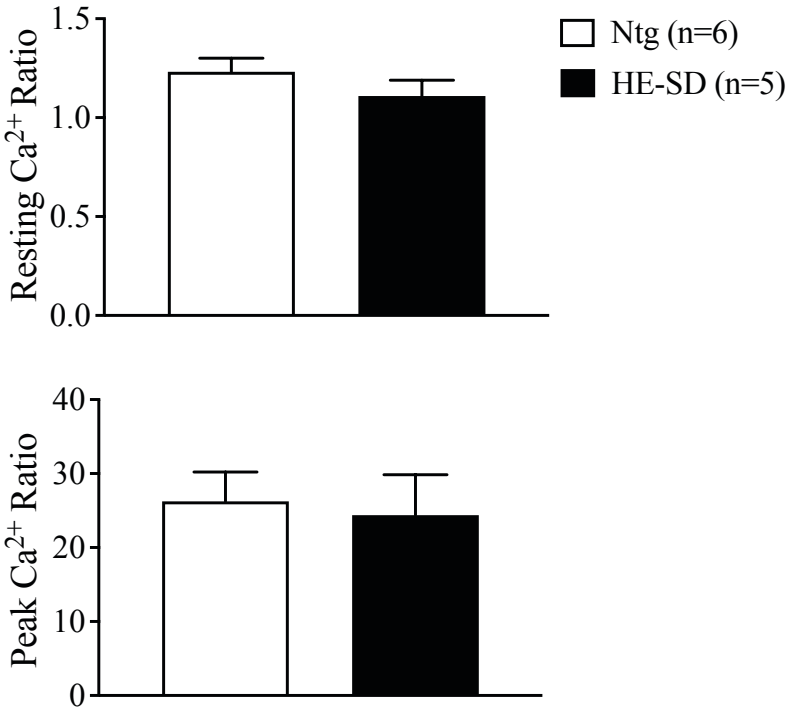

Supplemental Figure 4.3 Calcium transients measured in isolated cardiomyocytes loaded with Fura-2AM and isolated from cTnI HE-SD and ntg mice. Fura-2AM-loaded cardiomyocytes were paced at 0.5Hz, and signal-averaged Ca^{2+} transients for resting and peak Ca^{2+} ratios are shown. A student's unpaired t-test indicated no significant differences between HE-SD and ntg results ($p>0.05$).

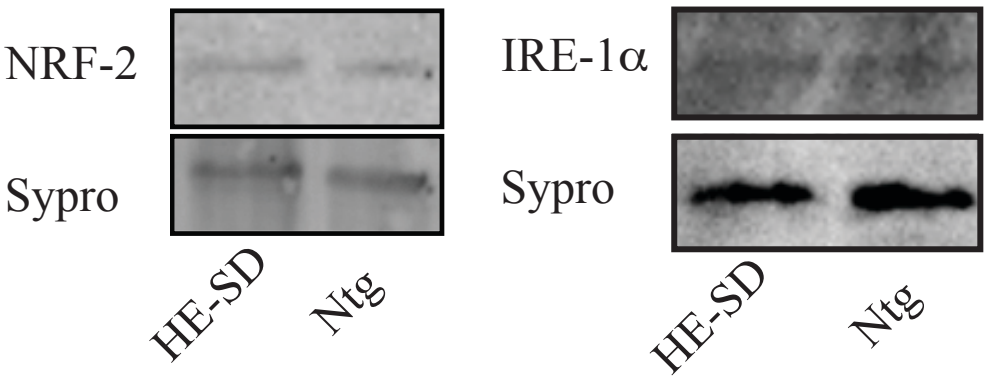

Supplemental Figure 4.4 Representative Western analysis of NRF-2 (left panel) and IRE-1α (right panel) protein expression 3 mos old cTnI HE-SD compared to ntg hearts. Expression of NRF-2 is used as a marker of nuclear stress while Ire-1α indicates sarcoplasmic reticulum stress. The Sypro Ruby Red stains are shown in each Western to indicate total protein loading control. This analysis indicates there is an absence of nuclear and SR stress, respectively.

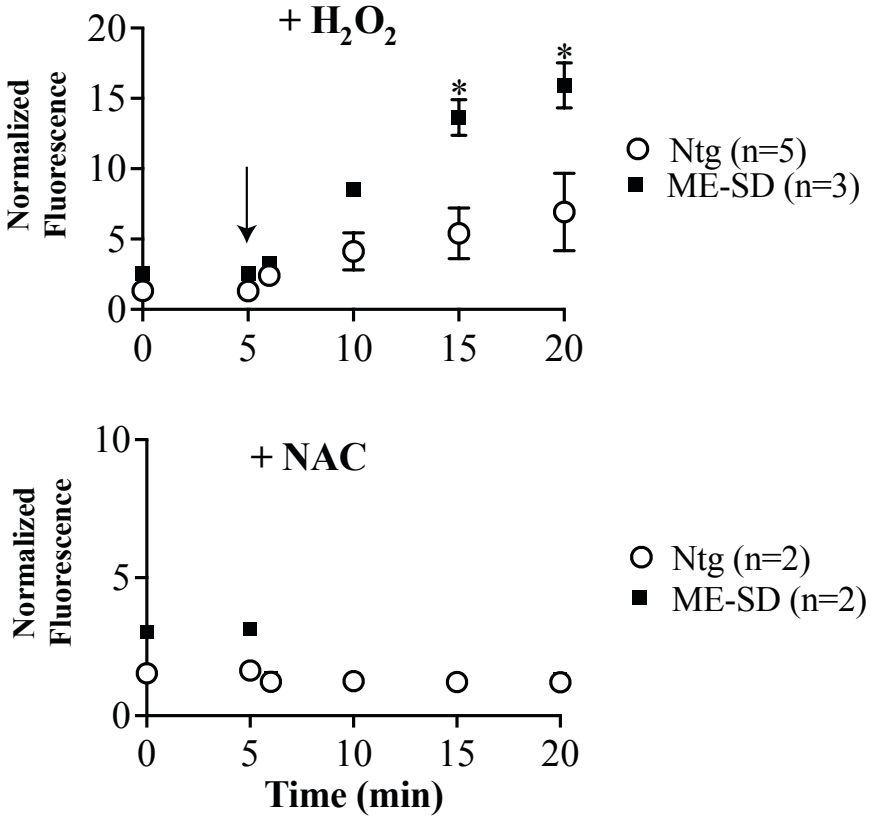

Supplemental Figure 4.5 ROS production in isolated mitochondria from 3 mos old ME-SD compared to ntg mitochondria. The production of ROS in mitochondria loaded with CMH_2DCF-DA is followed over 20 min in response to H_2O_2 (middle panel) and after the addition of both the H_2O_2 and ROS inhibitor, N-Acetyl Cysteine (lower panel). Arrows indicate addition of 1mM H_2O_2 in the absence (upper panel) and presence of N-Acetyl Cysteine (lower panel). Results are expressed as mean, and when appropriate the SEM are also reported (n= number of hearts). Simple linear regression analysis was conducted to compare the slopes of each line with statistical significance set to $p<0.05$. Statistical analysis shows increased ROS production by cTnI ME-SD compared to ntg samples in response to H_2O_2, as the slopes of H_2O_2-treated cTnI ME-SD is significantly different from the ntg ($p<0.05$ vs ntg; ntg: slope ± SEM = 0.3085 ± 0.086, $R^2 = 0.3151$; ME-SD slope ± SEM = 0.7879 ± 0.0686 $R^2 = 0.857$).

Chapter 5

Asparagine (N) Functions as an Appropriate Non-Phosphorylatable Substitution in Cardiac Troponin I at S43/45

Vani S. Ravichandran, Tabea M. Schatz, and Margaret V. Westfall

Abstract

Elevated protein kinase C (PKC) expression and activity, along with downstream phosphorylation of cardiac troponin I (cTnI) at S43/45 are linked to cardiac dysfunction. While chronic cTnIS43/45 phosphorylation is postulated to be a sarcomeric node for pathologically modulating contractile function in the heart, the exact functional *in vivo* impact of phosphorylation at this site remains unclear. To partially address this issue, the current set of studies determine if contractile function is similar to wildtype mice using a non-phosphorylatable substitution at this site. Previously, the conventional non-phosphorylatable substitution with nonpolar alanine (A) at cTnI S43/45 diminished basal myocyte and contractile function. Thus, alteration of contractile function by this substitution produces a response similar to PKC-induced phosphorylation at this site. As an alternative, we postulate that asparagine (N) at cTnIS43/45 acts as non-phosphorylatable substitution without overt effects on *in vivo* cTnI function. The generation of transgenic (tg) mice expressing cardiac-specific cTnI S43/45N to test this idea display *in vivo* cardiac function comparable to non-transgenic (ntg) littermates. In addition, structural or functional remodeling is absent in these mice for up to at least four months of age. These findings suggest the novel N substitution acts as a "functionally conservative" non-

phosphorylatable substitution at cTnI S43/45 in murine myocardium. The results also provide a foundation for future work testing whether this cTnIS43/45N substitution blocks and/or attenuates PKC-induced sarcomeric and cardiomyocyte contractile dysfunction.

Introduction

Protein kinase C (PKC) phosphorylation of cardiac troponin I (cTnI) at S23/24, S43/45, and T144 is well-documented for heart failure [69]. The S23/24 cluster accelerates relaxation during β-adrenergic stimulation by increasing the rate of dissociation of Ca^{2+} from cardiac troponin C (cTnC) [66, 70, 115]. However, the function of the cTnI S43/45 and T144 sites are less well characterized [10, 64, 69, 70, 111, 112, 240]. The role(s) of S43/45 is particularly important, given its elevated level of phosphorylation during heart failure (HF), along with elevated PKC activity [68, 69]. As a result, S43/45 is the focus of the current study.

Previous work suggests cTnI S43/45 phosphorylation acts as a dominant brake on contractile function by reducing Ca^{2+} sensitivity and maximum tension in the myofilament, sliding velocity in *in vivo* motility assays, and the rates of contraction and relaxation in cellular studies [3, 5, 240]. Historically, phospho-null/non-phosphorylatable substitutions are useful in evaluating the function of a phosphorylation site. The traditional phospho-null alanine (A) substitutions attenuate or block second messenger-induced responses because downstream site-specific phosphorylation is absent [244]. To adequately serve this purpose, function measured in samples with a phospho-null substitution should be comparable to wildtype when there is minimal phosphorylation of a site. In other words, the A substitution is "functionally conservative" in the absence of phosphorylation.

Based on the extensive use of A as a non-phosphorylatable substitution, previous investigators assumed cTnIS43/45A was functionally conservative and therefore, could show whether this site contributes to basal *in vivo* contractile function, and/or attenuates PKC-induced contractile dysfunction [66, 117, 245]. Instead, cTnI S43/45A contributed to confusion about the *in vivo* role played by this site. In one mouse model, the PKC agonist, endothelin increased

the rate of contraction and slowed relaxation in isolated myocytes after complete replacement of wildtype cTnI with cTnI containing A substitutions at the PKC-targeted S23/24, S43/45, and T144 residues, and abbreviated as cTnIAla$_5^{nb}$ [113, 114]. In contrast, multiple *in vitro* studies show cTnI S43/45 phosphorylation reduces cardiac contractile function [3-5]. In addition, the authors failed to compare basal contractile function in wildtype cTnI- versus cTnIAla$_5^{nb}$-expressing myocytes in the absence of the PKC agonist. Further analysis of the published data indicates cTnIAla$_5^{nb}$ myocytes develop dramatic decreases in myofilament Ca^{2+} sensitivity compared to wildtype cTnI. A similar Ca^{2+} sensitivity shift along with a reduction in maximum actomyosin ATPase activity also was reported in myofilament studies with cTnIS43/45A alone under conditions with no detectable cTnI phosphorylation [101]. These findings indicate A substitutions at S43/45 alter contractile function independent of cTnI phosphorylation.

There is also earlier work on the impact of the cTnIS43/45A alone. In a mouse model expressing cTnIS43/45A, there was little *in vivo* impact on cardiac function under basal conditions, and although the level of S43/45A replacement in mice was not specifically measured, it was predicted to be 50% [117, 245]. While this maintenance of cardiac function is desirable, the low replacement level could mitigate the ability of this model to act as a typical phospho-null if PKC phosphorylates the remaining endogenous cTnI in these hearts. In contrast, cellular studies from our laboratory achieved >50% replacement of endogenous cTnI with cTnIS43/45A, which reduced contractile function. Overall, the findings regarding the impact of cTnIS43/45A are largely consistent in the literature [113, 114, 116, 119], and suggest A is not a functionally conservative substitution at cTnIS43/45.

These earlier studies indicate a different strategy is necessary for developing a cTnIS43/45 phospho-null mouse model. Previous cellular work established that a polar

asparagine (N) substitution is a non-phosphorylatable substitution at S43/45, and it does not cause alterations in basal myocyte function [119]. As a result, we developed a mouse model with the cTnI S43/45N substitution to test whether this substitution maintains basal contractile function without detectable structural remodeling compared to ntg hearts. Results from these mice support our previous cellular findings, and may lay the groundwork for future studies testing whether PKC-induced cardiac dysfunction is ameliorated in hearts expressing cTnI S43/45N.

Methods

Animal Model

Transgenic mouse development. Animals generated and studied here were approved by the University of Michigan Institutional Animal Care and Use Committee and with the care and use of these animals following the PHS policy on Humane Care and Use of Laboratory animals. The cTnIS43/45N substitutions were incorporated into cTnI cDNA as described previously [5]. Briefly, the construct was inserted into a ~9.9 kb plasmid under the control of a minimal 4.5 kb α-myosin heavy chain promoter and 1.2 kb human GH poly-adenylation signal at the Sal-I site [219]. To generate transgenic (tg) mice, a 7kb Not-I plasmid fragment was purified and injected into C57BL6/J x SJL F1 mouse eggs and transferred into pseudo-pregnant females. Two separate lines of tg founder mice were generated, confirmed by polymerase chain reaction (PCR) with custom primers (Table 5.1; Geno2), and categorized into high (HE-) and low (LE-) expressing cTnI S43/45N (SN) mice based on Southern blot analysis of copy number using purified Bam-H1 digested liver DNA [246]. The HE-SN line is used for all functional studies. Copy number was verified using purified heart DNA analyzed in triplicate by quantitative PCR (qPCR) analysis with custom FAM-NFQ/MGB cTnI primers (Table 5.1) plus the VIC-TAMRA TFRC copy number reference assay (Thermo; 4310892E) in a Step-One Plus real time PCR system.

Table 5.1 Primers for Q/RT-PCR

Protein Encoded	Primer Name	Primer Sequences (5'-3') or commercial catalog
cTnI		Fw: ATGGCGGATGAGAGCAGCGATG Rev: CAATGTCCTCCTTCTTCACCTGCTTG
cTnI S43/45	CTNI1Q	Fw: AACCGGTGGGACATTTGAGTT Rev: TGGACCCAACGCATGAGA Probe: TTGCTTGGCACTGTC TFRC normalized Fisher Cat #4458367
Atrial Natriuretic Peptide (ANP)	NPPA	Mm01255747_g1 (Applied Biosciences)

Myofilament studies

Sarcomere replacement, incorporation, and thin filament stoichiometry were determined in hearts from 3 month (mos) old cTnI HE-S43/45N (SN) mice and nontransgenic (ntg) littermates. Myofibrils (50 μg) prepared from cTnI HE-SN and ntg littermates hearts [119] were separated on 12% SDS- polyacrylamide gels (PAGE) and stained overnight with Coomassie blue. The band containing cTnI at ~25 kDa was excised prior to trypsin digestion and purification, as described in chapter 4. The trypsin-digested band is analyzed using established AQUA peptides together with tandem mass spectroscopy (MS/MS) [69].

Thin filament stoichiometry was analyzed using 100 μg of whole cell lysates prepared from HE-SN and ntg hearts pulverized in liquid N_2, diluted in ice-cold sample buffer and stored at -80^{o}C [5]. Prior to separation on 12% SDS-PAGE gels, samples were boiled for 2 min, and sonicated in an ice bath for 10 min. Proteins from the gel were transferred to a PVDF membrane [5], and then probed with anti-troponin I (TnI) and anti-tropomyosin (Tm) primary antibodies ([4]; Table

5.2) followed by horseradish peroxidase (HRP)-conjugated goat anti-mouse (GAM) secondary antibody (Ab). Blots were imaged using a ChemiDoc MP imager and quantitated with ImageLab software (BioRad).

Table 5.2 Antibodies used for Western blot

Primary Antibody	**Catalog #**	**Dilution**	**Secondary Antibody**
Troponin I (TnI)	Sigma mAb1691 (C5 Clone)	1:1000	Goat anti-mouse (1:1000)
Tropomyosin (Tm)	Novus Biologicals T2780 (Clone Tm311)	1:10000	

Phenotypic Characterization

Morphology and histology. Structural evidence of remodeling was analyzed using morphology measurements and histological staining. Hearts were collected at 1, 2 and 3 mos of age for morphological comparison of heart weight/tibial length ratios from ntg and S43/45N mice. Structural analysis by histology was performed on formaldehyde fixed, paraffin-embedded 4-5 μm coronal sections from ≥3 mos-old S43/45N and ntg mice stained with H&E to determine myocyte and myofibrillar organization [223], and picrosirius Red (PR) to assess fibrosis [223, 224]. Pulmonary congestion, which is an indicator of congestive heart failure, was monitored with wet/dry lung weight ratios measured using 2 lobes of lungs excised from 2 and 3 mos old mice and weighed immediately after removal for wet weights. Dry weights were determined after placing lungs in a 55^{o}C incubator for ≥3 days.

Analysis of cell morphology. Cellular remodeling was monitored 2 and 3 mos old cTnISN and ntg mice. Rod-shaped, Ca^{2+}-tolerant cardiomyocytes were isolated as described in detail in Chapter 3 [91] and length-to-width aspect ratios of cells were determined using a Nikon Eclipse Ti-S Phase Contrast microscope. Specifically, 3-6 mice were sacrificed per genotype, and length and widths (μm) measured for 10 representative cells/coverslip and 3 coverslips/mouse prep. The L/W aspect ratios were calculated for comparison between tg vs ntg mice.

Cardiac function with echocardiography. In vivo cardiac function was measured in collaboration with the University of Michigan's Physiology Phenotyping Core. Isoflurane anesthetized mice from 1, 2, and 3 mos-old S43/45N and NTG mice were analyzed by 2D M-mode (short axis), B-mode (long axis), plus pulse wave and tissue Doppler echocardiography using the Vevo 2100 system, as described in chapter 4.

Statistical Analysis

Data are represented as mean +/-SEM. Statistical comparisons were made using a Student's t-test, or one or two-way analysis of variance (ANOVA) where appropriate by PRISM (Graphpad version 9). A Tukey's posthoc test was used for 2-way ANOVAs. The specific statistical test used for each group of data are described in the figure legends. For each comparison, statistical significance set at $p<0.05$.

Results

Quantification of copy number (Fig. 5.1A) in the 2 separate lines indicates high (>10 copies; HE-SN) and low (<5 copies; LE-SN) copy numbers in tg mice, which are validated by qPCR analysis of cardiac DNA (results not shown). In the sarcomere, transgenesis results in replacement of endogenous protein rather than in overexpression of exogenous protein [109]. In HE-SN tg mice, cTnISN replaces 30% of endogenous cTnI and 0% in ntg littermates (Fig. 5.1A-B). Thus, the remainder of this study focuses on analyzing whether there are alterations in basal cardiac structure and function in this HE-SN line. Western blot analysis of whole cell lysates shows that the cTnI/Tm ratio remained comparable between each cTnISN line and ntg mice (Fig 5.1C), and is consistent with preservation of stoichiometry in the sarcomere [109]. MS/MS-derived replacement together with maintenance of thin filament stoichiometry, and earlier work showing *in vitro* sarcomere incorporation of cTnISN are consistent with cTnISN expression and replacement of endogenous cTnI in the sarcomere [119].

In addition to altered function, hypertrophy developed in the cTnIAla$_5^{nb}$ mouse expressing cTnIS43/45A [113, 114]. Thus, cTnISN could initiate hypertrophy and/or remodeling, if this substitution is not functionally conservative. To test for this possibility, RNA expression of NPPA is measured, which encodes for atrial natrieuretic peptide (ANP) and is used a molecular marker for hypertrophy. This qPCR analysis indicates an absence of hypertrophy in 1-3 mos old HE-SN mice (Fig. 5.2A). Morphological analysis confirmed a lack of hypertrophy, as heart weight-to-tibia (HW/TL) length ratios are similar in cTnISN and ntg mice (Fig. 5.2B). Additional characteristics of cardiac hypertrophy, such as collagen deposition/fibrosis and myocyte disarray also are absent in histological H&E and picrosirius red stained heart samples (Fig. 5.2C), along with an absence of pulmonary congestion evaluated by measuring wet-to-dry

lung weights (Fig 5.2D). Pulmonary congestion is also a hallmark sign of cardiac dysfunction and heart failure [247], and is elevated in earlier heart failure models [222]. Finally, the length and width of 30 representative cells from 2 and 3 mos old mice do not differ in S43/45N compared to age-matched ntg myocytes (Fig. 5.2E). Taken together, molecular, morphological, histological and cellular analysis provide no evidence of cardiac hypertrophy and/or remodeling in cTnI HE-SN mice by 3 mos of age.

Two-dimensional M-mode echocardiography determine whether cTnISN causes any alterations in cardiac function (Fig. 5.3). No detectable differences in ejection fraction (EF) or fractional shortening (FS), which are indices of cardiac systolic function (Fig. 5.3B-C), are identified in cTnISN mice by 3 mos of age, nor are there detectable differences in heart rate (Fig. 5.3A) or in echocardiography-derived cardiac dimensions (Fig. 5.3E-F). B-mode measurements in cTnISN and ntg mice corroborate this finding (results not shown). Further analysis by pulse-wave and tissue doppler also demonstrate no change in diastolic function, including the lack of change in E/A ratio (Fig 5.3D). Collectively, the results indicated that S43/45N is a viable substitution to use as a non-phosphorylatable residue at cTnI S43/45.

Discussion

Results presented in this study show ~30% replacement with S43/45N in mouse hearts (Fig. 5.1) results in *in vivo* cardiac function comparable to ntg littermates (Fig. 5.3), and an absence of hypertrophy and remodeling (Fig 5.2). Previous studies indicate that phosphorylation of S43/45 acts as a dominant brake on contractile function [4, 5, 248]. However, earlier efforts to generate a phospho-deficient cTnIS43/45A, resulted in functional changes similar to phospho-mimetic aspartic acid (D) or glutamic acid (E) substitutions at this cluster [5, 113, 114, 116]. This *in vivo* replacement together with earlier *in vitro* studies using cTnISN are consistent with N acting as a functionally conservative substitution [116, 119]. Further work in these mice is desirable to determine if cellular contractile function also is maintained in HE-SN mice, and is consistent with previous results in rat myocytes expressing cTnISN after cellular gene transfer [99].

In previous studies, the reduced myofilament Ca^{2+} sensitivity and contractile function in mice with cTnIS43/45A added to the complexity arising from different *in vitro* versus *in vivo* responses produced by phospho-mimetic and/or phospho-deficient cTnI S43/45 substitutions [66, 111-114]. A non-phosphorylatable substitution that does not change cardiac function by itself is highly desirable to gain a thorough understanding of the functional impact produced by PKC-targeted S43/45 phosphorylation. The development of the current cTnISN model brings this field one step closer to testing whether PKC-targeted phosphorylation of cTnIS43/45 causes significant cardiac dysfunction.

The differences in contractile function with the A versus N substitutions at cTnIS43/45 most likely depends on the properties of the individual amino acids. Previous studies suggest that

cTnI S43/45 phosphorylation may alter interactions between cTnI and cTnC [118]. It is possible that removing polarity from this cluster further alters this interaction, which may explain why the A substitution disrupts contractile function at this cluster, while N preserves function (Fig. 5.4). The S43/45 cluster sits at the beginning of the H1 helix, and in the 3-dimensional crystal structure this cluster is in close proximity to the inhibitory peptide (IP) and H3 helix. As a result, S43/45 could interact with one or both of these domains to play a significant role in modulating switch function within cTnI. Phosphorylation at this critical cluster also could alter H1 helix rigidity, which alters switch function by the IP and H3 domains, or influences downstream switch functions mediated by the I-T arm of the Tn complex. Thus, choosing a phospho-null amino acid for use at this critical site requires careful consideration. Biochemical properties of other small amino acids indicate that N may be a viable alternative to A. Glycine, while small and nonpolar like alanine, is flexible and could cause additional disturbances in this critical region of cTnI. Cysteine is a reasonable option as it is small but given the presence of other cysteine residues within troponin, there is a reasonable risk of forming disulfide bonds and further confounding the results. Other possibilities include proline, a known helix-breaker, sterically bulky valine, or phosphorylatable threonine. Thus, a polar R group may be critical for maintaining cTnI function at S43/45 [119], making N a superior alternative to A (Fig. 5.4). It is important to note that this work does *not* suggest eliminating the use of A as a non-phosphorylatable residue at other sites in sarcomeric proteins. However, the rationale for the use of N in this study is that A does not function conservatively at cTnI S43/45. Understanding the impact of non-phosphorylatable S43/45 provides a more concrete understanding of the role played by S43/45 within the sarcomere.

The current transgenesis approach resulted in <50% replacement of endogenous cTnI. As a result, this mouse model is expected to be inadequate as a phospho-null mouse. Instead, complete replacement of endogenous cTnI by cTnIS43/45N is predicted to be necessary to test whether cardiac dysfunction is prevented by blockade of S43/45 phosphorylation during PKC activation. For this amino acid cluster, a mouse model with 100% cTnISN replacement is more likely to be achieved via a knock-in strategy, and using this approach is desirable in the future. A homozygous knock-in mouse could more definitively answer whether the lack of phosphorylation at cTnI S43/45 has an impact on basal function, and whether the absence of phosphorylation at S43/45 protects against cardiac dysfunction during chronic PKC activation. However, results from the current mouse in concert with previous cellular findings are consistent with the idea that PKC-targeted cTnI S43/45 phosphorylation is detrimental to cardiac, cellular, and myofilament function, while the lack of phosphorylation at this site is not. A knock-in approach also could address whether a threshold level of phosphorylation is required to induce a contractile or cardiac phenotype.

Future studies are expected to further elucidate the *in vivo* role of cTnIS43/45, as well as the functional impact of *in vivo* cTnIS43/45 phosphorylation. Further work using the current model could help determine whether cTnISN protects against dysfunction during chronic PKC phosphorylation of S43/45, which is possible during conditions leading to progressive heart failure, such as hypertension/diabetes [9, 242, 243]. Future studies are also needed to determine if this phospho-deficient substitution could attenuate cardiac dysfunction and remodeling when crossed with cTnIS43/45D mice and/or during sustained PKC activation by agonists and/or neurohormones. Future studies using the current model along with development of a knock-in mouse model having 100% cTnISN replacement would deepen understanding of the impact of

these critical residues and add to current understanding of how troponin I modulates contractile function in the heart.

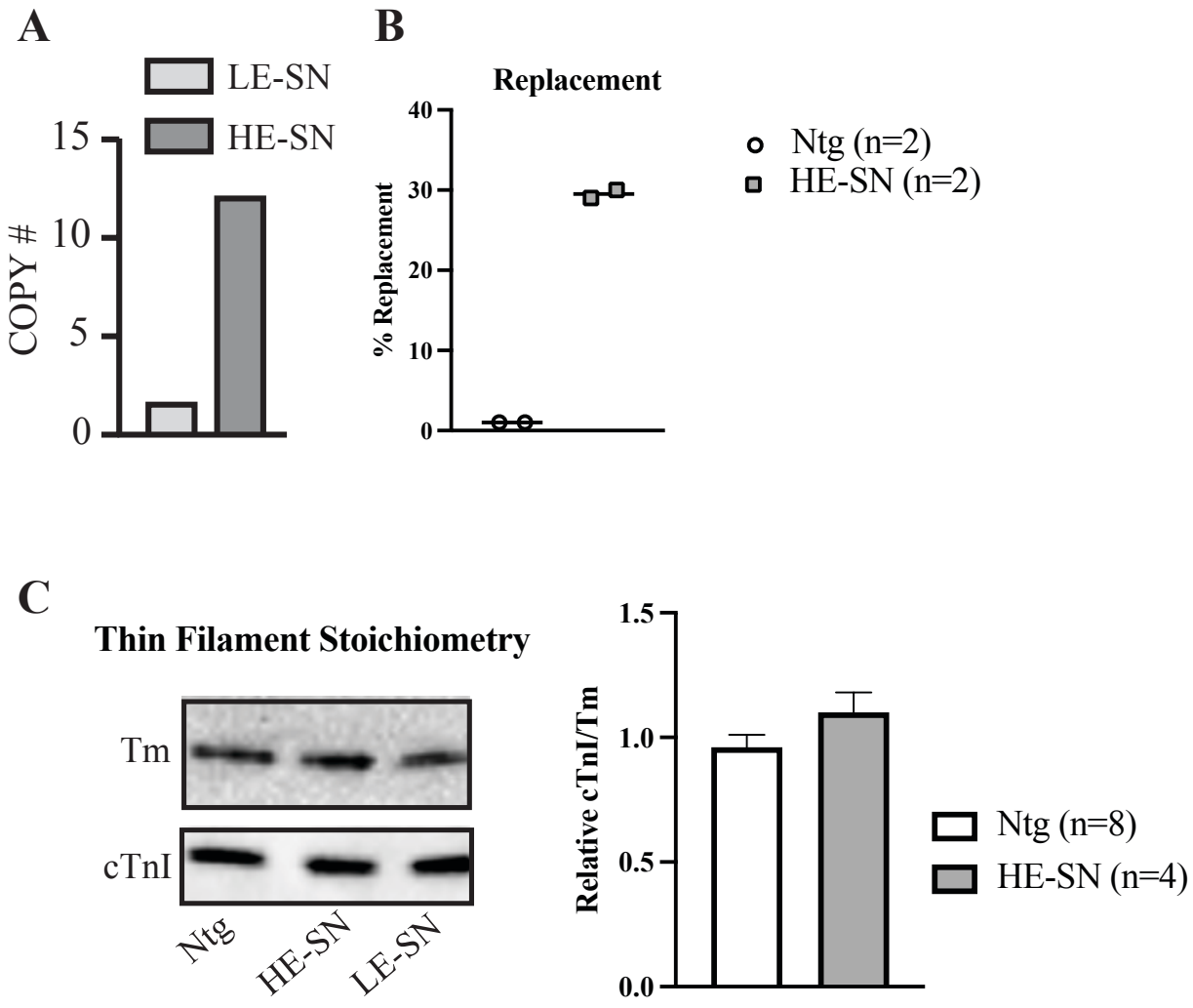

Figure 5.1 Analysis of copy number, replacement level and thin filament stoichiometry. A, Southern blot quantification of cTnISN mice in 2 lines of mice. Lines are designated as low (LE)- and high (HE)- expressing cTnISN mice. **B,** AQUA and MS/MS analysis of myofilaments from ntg and cTnI HE-SN mice (n=2) showed 30% replacement of endogenous cTnI with cTnISN in the HE-SN line. There was no cTnISN detected in ntg mice. **C,** Western analysis shows cTnI and Tm expression in myofilaments from ntg, plus cTnI HE-SN and LE-SN mice (left panel). Quantitative analysis of cTnI/Tm ratio (right panel) shows no differences between cTnI HE-SN and ntg samples, which indicates preserved thin filament stoichiometry in cTnISN mice. The n is listed on each figure panel. For graphical comparisons, a Student's unpaired t-test was performed with significance set to $p<0.05$.

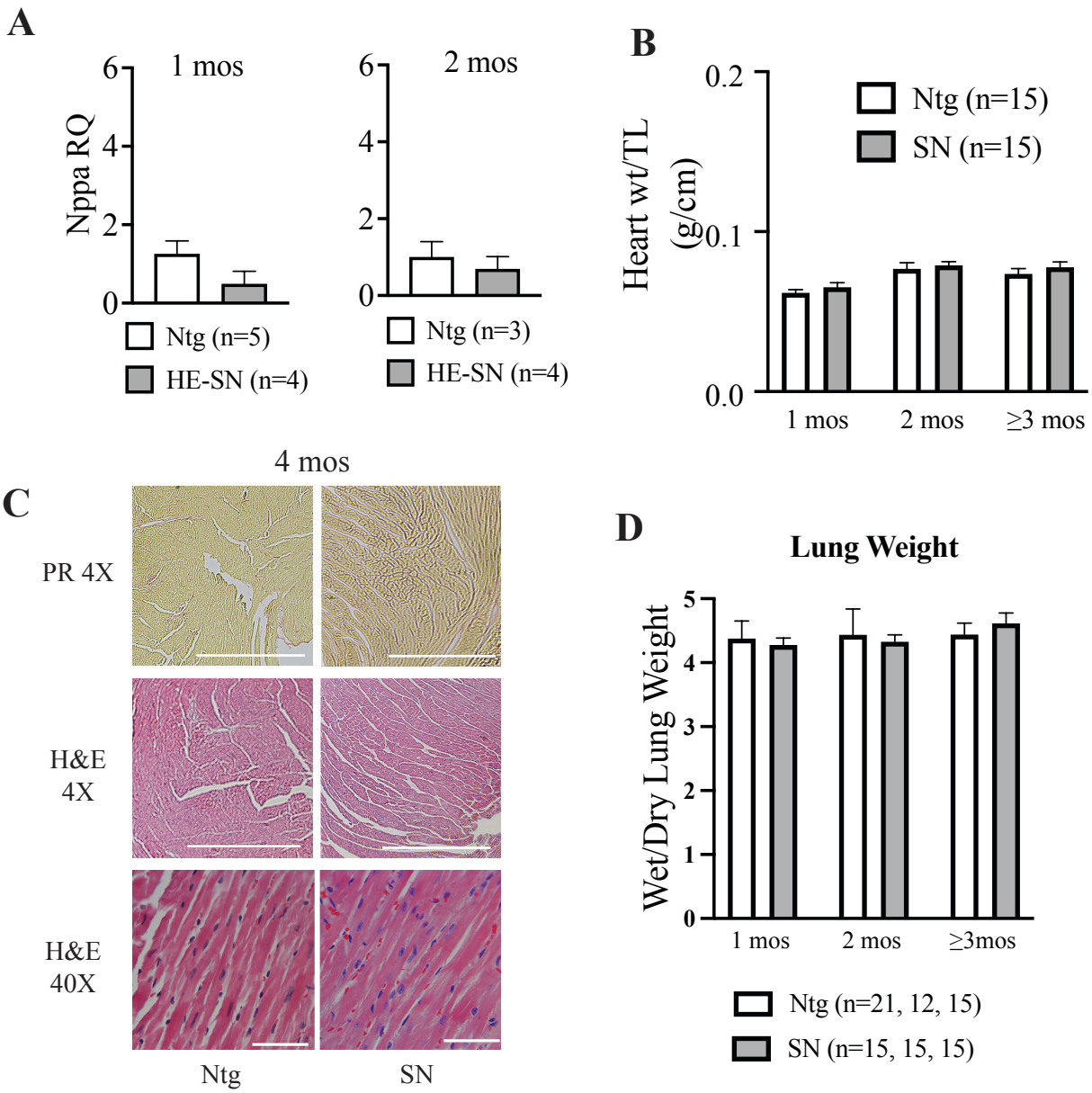
A
1 mos
2 mos
Nppa RQ
6
4
2
0
Ntg (n=5)
HE-SN (n=4)
Ntg (n=3)
HE-SN (n=4)
B
Heart wt/TL (g/cm)
0.2
0.1
0.0
Ntg (n=15)
SN (n=15)
1 mos
2 mos
≥3 mos
C
4 mos
PR 4X
H&E 4X
H&E 40X
Ntg
SN
D
Lung Weight
Wet/Dry Lung Weight
5
4
3
2
1
0
1 mos
2 mos
≥3mos
Ntg (n=21, 12, 15)
SN (n=15, 15, 15)
E
L/W ratio
15
10
5
0
Ntg (n= 6, 6)
SN (n= 3, 6)
2 mos
≥3 mos
Width (μm)
50
25
2 mos
≥3 mos

Figure 5.2 Analysis of ntg and cTnI HE-SN hearts for structural remodeling and hypertrophy. A, NPPA transcript levels in 1 (left panel) and 2 (right panel) mos old cTnI HE-SN are not different from ntg hearts when analyzed by qPCR ($p>0.05$). **B,** The heart weight-to-tibial length (TL) ratio also is not significantly different in cTnI HE-SN vs ntg mice between 1 and 3 mos of age ($p>0.05$). **C,** Paraffin- embedded ventricular sections from 4 mos-old cTnI HE-SN and ntg mice were stained with PR to detect fibrosis (top panel) or H&E to detect cardiomyocyte disarray (middle, bottom panels). The histological images indicate no significant fibrosis or disarray in hearts from cTnI HE-SN vs ntg mice. H&E is shown at 4X (middle) and 40X (bottom) for ease of viewing. Scale bars 500µm for 4X images; 50µm for 40X images. **D,** The lung wet/dry weight ratio is similar in cTnI HE-SN and ntg mice between 1-3 mos of age ($p>0.05$). **E,** Length-to-width aspect ratios measured in isolated Ca^{2+} tolerant cardiomyocytes indicate no cellular hypertrophy in hearts from cTnI HE-SN compared to ntg mice. Widths are provided to illustrate the lack of concentric hypertrophy. The n for each experiment is listed in each figure panel. For **A,** Results were compared using a Student's unpaired t-test with statistical significance set to $p<0.05$ (*). For **B-E,** two-way ANOVA analyses were conducted, with statistical significance set to $p<0.05$. None of these comparisons showed a significant difference between ntg and S43/45N samples ($p>0.05$), and thus, no post-hoc analyses were performed.

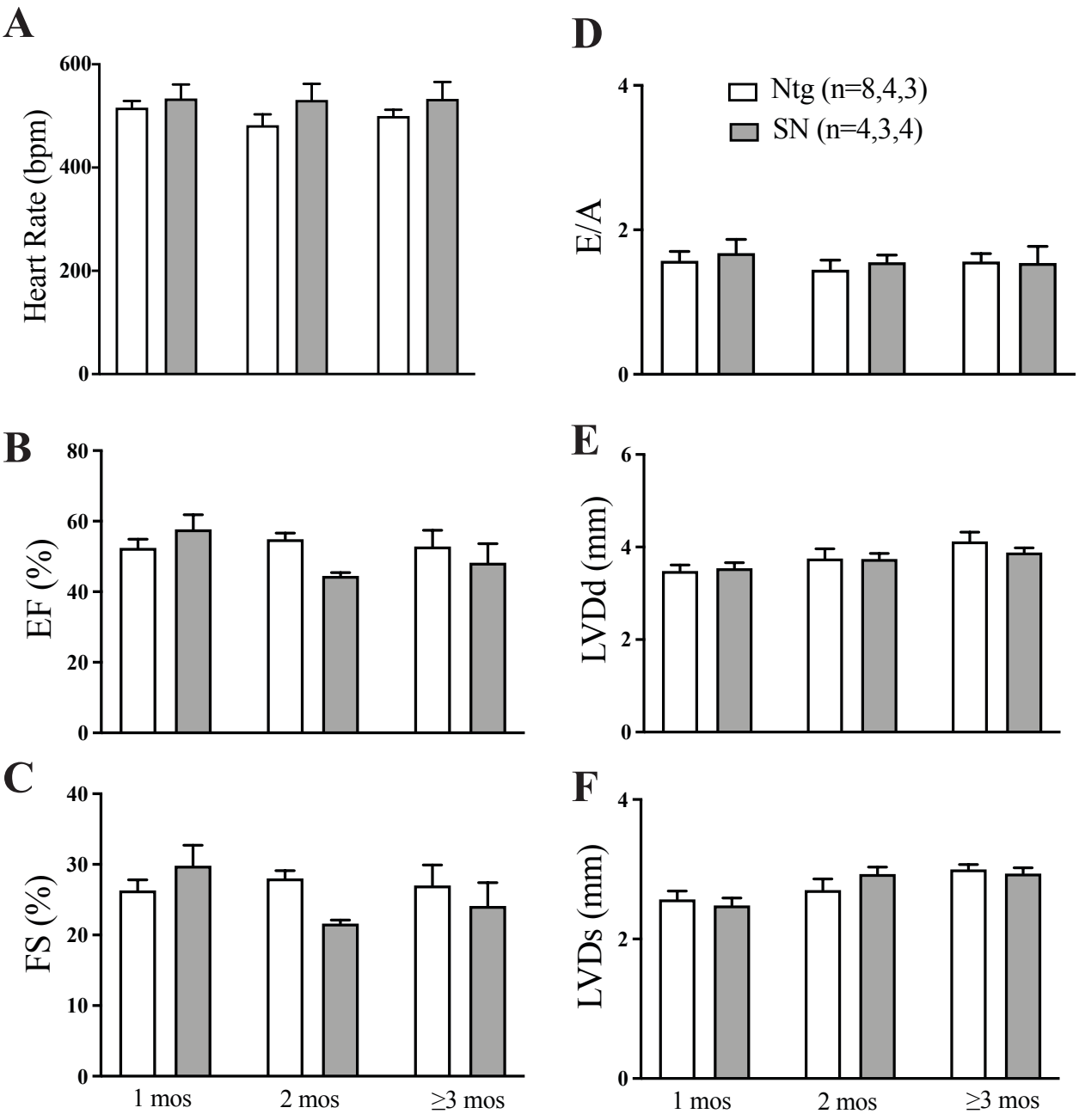

Figure 5.3 Two-dimensional (2D) echo analysis shows no changes in *in vivo* cardiac function in cTnI HE-SN compared to ntg mice between 1-3 months of age. A-C, Echocardiography analysis shows that cTnI HE-SN mice maintain heart rate and systolic function, as measured by ejection fraction (EF) and fractional shortening (FS). **D,** Pulse-Wave Doppler imaging shows no change in diastolic function based on the lack of change in E/A ratio. **E-F,** echocardiography additionally does not detect *in vivo* cardiac remodeling using the left ventricular dimension at end diastole (LVDd) and at end systole (LVDs). The number of mice (n) for each experiment is indicated in the figure. Statistical analysis was performed by a 2-WAN, with statistical significance set to $p<0.05$. Post-hoc tests were not performed, as there was no significant difference between results from ntg and cTnI HE-SN mice ($p>0.05$).

Small/Tiny Amino Acids for cTnI S43/45 replacement

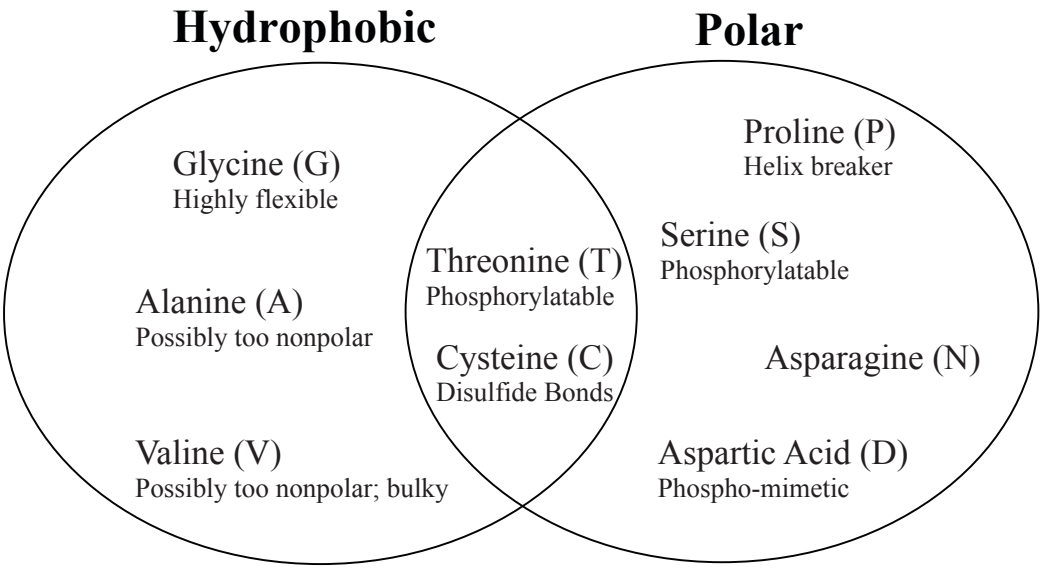

Figure 5.4 Possible substitutions for use at cTnI S43/45. A schematic representation of small and tiny amino acids based on chemical and physical properties. Properties that may confound the ability to use a residue as a phospho-deficient substitution at S43/45 are listed below the name and single-letter abbreviation of each amino acid. To achieve phospho-deficiency at cTnI S43/45, asparagine was chosen due to its relatively small size and polar properties.

Chapter 6

Conclusions and Future Directions

PKC: An Enigma

Despite over forty years of study, protein kinase C (PKC) remains one of the more enigmatic kinases due to its myriad roles in each organ and in pathophysiology [249]. Further investigation into PKC's role in pathological signaling is needed, as the relationship between PKC and heart pathology is still correlative. The mere existence of many PKC isoforms suggests that PKC's may have functionally divergent roles in different cell types (Fig. 1.5). A deeper understanding of PKC targets and their biological roles would greatly help to advance the understanding of PKC signaling in the heart and during heart failure.

More advanced knowledge about PKC may also enable the successful pursuit of PKC as a therapeutic target in heart failure and in other pathologies. Successfully targeting PKC in pathology is difficult because: i) close sequence homology of PKC isoenzymes makes designing pharmacological agents to target PKC challenging; ii) adaptive increases in expression and activity of PKC isoenzymes makes it difficult to study the role of each isoenzyme; and iii) there is no canonical model with which to fit PKC signaling in the heart. Despite these obstacles, PKC is implicated in many cardiovascular diseases [9-11] and developing a deeper understanding of its function in various contexts can inform rational drug design for pathologies related to upregulated PKC activity.

PKC phosphorylation of cTnI

The *in vivo* role of PKC-induced cTnI S43/45 phosphorylation (p-S43/45) also is controversial due in part to unpredicted phenotypes in animal models [66, 111, 112]. Results presented in Chapter 2 of this dissertation show a strong correlation between PKC-targeted cTnI p-S43/45 and heart failure. The functional results also are consistent with prior work showing p-S43/45 diminished contractile function on a cellular and myofilament level [3-5]. The increased PKC expression in human heart failure, along with elevated S45 phosphorylation, indicate chronic phosphorylation of this cluster develops during progressive heart failure (Ch. 2; Fig. 2.1, Supp Fig 2.2). The modest reduction in phosphorylation at S45 after VAD together with improved cellular contractile function (Fig. 2.1) suggests that phosphorylation at this residue reversibly diminished contractile function in response to mechanical unloading.

Studies in chapter 2 also focused on the PKCα isoform during heart failure. In a proof of concept experiment, dominant negative PKCα improved myocyte shortening in rat models of heart failure and aging to highlight the pathological role for PKCα in heart failure (Fig. 2.2). Contractile dysfunction correlated with a dispersed distribution of PKCα following pressure overload, compared to the tight accumulation of PKCα around intercalated disks in sham control rats (Supp Fig. 2.3). Ca^{2+}-activated PKCα is expected to congregate around the intercalated disk within the cardiomyocyte, which also contains many ion channels, including Ca^{2+} involved in PKC activation ([91]). The explanation for the trafficking pattern and potential PKCα localization to the myofilament is unclear, and further investigation is needed to understand both phenomena in cardiomyocytes. Given the domain structure of classical PKCs, it is also difficult to visualize how an activated classical PKC phosphorylates cTnI without a nearby membrane anchor, but cleavage or alterations within the regulatory domain to produce a constitutively

active PKCα [90] could result in the altered trafficking and/or localization to myofilaments. Additionally, kinase docking within the myofilament to phosphorylate cTnI is unclear, and could instead target newly synthesized cTnI as it is shuttled and incorporated in the sarcomere. Future work to address these questions could employ reagents such as PKC-labeled for FRET {Swanson, 2014 #474} to provide insight into this question.

Prior work showed the cTnI p-S43/45 sites work independently but not additively to act as dominant breaks on contractile function [3-5]. This cluster also modulated phosphorylation at other sites within cTnI [4, 5, 116, 248], as shown for cTnI residues S23/24, and T144 [4]. More importantly, the ability of p-S43/45 to reduce contractile function can be modified by phosphorylation at least one other site cTnI, as illustrated by the less severe contractile dysfunction observed in myoytes expressing phospho-mimetic cTnI S23/24/43/45D (S4D) [4]. In contrast, S43/45 remained a more dominant negative modulator of contractile function in myocytes expressing a cTnI S43/45D+T144D (SDTD) construct [4]. These earlier findings together with the development of progressive cardiac dysfunction and early mortality in cTnIS43/45D-expressing mice (Fig. 4.2) indicate this site may be a central node for modulating contractile function in the heart. A mouse expressing phospho-mimetic substitutions on 2 different cTnI proteins (cTnIS23/24D and cTnIS43/45D) could test this idea.

While dysregulated myocardial contraction is often linked to alterations in Ca^{2+} handling [250] the current work shows cardiac dysfunction also develops in response to chronic changes within the sarcomere. Specifically, work presented in chapter 4 showed the onset of significant contractile dysfunction by 2 mos of age in mice expressing phospho-mimetic cTnIS43/45D in myocardium (Figs. 4.2-4.3). While Ca^{2+} transients did not change in myocytes isolated from these mice, alterations are likely to develop at a later stage of progressive dysfunction. A key

conclusion from the work in the cTnIS43/45D mouse models is that cardiac dysfunction originates within the sarcomere before significant changes develop in Ca^{2+} handling. To better understand sarcomere-based dysfunction in the future will require insight into the complex molecular switching mechanism within the Tn complex including S43/45 interactions with other cTnI phosphorylation sites These insights are needed to achieve the long-term goal of decoding functional responses caused by dynamic changes in the sarcomere.

Chronic phospho-mimetic cTnIS43/45D (SD) caused dose- and time-dependent *in vivo* cardiac dysfunction in mice, with initial cardiac dysfunction originating from the sarcomere (Fig. 4.2B, S4.1) and later onset of remodeling and progressive deterioration in cardiac function (Fig. 4.2-4.3) resulting from alterations beyond the sarcomere. The chronic negative charge at cTnIS43/45 may disrupt a sarcomere "steady state" to which the sarcomere responds followed by changes throughout the cardiomyocyte. This idea is supported by previous work showing that phosphorylation at S43 and S45 resulted in secondary phosphorylation in other regions of cTnI [4, 248].

To address the later changes in function, studies in chapter 4 tested whether chronic cTnIS43/45D in the sarcomere triggers early alterations in mitochondria. While compromised mitochondrial function is well-documented in end-stage heart failure [125], our work tested the novel idea that cardiac dysfunction originating from the sarcomere causes early mitochondrial responses to lay the foundation for progressive deterioration in heart. The rationale for this idea came from earlier studies showing that the sarcomere uses >75% of mitochondrial ATP to generate a force [124]. As a result, early reductions in function observed in cTnIS43/45D hearts could result from slowed crossbridge cycling with ATP depletion (Fig 4.5B). Although our work shows early changes, reduced energy availability is not the first change detected in mitochondria

(Fig. 4.4). Instead, the first early mitochondrial change was a dose-dependent decrease in Mt/Nuc DNA ratio observed in cTnIS43/45D hearts prior to detectable remodeling (Fig. 4.4A). Decreased Mt/Nuc DNA could indicate a decrease in mitochondrial biogenesis, or a decrease in the number of mitochondria. There is also the possibility that the decrease in mitochondrial number results from a cTnIS43/45D-induced increase in fusion. Though an interesting question, this idea was not tested here, and would require exploring complex upstream pathway(s).

Additional studies tested whether there is evidence of early oxidative stress, which could reduce the number of mitochondria [251]. In cTnIS43/45D mice, there were early increases in reactive oxygen species (ROS) production (Fig 4.6, S4.5). Upon further probing, aberrant oxidative stress preceded decreases in mitochondrial number, respiration, or adenine nucleotides (Fig 4.4-4.6). The decreased amount of a gene encoding a component of complex III (cytochrome B) as our marker for mitochondrial DNA also is consistent with early increases in mitochondrial ROS (Fig. 4.3A, 4.6A). Furthermore, this ROS production proved to be detrimental for contractile function, as targeting mitochondrial ROS with a cardiolipin stabilizer not only reduced ROS but also improved contractile dysfunction in myocytes from cTnISD mice (Fig. 4.7). These findings supported the hypothesis that sarcomere stress triggered by chronic p-S43/45 is communicated to mitochondria during an early stage of cardiac dysfunction.

The nature of sarcomere communication with mitochondria appears to rely at least in part on increased generation of ROS (Fig. 4.6). ROS can have a myriad of impacts on the cell, including intercalation into DNA, mitochondrial depolarization via enhancement of mitochondrial calcium uniporter activity, and peroxidation of nearby lipids [235, 252, 253]. Our findings also suggest the reduction in the mitochondrial ROS scavenger, SOD2 could further contribute to oxidative stress in cTnI S43/45D mouse hearts. In the future, it is desirable to

confirm reduced ROS improves contractile function in the cTnIS43/45D mouse model using genetic manipulation to increase the levels of protein scavengers. For example, a cross of S43/45D mice with mice overexpressing SOD2 (SOD2 OE) could attenuate or delay progressive dysfunction, given that there is enhanced respiration and decreased permeability transition pore opening in SOD OE mice [254, 255]. Attenuated or delayed progression of cardiac dysfunction would add further support to the idea that ROS is a primary driver of cardiac dysfunction in S43/45D hearts.

While the exact mechanism(s) involved in sarcomere communication with the mitochondria is unknown, it was promise ng to observe that the targeted mitochondrial antioxidant, CTP-03, improved SD myocyte shortening (Fig. 4.7C). This proof-of-concept therapeutic strategy was based on targeting the inner mitochondrial membrane to stabilize the primary sources of physiological ROS within the mitochondria, namely complexes I and III, as a means of mitigating contractile dysfunction (Fig 4.6-4.7 [252]). CTP-03 is the second generation version of elamipretide (also known as SS-31, Bendavia, and MTP-131), a tetrapeptide known to target and preserve cardiolipin within the mitochondrial inner membrane to stabilize electron transport and minimize aberrant ROS generation [256, 257]. While elamipretide was well-tolerated, it did not improve heart failure outcomes in clinical trials [258], although these trials focused on patients in a later stage of HF. Our data support the idea that CTP-03 improved contractile function (Fig. 4.7B) by stabilizing the mitochondrial inner membrane, although this drug could also work via additional mechanisms. Future studies to elucidate the specific cellular process(es) altered by CTP-03.

While mitochondrial dysfunction is routinely noted in HF [125], its role as an early event laying the foundation for progressive cardiac dysfunction in response to chronic changes within

the myofilament also requires further exploration. Specifically, future investigations could determine whether early *in vivo* intervention with CTP-03 can restore mitochondrial DNA levels, ETC complex stoichiometry, or the balance of ROS scavenging enzymes in the hearts of cTnISN mice. Because the novelty in these studies lies in the fact that mitochondrial dysfunction is being targeted as an *early* event, it would be important to begin CTP-03 treatment before the onset of cardiac remodeling and severe cardiac dysfunction. Important outcomes to consider include whether *in vitro and in vivo* mitochondrial alterations and contractile dysfunction are mitigated by *in vivo* delivery of CTP-03 to cTnIS43/45D mice. These studies could be especially useful to determine if mitochondrial-targeted drugs preemptively improve or delay cardiac dysfunction in patient populations with a high risk for elevated PKC activity, such as those with hypertension and diabetes [9-11].

Phospho-deficient substitutions for cTnI S43/45

This dissertation also tested for the role of cTnI p-S43/45 by showing that the phospho-deficient N substitution in cTnIS43/45N does not produce overt changes in remodeling or basal cardiac function (Fig. 5.2-5.3). The findings support prior results obtained in the Westfall laboratory which demonstrated that N is a reasonable non-phosphorylatable residue to study the *in vivo* role of cTnIS43/45 [116, 119]. In earlier work, the traditional phospho-null A residue was substituted in all PKC-targeted cTnI residues (S23/24, S43/45, T144) and 100% replacement of endogenous cTnI in the $cTnIAla_5^{nb}$ mouse model [113, 114]. Although there was no comment in the publications on this mouse, the A substitutions in S43/45 and/or T144 produced a dramatic rightward shift in Ca^{2+} sensitivity [113, 114]. *In vivo* studies also were not pursued in these mice [113, 114], although the shift in myofilament function suggests that there is likely cardiac

contractile dysfunction in these hearts. In addition, results obtained after PKC activation produced an increase in myofilament Ca^{2+} sensitivity, in contrast to *in vitro* decreases reported after cTnI p-S43/45 and/or in response to phospho-mimetic substitutions at cTnIS43/45 [5, 66, 111]. Previous work in our laboratory showed that while cTnIS43/45A decreased Ca^{2+} sensitivity in rat myocytes, comparable levels of replacement with the alternative cTnIS43/45N did not change contractile function compared to myocytes expressing wildtype cTnI [116, 119]. Though it is unclear why the A substitution reduces myofilament function at S43/45, it may cause local changes within cTnI that could alter switch function within the thin filament. While our work does not directly test whether the A substitution causes local changes in the myofilament, it does suggest that cTnIS43/45N does not cause alterations in contractile function that are comparable to cTnIS43/45A. Thus, it is crucial to carefully consider the amino acid residue chosen as a phospho-deficient substitution at this phosphorylation site. Additionally, the *in vivo* work in cTnIS43/45N mice supports previous *in vitro* findings that N is an appropriate residue for studying a phospho-deficient substitution at S43/45 [116, 119] . A future study with mice expressing complete replacement with cTnI S43/45N is highly desirable to determine whether there is a threshold needed to see any changes in basal contractile function with this substitution, and investigate whether a functionally conservative phospho-null substitution at cTnI S43/45 protects against the onset and progression of heart dysfunction in response to environmental conditions that produce increased PKC activity and heart failure, such as myocardial ischemia and/or hypertension [88, 259].

The S43/45 cluster in cTnI: A critical node for beat-to-beat regulation of contraction

Our results suggest that S43/45 serves as a critical node within cTnI for modulating contractile function, and when chronically modified or phosphorylated, it detrimentally impacts cardiac contractile function. The mechanistic changes within the thin filament caused by phospho-mimetic and/or phosphorylation of cTnI S43/45 are not known, but this cluster sits within a critical region of the 3-dimensional cTnI structure, and could have several functions (Fig. 1.4). First, cTnI S43/45 is close in proximity to the inhibitory peptide (IP) region of cTnI, which is necessary to inhibit the interaction between actin and myosin in the absence of Ca^{2+}. Thus, it is possible that p-S43/45 interferes with the switch function of cTnI by altering the ability of the IP region to toggle between actin and TnC, and therefore, inhibit and disinhibit strong force-generating interactions between myosin and actin [51] (Fig. 1.4). Additionally, it sits at the start of the H1 α-helix, which may communicate with the adjacent H2 helix that forms the IT arm along with cardiac troponin T (cTnT). It is possible that cTnI p-S43/45 could produce an increase in H1 helix rigidity, which in turn could be transmitted to the IT arm, and/or disrupt interactions between cTnI and the Ca^{2+}-binding N-lobe of cTnC [51, 118, 260]. In general, cTnI is well-conserved and there are few patient-reported mutations near S43/45. One exception is the cTnI K36Q mutation, which sits slightly upstream of S43/45 at the H1 helix, but causes a severe dilated cardiomyopathy similar to the cTnI HE-SD mice [17]. It is possible that this mutation also could disrupt the IP domain, H1 helix rigidity and/or interactions with the N lobe of TnC similar to the potential changes caused by S43/45D, and thereby damage or interrupt cTnI function during contraction [29]. While testing this possibility is outside of the scope of this dissertation research, it would be interesting to test whether altering specific amino acids in the

region between cTnI residues 36 and 45 also causes contractile dysfunction and similar dilated cardiomyopathy phenotypes.

While mechanistic insight into how cTnI p-S43/45 impacts cTnI and thin filament function at the biophysical level is poorly understood, previous studies show that phospho-mimetic cTnIS43/45 substitutions slow Ca^{2+}-binding to cTnC, slow myosin detachment from the thin filament, and place the thin filament in a conformation that is less able to be activated [3, 40, 41]. These findings together with the current results in cTnIS43/45D mice showing slowed shortening and re-lengthening indicate there is a need to consider additional states beyond the current three-state model for thin filament activation [37, 42, 43]. This model accounts for Ca^{2+} binding to cTnC, as well as the cooperativity which occurs in the myofilament due to one strongly bound myosin crossbridge causing an increased propensity for the neighboring myosin crossbridges to form strong force-generating interactions with actin [37, 42]. This model relies on the positioning of tropomyosin (Tm) within the thin filament, by occupying either a "blocked", "closed" or "open" conformation [217, 261]. In the blocked position, the myosin head is unable to attach to the thin filament, while in the "closed" position, it can form a weak bond, and in the "open" position, it forms a strong, force-generating interaction with actin (see Fig 1.3). Our data support the need for at least 3 states, but the observed slowing of both contraction and relaxation rates in cTnIS43/45D myocytes also could require a fourth state to explain how this change produces hysteresis to slow both contraction and relaxation. Testing this idea will require sophisticated measurements of cardiac kinetics in muscle preparations from cTnIS43/45D mice.

A commonality between aforementioned *in vivo* studies mimicking cTnI phosphorylation in transgenic mice, is that phospho-mimetic substitutions were made at multiple residues on the

same cTnI. An interesting question to consider is whether the functional impact of site-specific cTnI phosphorylation differs if there is phosphorylation of a different residue on another cTnI protein. In an early study, mice with a homozygous cTnI knockout died by 18 days of age [262]. However, this study also showed that the heterozygous knockout mice survived beyond day 18. An interesting question to consider is whether some level of endogenous cTnI is required for proper function of the heart. Crossing different mice to obtain double transgenic animals could answer this question.

By crossing our mouse models, we can begin to answer the question of whether the functional response is the same if alternative changes are made to the same residue on 2 different cTnI proteins. Based on our findings that cTnI S43/45N mice do not develop a phenotype (Ch. 5), and crossing cTnIS43/45D and cTnIS43/45N mice would provide interesting insight into 1) whether a double transgenic mouse is viable, and 2) whether the presence of cTnIS43/45N plays a cardioprotective role in mice which also express cTnIS43/45D (e.g. cTnIS43/45DN). If a pathological phenotype does not differ between cTnIS43/45D and cTnIS43/45DN mice, it may imply that the chronic cTnI p-S43/45 is a critical node for contractile function. Alternatively, a delayed or less severe phenotype could indicate reducing the number of cTnIS43/45 sites available or phosphorylation is protective.

Our lab has additionally investigated *in vitro* communication between cTnI phosphorylation sites (S23/24, S43/45, and T144) [4]. Our findings support the idea that S43/45 is the master brake on contractile function even in the presence of S23/24 and T144 phosphorylation, although these sites can modestly attenuate the impact of S43/45 [4, 5]. A next step is to address whether *in vivo* crosses between mice expressing cTnIS43/45D and mice expressing cTnIS23/24D and/or cTnIT144D, support *in vitro* results. Based on previous findings,

it is expected that combining mice expressing cTnIS23/24D or cTnIT144D with a mouse expressing cTnIS43/45D will develop contractile dysfunction, but the time course may be delayed and/or the severity may be reduced [4]. Additionally, the response of cTnIS43/45D, cTnIS23/24D, and cTnIS4D mice to a β-agonist also could provide insight into the interplay between these sites during the β-adrenergic response.

The present work adds greatly to existing knowledge about sarcomere modification and its impact on cardiac function by addressing a longstanding gap in knowledge regarding the *in vivo* role played by cTnI p-S43/45. The present work establishes the *in vivo* impact of cTnI p-S43/45 alone on cardiac and myocyte function. Collectively, the results suggest that phenotypes in previous mouse models with phospho-mimetic substitutions on multiple residues may help to compensate for the impact of cTnI p-S43/45 on contractile function. Our work also provides an impetus for gaining mechanistic insight into compensations within the sarcomere at the onset of cardiac dysfunction. Additionally, by studying differing levels of cTnI p-S43/45, we showed there is an important physiological impact of cTnI p-S43/45. Phosphorylation is meant to be a modulator rather than an on-off switch; and studying varying levels of phosphorylation in a transgenic mouse model provides a powerful addition to the current body of knowledge. Finally, our work explores a novel mechanism that may be responsible for the progressive cardiac dysfunction and heart failure observed in the cTnIS43/45D mouse by testing the novel idea that mitochondrial dysfunction could be a key player when chronic changes within the sarcomere produce contractile dysfunction. The work presented here encourages future studies to consider the impact that sarcomere modification has on cellular function, as it could inform further mechanistic studies and the development of key therapeutic targets in the treatment against heart failure.

References

1. Widmaier, E.P., et al., *Vander's human physiology : the mechanisms of body function*. Fifteenth edition, International student edition / ed. 1 volume (various pagings).
2. Delicce, A.V. and A.N. Makaryus, *Physiology, Frank Starling Law*, in *StatPearls*. 2021: Treasure Island (FL).
3. Burkart, E.M., et al., *Phosphorylation or glutamic acid substitution at protein kinase C sites on cardiac troponin I differentially depress myofilament tension and shortening velocity.* J Biol Chem, 2003. **278**(13): p. 11265-72.
4. Lang, S.E., et al., *Functional communication between PKC-targeted cardiac troponin I phosphorylation sites.* Arch Biochem Biophys, 2017. **627**: p. 1-9.
5. Lang, S.E., et al., *Independent modulation of contractile performance by cardiac troponin I Ser43 and Ser45 in the dynamic sarcomere.* J Mol Cell Cardiol, 2015. **79**: p. 264-74.
6. Bers, D.M., *Cardiac excitation-contraction coupling.* Nature, 2002. **415**(6868): p. 198-205.
7. Bers, D.M. and T. Guo, *Calcium signaling in cardiac ventricular myocytes.* Ann N Y Acad Sci, 2005. **1047**: p. 86-98.
8. Benjamin, E.J., et al., *Heart Disease and Stroke Statistics-2018 Update: A Report From the American Heart Association.* Circulation, 2018. **137**(12): p. e67-e492.
9. Johnsen, D.D., et al., *Protein kinase C isozymes in hypertension and hypertrophy: insight from SHHF rat hearts.* Mol Cell Biochem, 2005. **270**(1-2): p. 63-9.
10. Dong, X., et al., *Augmented phosphorylation of cardiac troponin I in hypertensive heart failure.* J Biol Chem, 2012. **287**(2): p. 848-57.
11. Geraldes, P. and G.L. King, *Activation of protein kinase C isoforms and its impact on diabetic complications.* Circ Res, 2010. **106**(8): p. 1319-31.
12. Burchfield, J.S., M. Xie, and J.A. Hill, *Pathological ventricular remodeling: mechanisms: part 1 of 2.* Circulation, 2013. **128**(4): p. 388-400.
13. Simmonds, S.J., et al., *Cellular and Molecular Differences between HFpEF and HFrEF: A Step Ahead in an Improved Pathological Understanding.* Cells, 2020. **9**(1).
14. Cheng, Y., et al., *Troponin I Mutations R146G and R21C Alter Cardiac Troponin Function, Contractile Properties, and Modulation by Protein Kinase A (PKA)-mediated Phosphorylation.* J Biol Chem, 2015. **290**(46): p. 27749-66.
15. Tsoutsman, T., et al., *Molecular insights from a novel cardiac troponin I mouse model of familial hypertrophic cardiomyopathy.* J Mol Cell Cardiol, 2006. **41**(4): p. 623-32.
16. Deng, Y., et al., *Phosphorylation of human cardiac troponin I G203S and K206Q linked to familial hypertrophic cardiomyopathy affects actomyosin interaction in different ways.* J Mol Cell Cardiol, 2003. **35**(11): p. 1365-74.
17. Carballo, S., et al., *Identification and functional characterization of cardiac troponin I as a novel disease gene in autosomal dominant dilated cardiomyopathy.* Circ Res, 2009. **105**(4): p. 375-82.

18. Lu, Q.W., X.Y. Wu, and S. Morimoto, *Inherited cardiomyopathies caused by troponin mutations.* J Geriatr Cardiol, 2013. **10**(1): p. 91-101.
19. Owan, T.E., et al., *Trends in prevalence and outcome of heart failure with preserved ejection fraction.* N Engl J Med, 2006. **355**(3): p. 251-9.
20. Camelliti, P., T.K. Borg, and P. Kohl, *Structural and functional characterisation of cardiac fibroblasts.* Cardiovasc Res, 2005. **65**(1): p. 40-51.
21. Ivey, M.J. and M.D. Tallquist, *Defining the Cardiac Fibroblast.* Circ J, 2016. **80**(11): p. 2269-2276.
22. Banerjee, I., et al., *Dynamic interactions between myocytes, fibroblasts, and extracellular matrix.* Ann N Y Acad Sci, 2006. **1080**: p. 76-84.
23. Davis, J. and J.D. Molkentin, *Myofibroblasts: trust your heart and let fate decide.* J Mol Cell Cardiol, 2014. **70**: p. 9-18.
24. Alem, M.M., *Endothelial Dysfunction in Chronic Heart Failure: Assessment, Findings, Significance, and Potential Therapeutic Targets.* Int J Mol Sci, 2019. **20**(13).
25. Dick, S.A. and S. Epelman, *Chronic Heart Failure and Inflammation: What Do We Really Know?* Circ Res, 2016. **119**(1): p. 159-76.
26. Tajsharghi, H., *Thick and thin filament gene mutations in striated muscle diseases.* Int J Mol Sci, 2008. **9**(7): p. 1259-75.
27. Lange, S., et al., *The M-band: The underestimated part of the sarcomere.* Biochim Biophys Acta Mol Cell Res, 2020. **1867**(3): p. 118440.
28. Potter, J.D., *The content of troponin, tropomyosin, actin, and myosin in rabbit skeletal muscle myofibrils.* Arch Biochem Biophys, 1974. **162**(2): p. 436-41.
29. Katrukha, I.A., *Human cardiac troponin complex. Structure and functions.* Biochemistry (Mosc), 2013. **78**(13): p. 1447-65.
30. Farah, C.S. and F.C. Reinach, *The troponin complex and regulation of muscle contraction.* FASEB J, 1995. **9**(9): p. 755-67.
31. Day, S.M., M.V. Westfall, and J.M. Metzger, *Tuning cardiac performance in ischemic heart disease and failure by modulating myofilament function.* J Mol Med (Berl), 2007. **85**(9): p. 911-21.
32. Kobayashi, T. and R.J. Solaro, *Calcium, thin filaments, and the integrative biology of cardiac contractility.* Annu Rev Physiol, 2005. **67**: p. 39-67.
33. Galinska, A., et al., *The C terminus of cardiac troponin I stabilizes the Ca2+-activated state of tropomyosin on actin filaments.* Circ Res, 2010. **106**(4): p. 705-11.
34. Janco, M., et al., *The impact of tropomyosins on actin filament assembly is isoform specific.* Bioarchitecture, 2016. **6**(4): p. 61-75.
35. Michele, D.E., F.P. Albayya, and J.M. Metzger, *Direct, convergent hypersensitivity of calcium-activated force generation produced by hypertrophic cardiomyopathy mutant alpha-tropomyosins in adult cardiac myocytes.* Nat Med, 1999. **5**(12): p. 1413-7.
36. Gordon, A.M., M. Regnier, and E. Homsher, *Skeletal and cardiac muscle contractile activation: tropomyosin "rocks and rolls".* News Physiol Sci, 2001. **16**: p. 49-55.
37. Geeves, M.A. and P.B. Conibear, *The role of three-state docking of myosin S1 with actin in force generation.* Biophys J, 1995. **68**(4 Suppl): p. 194S-199S; discussion 199S-201S.
38. Hill, T.L., E. Eisenberg, and L. Greene, *Theoretical model for the cooperative equilibrium binding of myosin subfragment 1 to the actin-troponin-tropomyosin complex.* Proc Natl Acad Sci U S A, 1980. **77**(6): p. 3186-90.

39. Hitchcock, S.E., H.E. Huxley, and A.G. Szent-Gyorgyi, *Calcium sensitive binding of troponin to actin-tropomyosin: a two-site model for troponin action.* J Mol Biol, 1973. **80**(4): p. 825-36.
40. Mathur, M.C., T. Kobayashi, and J.M. Chalovich, *Negative charges at protein kinase C sites of troponin I stabilize the inactive state of actin.* Biophys J, 2008. **94**(2): p. 542-9.
41. Mathur, M.C., T. Kobayashi, and J.M. Chalovich, *Some cardiomyopathy-causing troponin I mutations stabilize a functional intermediate actin state.* Biophys J, 2009. **96**(6): p. 2237-44.
42. McKillop, D.F. and M.A. Geeves, *Regulation of the interaction between actin and myosin subfragment 1: evidence for three states of the thin filament.* Biophys J, 1993. **65**(2): p. 693-701.
43. Solaro, R.J. and J. Van Eyk, *Altered interactions among thin filament proteins modulate cardiac function.* J Mol Cell Cardiol, 1996. **28**(2): p. 217-30.
44. McNamara, J.W., et al., *The role of super-relaxed myosin in skeletal and cardiac muscle.* Biophys Rev, 2015. **7**(1): p. 5-14.
45. Tiso, N., et al., *Fine mapping of five human skeletal muscle genes: alpha-tropomyosin, beta-tropomyosin, troponin-I slow-twitch, troponin-I fast-twitch, and troponin-C fast.* Biochem Biophys Res Commun, 1997. **230**(2): p. 347-50.
46. Bhavsar, P.K., et al., *Isolation and characterization of the human cardiac troponin I gene (TNNI3).* Genomics, 1996. **35**(1): p. 11-23.
47. Bhavsar, P.K., et al., *Developmental expression of troponin I isoforms in fetal human heart.* FEBS Lett, 1991. **292**(1-2): p. 5-8.
48. Dhoot, G.K. and S.V. Perry, *Distribution of polymorphic forms of troponin components and tropomyosin in skeletal muscle.* Nature, 1979. **278**(5706): p. 714-8.
49. Dellow, K.A., et al., *Identification of novel, cardiac-restricted transcription factors binding to a CACC-box within the human cardiac troponin I promoter.* Cardiovasc Res, 2001. **50**(1): p. 24-33.
50. Bodor, G.S., et al., *Cardiac troponin-I is not expressed in fetal and healthy or diseased adult human skeletal muscle tissue.* Clin Chem, 1995. **41**(12 Pt 1): p. 1710-5.
51. Takeda, S., et al., *Structure of the core domain of human cardiac troponin in the Ca(2+)-saturated form.* Nature, 2003. **424**(6944): p. 35-41.
52. Marston, S. and J.E. Zamora, *Troponin structure and function: a view of recent progress.* J Muscle Res Cell Motil, 2020. **41**(1): p. 71-89.
53. Yamada, Y., K. Namba, and T. Fujii, *Cardiac muscle thin filament structures reveal calcium regulatory mechanism.* Nat Commun, 2020. **11**(1): p. 153.
54. Andrew, C.D., et al., *Effect of phosphorylation on alpha-helix stability as a function of position.* Biochemistry, 2002. **41**(6): p. 1897-905.
55. Hanks, S.K. and T. Hunter, *Protein kinases 6. The eukaryotic protein kinase superfamily: kinase (catalytic) domain structure and classification.* FASEB J, 1995. **9**(8): p. 576-96.
56. Kemp, B.E., et al., *Substrate specificity of the cyclic AMP-dependent protein kinase.* Proc Natl Acad Sci U S A, 1975. **72**(9): p. 3448-52.
57. Zetterqvist, O., et al., *The minimum substrate of cyclic AMP-stimulated protein kinase, as studied by synthetic peptides representing the phosphorylatable site of pyruvate kinase (type L) of rat liver.* Biochem Biophys Res Commun, 1976. **70**(3): p. 696-703.
58. Kemp, B.E. and R.B. Pearson, *Protein kinase recognition sequence motifs.* Trends Biochem Sci, 1990. **15**(9): p. 342-6.

59. Knighton, D.R., et al., *Crystal structure of the catalytic subunit of cyclic adenosine monophosphate-dependent protein kinase.* Science, 1991. **253**(5018): p. 407-14.
60. Johnson, L.N., M.E. Noble, and D.J. Owen, *Active and inactive protein kinases: structural basis for regulation.* Cell, 1996. **85**(2): p. 149-58.
61. Yang, J., et al., *Molecular mechanism for the regulation of protein kinase B/Akt by hydrophobic motif phosphorylation.* Mol Cell, 2002. **9**(6): p. 1227-40.
62. Komander, D., et al., *Role of T-loop phosphorylation in PDK1 activation, stability, and substrate binding.* J Biol Chem, 2005. **280**(19): p. 18797-802.
63. Moir, A.J., R.J. Solaro, and S.V. Perry, *The site of phosphorylation of troponin I in the perfused rabbit heart. The effect of adrenaline.* Biochem J, 1980. **185**(2): p. 505-13.
64. Zhang, R., et al., *Cardiac troponin I phosphorylation increases the rate of cardiac muscle relaxation.* Circ Res, 1995. **76**(6): p. 1028-35.
65. Dong, W.J., et al., *Effects of PKA phosphorylation of cardiac troponin I and strong crossbridge on conformational transitions of the N-domain of cardiac troponin C in regulated thin filaments.* Biochemistry, 2007. **46**(34): p. 9752-61.
66. Sakthivel, S., et al., *In vivo and in vitro analysis of cardiac troponin I phosphorylation.* J Biol Chem, 2005. **280**(1): p. 703-14.
67. Robertson, S.P., et al., *The effect of troponin I phosphorylation on the Ca2+-binding properties of the Ca2+-regulatory site of bovine cardiac troponin.* J Biol Chem, 1982. **257**(1): p. 260-3.
68. Bowling, N., et al., *Increased protein kinase C activity and expression of Ca2+-sensitive isoforms in the failing human heart.* Circulation, 1999. **99**(3): p. 384-91.
69. Zhang, P., et al., *Multiple reaction monitoring to identify site-specific troponin I phosphorylated residues in the failing human heart.* Circulation, 2012. **126**(15): p. 1828-37.
70. Liu, B., et al., *Protein kinase C phosphomimetics alter thin filament Ca2+ binding properties.* PLoS One, 2014. **9**(1): p. e86279.
71. de Lucia, C., A. Eguchi, and W.J. Koch, *New Insights in Cardiac beta-Adrenergic Signaling During Heart Failure and Aging.* Front Pharmacol, 2018. **9**: p. 904.
72. Takai, Y., et al., *Studies on a cyclic nucleotide-independent protein kinase and its proenzyme in mammalian tissues. I. Purification and characterization of an active enzyme from bovine cerebellum.* J Biol Chem, 1977. **252**(21): p. 7603-9.
73. Inoue, M., et al., *Studies on a cyclic nucleotide-independent protein kinase and its proenzyme in mammalian tissues. II. Proenzyme and its activation by calcium-dependent protease from rat brain.* J Biol Chem, 1977. **252**(21): p. 7610-6.
74. Newton, A.C., *Regulation of the ABC kinases by phosphorylation: protein kinase C as a paradigm.* Biochem J, 2003. **370**(Pt 2): p. 361-71.
75. Assert, R., H. Schatz, and A. Pfeiffer, *Upregulation of PKC delta- and downregulation of PKC alpha-mRNA and protein by phorbol ester in human T84 cells.* FEBS Lett, 1996. **388**(2-3): p. 195-9.
76. Mellor, H. and P.J. Parker, *The extended protein kinase C superfamily.* Biochem J, 1998. **332 (Pt 2)**: p. 281-92.
77. Castagna, M., et al., *Direct activation of calcium-activated, phospholipid-dependent protein kinase by tumor-promoting phorbol esters.* J Biol Chem, 1982. **257**(13): p. 7847-51.

78. Kishimoto, A., et al., *Activation of calcium and phospholipid-dependent protein kinase by diacylglycerol, its possible relation to phosphatidylinositol turnover.* J Biol Chem, 1980. **255**(6): p. 2273-6.
79. Steinberg, S.F., *Structural basis of protein kinase C isoform function.* Physiol Rev, 2008. **88**(4): p. 1341-78.
80. Yoshida, Y., et al., *Tissue distribution and developmental expression of protein kinase C isozymes.* J Biol Chem, 1988. **263**(20): p. 9868-73.
81. Abe, M.K., et al., *Hydrogen peroxide activates extracellular signal-regulated kinase via protein kinase C, Raf-1, and MEK1.* Am J Respir Cell Mol Biol, 1998. **18**(4): p. 562-9.
82. Dempsey, E.C., I.F. McMurtry, and R.F. O'Brien, *Protein kinase C activation allows pulmonary artery smooth muscle cells to proliferate to hypoxia.* Am J Physiol, 1991. **260**(2 Pt 1): p. L136-45.
83. Dempsey, E.C., et al., *Enhanced growth capacity of neonatal pulmonary artery smooth muscle cells in vitro: dependence on cell size, time from birth, insulin-like growth factor I, and auto-activation of protein kinase C.* J Cell Physiol, 1994. **160**(3): p. 469-81.
84. Qvit, N., O.S. Kornfeld, and D. Mochly-Rosen, *Engineered Substrate-Specific Delta PKC Antagonists to Enhance Cardiac Therapeutics.* Angew Chem Int Ed Engl, 2016. **55**(50): p. 15672-15679.
85. Capogrossi, M.C., et al., *Ca2+ dependence of alpha-adrenergic effects on the contractile properties and Ca2+ homeostasis of cardiac myocytes.* Circ Res, 1991. **69**(2): p. 540-50.
86. Palaniyandi, S.S., et al., *Protein kinase C in heart failure: a therapeutic target?* Cardiovasc Res, 2009. **82**(2): p. 229-39.
87. Puri, T.S., et al., *Differential effects of subunit interactions on protein kinase A- and C-mediated phosphorylation of L-type calcium channels.* Biochemistry, 1997. **36**(31): p. 9605-15.
88. Benjamin, E.J., et al., *Heart Disease and Stroke Statistics-2019 Update: A Report From the American Heart Association.* Circulation, 2019. **139**(10): p. e56-e528.
89. Wende, A.R., et al., *Metabolic Origins of Heart Failure.* JACC Basic Transl Sci, 2017. **2**(3): p. 297-310.
90. Kang, M.Y., et al., *Receptor-independent cardiac protein kinase Calpha activation by calpain-mediated truncation of regulatory domains.* Circ Res, 2010. **107**(7): p. 903-12.
91. Ravichandran, V.S., et al., *Cardiac contractile dysfunction and protein kinase C-mediated myofilament phosphorylation in disease and aging.* J Gen Physiol, 2019.
92. Braz, J.C., et al., *PKC-alpha regulates cardiac contractility and propensity toward heart failure.* Nat Med, 2004. **10**(3): p. 248-54.
93. Wakasaki, H., et al., *Targeted overexpression of protein kinase C beta2 isoform in myocardium causes cardiomyopathy.* Proc Natl Acad Sci U S A, 1997. **94**(17): p. 9320-5.
94. Takeishi, Y., et al., *Transgenic overexpression of constitutively active protein kinase C epsilon causes concentric cardiac hypertrophy.* Circ Res, 2000. **86**(12): p. 1218-23.
95. Montgomery, D.E., et al., *Protein kinase C epsilon induces systolic cardiac failure marked by exhausted inotropic reserve and intact Frank-Starling mechanism.* Am J Physiol Heart Circ Physiol, 2005. **289**(5): p. H1881-8.
96. Kooij, V., G.J.M. Stienen, and J. van der Velden, *The role of protein kinase C-mediated phosphorylation of sarcomeric proteins in the heart-detrimental or beneficial?* Biophys Rev, 2011. **3**(3): p. 107.

97. Puceat, M., et al., *Differential regulation of protein kinase C isoforms in isolated neonatal and adult rat cardiomyocytes.* J Biol Chem, 1994. **269**(24): p. 16938-44.
98. Perry, S.V. and H.A. Cole, *Phosphorylation of troponin and the effects of interactions between the components of the complex.* Biochem J, 1974. **141**(3): p. 733-43.
99. Layland, J., R.J. Solaro, and A.M. Shah, *Regulation of cardiac contractile function by troponin I phosphorylation.* Cardiovasc Res, 2005. **66**(1): p. 12-21.
100. Solaro, R.J., A.J. Moir, and S.V. Perry, *Phosphorylation of troponin I and the inotropic effect of adrenaline in the perfused rabbit heart.* Nature, 1976. **262**(5569): p. 615-7.
101. Noland, T.A., Jr., et al., *Differential regulation of cardiac actomyosin S-1 MgATPase by protein kinase C isozyme-specific phosphorylation of specific sites in cardiac troponin I and its phosphorylation site mutants.* Biochemistry, 1996. **35**(47): p. 14923-31.
102. Wittkopper, K., et al., *Phosphatase-1 inhibitor-1 in physiological and pathological beta-adrenoceptor signalling.* Cardiovasc Res, 2011. **91**(3): p. 392-401.
103. Keane, N.E., et al., *The ordered phosphorylation of cardiac troponin I by the cAMP-dependent protein kinase--structural consequences and functional implications.* Eur J Biochem, 1997. **248**(2): p. 329-37.
104. Noland, T.A., Jr. and J.F. Kuo, *Protein kinase C phosphorylation of cardiac troponin I or troponin T inhibits Ca2(+)-stimulated actomyosin MgATPase activity.* J Biol Chem, 1991. **266**(8): p. 4974-8.
105. Jideama, N.M., et al., *Phosphorylation specificities of protein kinase C isozymes for bovine cardiac troponin I and troponin T and sites within these proteins and regulation of myofilament properties.* J Biol Chem, 1996. **271**(38): p. 23277-83.
106. Braz, J.C., et al., *PKC alpha regulates the hypertrophic growth of cardiomyocytes through extracellular signal-regulated kinase1/2 (ERK1/2).* J Cell Biol, 2002. **156**(5): p. 905-19.
107. Wijnker, P.J., et al., *A novel phosphorylation site, Serine 199, in the C-terminus of cardiac troponin I regulates calcium sensitivity and susceptibility to calpain-induced proteolysis.* J Mol Cell Cardiol, 2015. **82**: p. 93-103.
108. Walker, L.A., et al., *Stage-specific changes in myofilament protein phosphorylation following myocardial infarction in mice.* J Mol Cell Cardiol, 2010. **48**(6): p. 1180-6.
109. Michele, D.E., F.P. Albayya, and J.M. Metzger, *Thin filament protein dynamics in fully differentiated adult cardiac myocytes: toward a model of sarcomere maintenance.* J Cell Biol, 1999. **145**(7): p. 1483-95.
110. Chandra, M., et al., *Effects of protein kinase A phosphorylation on signaling between cardiac troponin I and the N-terminal domain of cardiac troponin C.* Biochemistry, 1997. **36**(43): p. 13305-11.
111. Bilchick, K.C., et al., *Heart failure-associated alterations in troponin I phosphorylation impair ventricular relaxation-afterload and force-frequency responses and systolic function.* Am J Physiol Heart Circ Physiol, 2007. **292**(1): p. H318-25.
112. Kirk, J.A., et al., *Left ventricular and myocardial function in mice expressing constitutively pseudophosphorylated cardiac troponin I.* Circ Res, 2009. **105**(12): p. 1232-9.
113. Pi, Y., et al., *Protein kinase C and A sites on troponin I regulate myofilament Ca2+ sensitivity and ATPase activity in the mouse myocardium.* J Physiol, 2003. **552**(Pt 3): p. 845-57.

114. Pi, Y., et al., *Phosphorylation of troponin I controls cardiac twitch dynamics: evidence from phosphorylation site mutants expressed on a troponin I-null background in mice.* Circ Res, 2002. **90**(6): p. 649-56.
115. Noland, T.A., Jr., et al., *Cardiac troponin I mutants. Phosphorylation by protein kinases C and A and regulation of Ca(2+)-stimulated MgATPase of reconstituted actomyosin S-1.* J Biol Chem, 1995. **270**(43): p. 25445-54.
116. Lang, S.E., et al., *Myofilament incorporation and contractile function after gene transfer of cardiac troponin I Ser43/45Ala.* Arch Biochem Biophys, 2013. **535**(1): p. 49-55.
117. MacGowan, G.A., et al., *Ischemic dysfunction in transgenic mice expressing troponin I lacking protein kinase C phosphorylation sites.* Am J Physiol Heart Circ Physiol, 2001. **280**(2): p. H835-43.
118. Finley, N.L. and P.R. Rosevear, *Introduction of negative charge mimicking protein kinase C phosphorylation of cardiac troponin I. Effects on cardiac troponin C.* J Biol Chem, 2004. **279**(52): p. 54833-40.
119. Lang, S.E., et al., *Functionally conservative substitutions at cardiac troponin I S43/45.* Arch Biochem Biophys, 2016. **601**: p. 42-7.
120. Martin, W.F., S. Garg, and V. Zimorski, *Endosymbiotic theories for eukaryote origin.* Philos Trans R Soc Lond B Biol Sci, 2015. **370**(1678): p. 20140330.
121. Zhao, Q., et al., *Complex Regulation of Mitochondrial Function During Cardiac Development.* J Am Heart Assoc, 2019. **8**(13): p. e012731.
122. Bruggisser, J., et al., *Biogenesis of a Mitochondrial Outer Membrane Protein in Trypanosoma brucei: TARGETING SIGNAL AND DEPENDENCE ON A UNIQUE BIOGENESIS FACTOR.* J Biol Chem, 2017. **292**(8): p. 3400-3410.
123. Chaban, Y., E.J. Boekema, and N.V. Dudkina, *Structures of mitochondrial oxidative phosphorylation supercomplexes and mechanisms for their stabilisation.* Biochim Biophys Acta, 2014. **1837**(4): p. 418-26.
124. Schramm, M., H.G. Klieber, and J. Daut, *The energy expenditure of actomyosin-ATPase, Ca(2+)-ATPase and Na+,K(+)-ATPase in guinea-pig cardiac ventricular muscle.* J Physiol, 1994. **481 (Pt 3)**: p. 647-62.
125. Zhou, B. and R. Tian, *Mitochondrial dysfunction in pathophysiology of heart failure.* J Clin Invest, 2018. **128**(9): p. 3716-3726.
126. Hill, M.F. and P.K. Singal, *Antioxidant and oxidative stress changes during heart failure subsequent to myocardial infarction in rats.* Am J Pathol, 1996. **148**(1): p. 291-300.
127. Belch, J.J., et al., *Oxygen free radicals and congestive heart failure.* Br Heart J, 1991. **65**(5): p. 245-8.
128. Siwik, D.A., et al., *Inhibition of copper-zinc superoxide dismutase induces cell growth, hypertrophic phenotype, and apoptosis in neonatal rat cardiac myocytes in vitro.* Circ Res, 1999. **85**(2): p. 147-53.
129. Sam, F., et al., *Increased reactive oxygen species production and functional alterations in antioxidant enzymes in human failing myocardium.* J Card Fail, 2005. **11**(6): p. 473-80.
130. Orsini, F., et al., *The life span determinant p66Shc localizes to mitochondria where it associates with mitochondrial heat shock protein 70 and regulates trans-membrane potential.* J Biol Chem, 2004. **279**(24): p. 25689-95.
131. Nemoto, S. and T. Finkel, *Redox regulation of forkhead proteins through a p66shc-dependent signaling pathway.* Science, 2002. **295**(5564): p. 2450-2.

132. Guo, J., et al., *p66Shc links alpha1-adrenergic receptors to a reactive oxygen species-dependent AKT-FOXO3A phosphorylation pathway in cardiomyocytes.* Circ Res, 2009. **104**(5): p. 660-9.
133. Katoh, N., B.C. Wise, and J.F. Kuo, *Phosphorylation of cardiac troponin inhibitory subunit (troponin I) and tropomyosin-binding subunit (troponin T) by cardiac phospholipid-sensitive Ca2+-dependent protein kinase.* Biochem J, 1983. **209**(1): p. 189-95.
134. England, P.J., *Studies on the phosphorylation of the inhibitory subunit of troponin during modification of contraction in perfused rat heart.* Biochem J, 1976. **160**(2): p. 295-304.
135. Savarese, G. and L.H. Lund, *Global Public Health Burden of Heart Failure.* Card Fail Rev, 2017. **3**(1): p. 7-11.
136. Miller, L.W. and J.G. Rogers, *Evolution of Left Ventricular Assist Device Therapy for Advanced Heart Failure: A Review.* JAMA Cardiol, 2018. **3**(7): p. 650-658.
137. Uriel, N., G. Kim, and D. Burkhoff, *Myocardial Recovery After LVAD Implantation: A Vision or Simply an Illusion?* J Am Coll Cardiol, 2017. **70**(3): p. 355-357.
138. Wever-Pinzon, O., et al., *Cardiac Recovery During Long-Term Left Ventricular Assist Device Support.* J Am Coll Cardiol, 2016. **68**(14): p. 1540-53.
139. Morgan, J.A., et al., *Left ventricular reverse remodeling with a continuous flow left ventricular assist device measured by left ventricular end-diastolic dimensions and severity of mitral regurgitation.* ASAIO J, 2012. **58**(6): p. 574-7.
140. Smith, L.A., L.T. Yarboro, and J.L. Kennedy, *Left ventricular assist device implantation strategies and outcomes.* J Thorac Dis, 2015. **7**(12): p. 2088-96.
141. Kim, E.H., et al., *Differential protein expression and basal lamina remodeling in human heart failure.* Proteomics Clin Appl, 2016. **10**(5): p. 585-96.
142. Noguchi, T., et al., *Thin-filament-based modulation of contractile performance in human heart failure.* Circulation, 2004. **110**(8): p. 982-7.
143. Hambleton, M., et al., *Pharmacological- and gene therapy-based inhibition of protein kinase Calpha/beta enhances cardiac contractility and attenuates heart failure.* Circulation, 2006. **114**(6): p. 574-82.
144. Piacentino, V., 3rd, et al., *Cellular basis of abnormal calcium transients of failing human ventricular myocytes.* Circ Res, 2003. **92**(6): p. 651-8.
145. Murriel, C.L., et al., *Protein kinase Cdelta activation induces apoptosis in response to cardiac ischemia and reperfusion damage: a mechanism involving BAD and the mitochondria.* J Biol Chem, 2004. **279**(46): p. 47985-91.
146. Castillero, E., et al., *Structural and functional cardiac profile after prolonged duration of mechanical unloading: potential implications for myocardial recovery.* Am J Physiol Heart Circ Physiol, 2018. **315**(5): p. H1463-H1476.
147. Day, S.M., et al., *Histidine button engineered into cardiac troponin I protects the ischemic and failing heart.* Nat Med, 2006. **12**(2): p. 181-9.
148. Dipla, K., et al., *Myocyte recovery after mechanical circulatory support in humans with end-stage heart failure.* Circulation, 1998. **97**(23): p. 2316-22.
149. Goldberg, A.T., et al., *Endothelin receptor pathway in human left ventricular myocytes: relation to contractility.* Ann Thorac Surg, 2000. **69**(3): p. 711-5; discussion 716.
150. Chaudhary, K.W., et al., *Altered myocardial Ca2+ cycling after left ventricular assist device support in the failing human heart.* J Am Coll Cardiol, 2004. **44**(4): p. 837-45.

151. Wahr, P.A., D.E. Michele, and J.M. Metzger, *Effects of aging on single cardiac myocyte function in Fischer 344 x Brown Norway rats.* Am J Physiol Heart Circ Physiol, 2000. **279**(2): p. H559-65.
152. Hwang, H., et al., *PKCbetaII modulation of myocyte contractile performance.* J Mol Cell Cardiol, 2012. **53**(2): p. 176-86.
153. Milting, H., et al., *Selective upregulation of beta1-adrenergic receptors and dephosphorylation of troponin I in end-stage heart failure patients supported by ventricular assist devices.* J Mol Cell Cardiol, 2006. **41**(3): p. 441-50.
154. Venema, R.C. and J.F. Kuo, *Protein kinase C-mediated phosphorylation of troponin I and C-protein in isolated myocardial cells is associated with inhibition of myofibrillar actomyosin MgATPase.* J Biol Chem, 1993. **268**(4): p. 2705-11.
155. Bayer, A.L., et al., *Alterations in protein kinase C isoenzyme expression and autophosphorylation during the progression of pressure overload-induced left ventricular hypertrophy.* Mol Cell Biochem, 2003. **242**(1-2): p. 145-52.
156. Lange, S., et al., *MLP and CARP are linked to chronic PKCalpha signalling in dilated cardiomyopathy.* Nat Commun, 2016. **7**: p. 12120.
157. Belin, R.J., et al., *Left ventricular myofilament dysfunction in rat experimental hypertrophy and congestive heart failure.* Am J Physiol Heart Circ Physiol, 2006. **291**(5): p. H2344-53.
158. Bohm, M., et al., *Dose-dependent dissociation of ACE-inhibitor effects on blood pressure, cardiac hypertrophy, and beta-adrenergic signal transduction.* Circulation, 1995. **92**(10): p. 3006-13.
159. Chung, E. and G.M. Diffee, *Effect of aging on power output properties in rat skinned cardiac myocytes.* J Gerontol A Biol Sci Med Sci, 2011. **66**(12): p. 1267-73.
160. Turturro, A., et al., *Growth curves and survival characteristics of the animals used in the Biomarkers of Aging Program.* J Gerontol A Biol Sci Med Sci, 1999. **54**(11): p. B492-501.
161. Li, Z., C.S. Abdullah, and Z.Q. Jin, *Inhibition of PKC-theta preserves cardiac function and reduces fibrosis in streptozotocin-induced diabetic cardiomyopathy.* Br J Pharmacol, 2014. **171**(11): p. 2913-24.
162. Newton, A.C., C.E. Antal, and S.F. Steinberg, *Protein kinase C mechanisms that contribute to cardiac remodelling.* Clin Sci (Lond), 2016. **130**(17): p. 1499-510.
163. Singh, R.M., et al., *Protein kinase C and cardiac dysfunction: a review.* Heart Fail Rev, 2017. **22**(6): p. 843-859.
164. Belin, R.J., et al., *Augmented protein kinase C-alpha-induced myofilament protein phosphorylation contributes to myofilament dysfunction in experimental congestive heart failure.* Circ Res, 2007. **101**(2): p. 195-204.
165. Mukherjee, A., et al., *Spatio-Temporal Regulation of PKC Isoforms Imparts Signaling Specificity.* Front Immunol, 2016. **7**: p. 45.
166. Sakai, M., et al., *Decrease with senescence in the norepinephrine-induced phosphorylation of myofilament proteins in isolated rat cardiac myocytes.* J Mol Cell Cardiol, 1989. **21**(12): p. 1327-36.
167. Li, C., M.E. Fultz, and G.L. Wright, *PKC-alpha shows variable patterns of translocation in response to different stimulatory agents.* Acta Physiol Scand, 2002. **174**(3): p. 237-46.
168. Stehle, R. and B. Iorga, *Kinetics of cardiac sarcomeric processes and rate-limiting steps in contraction and relaxation.* J Mol Cell Cardiol, 2010. **48**(5): p. 843-50.

169. Westfall, M., *Post-translational modifications of troponin. In: Troponin: Regulator of muscle contraction (Editor: J-P Jin)*
. 2014: p. 163-202.
170. Takimoto, E., et al., *Frequency- and afterload-dependent cardiac modulation in vivo by troponin I with constitutively active protein kinase A phosphorylation sites.* Circ Res, 2004. **94**(4): p. 496-504.
171. Yasuda, S., et al., *Cardiac transgenic and gene transfer strategies converge to support an important role for troponin I in regulating relaxation in cardiac myocytes.* Circ Res, 2007. **101**(4): p. 377-86.
172. Messer, A.E., A.M. Jacques, and S.B. Marston, *Troponin phosphorylation and regulatory function in human heart muscle: dephosphorylation of Ser23/24 on troponin I could account for the contractile defect in end-stage heart failure.* J Mol Cell Cardiol, 2007. **42**(1): p. 247-59.
173. van der Velden, J., et al., *Alterations in myofilament function contribute to left ventricular dysfunction in pigs early after myocardial infarction.* Circ Res, 2004. **95**(11): p. e85-95.
174. van der Velden, J., et al., *Functional effects of protein kinase C-mediated myofilament phosphorylation in human myocardium.* Cardiovasc Res, 2006. **69**(4): p. 876-87.
175. Cleland, J.G., et al., *The effects of the cardiac myosin activator, omecamtiv mecarbil, on cardiac function in systolic heart failure: a double-blind, placebo-controlled, crossover, dose-ranging phase 2 trial.* Lancet, 2011. **378**(9792): p. 676-83.
176. Kirklin, J.K., et al., *Seventh INTERMACS annual report: 15,000 patients and counting.* J Heart Lung Transplant, 2015. **34**(12): p. 1495-504.
177. Ogletree, M.L., et al., *Duration of left ventricular assist device support: Effects on abnormal calcium cycling and functional recovery in the failing human heart.* J Heart Lung Transplant, 2010. **29**(5): p. 554-61.
178. McCall, E., et al., *Ca flux, contractility, and excitation-contraction coupling in hypertrophic rat ventricular myocytes.* Am J Physiol, 1998. **274**(4): p. H1348-60.
179. Kagaya, Y., et al., *Long-term angiotensin-converting enzyme inhibition with fosinopril improves depressed responsiveness to Ca2+ in myocytes from aortic-banded rats.* Circulation, 1996. **94**(11): p. 2915-22.
180. Orchard, C.H. and E.G. Lakatta, *Intracellular calcium transients and developed tension in rat heart muscle. A mechanism for the negative interval-strength relationship.* J Gen Physiol, 1985. **86**(5): p. 637-51.
181. Davis, J., et al., *Designing heart performance by gene transfer.* Physiol Rev, 2008. **88**(4): p. 1567-651.
182. Sasse, S., et al., *Troponin I gene expression during human cardiac development and in end-stage heart failure.* Circ Res, 1993. **72**(5): p. 932-8.
183. Anderson, P.A., et al., *Troponin T isoform expression in humans. A comparison among normal and failing adult heart, fetal heart, and adult and fetal skeletal muscle.* Circ Res, 1991. **69**(5): p. 1226-33.
184. Westfall, M.V., et al., *Adenovirus-mediated myofilament gene transfer into adult cardiac myocytes.* Methods Cell Biol, 1997. **52**: p. 307-22.
185. Panchal, R.G., et al., *Gene transfer: manipulating and monitoring function in cells and tissues.* Clin Exp Pharmacol Physiol, 2001. **28**(8): p. 687-91.
186. Louch, W.E., K.A. Sheehan, and B.M. Wolska, *Methods in cardiomyocyte isolation, culture, and gene transfer.* J Mol Cell Cardiol, 2011. **51**(3): p. 288-98.

187. Monge, C., et al., *Comparative analysis of the bioenergetics of adult cardiomyocytes and nonbeating HL-1 cells: respiratory chain activities, glycolytic enzyme profiles, and metabolic fluxes.* Can J Physiol Pharmacol, 2009. **87**(4): p. 318-26.
188. Rust, E.M., M.V. Westfall, and J.M. Metzger, *Stability of the contractile assembly and Ca2+-activated tension in adenovirus infected adult cardiac myocytes.* Mol Cell Biochem, 1998. **181**(1-2): p. 143-55.
189. Kirshenbaum, L.A., et al., *Highly efficient gene transfer into adult ventricular myocytes by recombinant adenovirus.* J Clin Invest, 1993. **92**(1): p. 381-7.
190. Jaenisch, R., *Germ line integration and Mendelian transmission of the exogenous Moloney leukemia virus.* Proc Natl Acad Sci U S A, 1976. **73**(4): p. 1260-4.
191. Pfeifer, A., *Lentiviral transgenesis.* Transgenic Res, 2004. **13**(6): p. 513-22.
192. Fassler, R., *Lentiviral transgene vectors.* EMBO Rep, 2004. **5**(1): p. 28-9.
193. Wells, K., K. Moore, and R. Wall, *Transgene vectors go retro.* Nat Biotechnol, 1999. **17**(1): p. 25-6.
194. Kass-Eisler, A., et al., *Quantitative determination of adenovirus-mediated gene delivery to rat cardiac myocytes in vitro and in vivo.* Proc Natl Acad Sci U S A, 1993. **90**(24): p. 11498-502.
195. Hofmann, A., et al., *Efficient transgenesis in farm animals by lentiviral vectors.* EMBO Rep, 2003. **4**(11): p. 1054-60.
196. Izsvak, Z., et al., *Efficient stable gene transfer into human cells by the Sleeping Beauty transposon vectors.* Methods, 2009. **49**(3): p. 287-97.
197. Merkulov, S., et al., *In vivo cardiac myosin binding protein C gene transfer rescues myofilament contractile dysfunction in cardiac myosin binding protein C null mice.* Circ Heart Fail, 2012. **5**(5): p. 635-44.
198. Lee, C.J., et al., *Promoter-specific lentivectors for long-term, cardiac-directed therapy of Fabry disease.* J Cardiol, 2011. **57**(1): p. 115-22.
199. Fassler, M., et al., *Preferential lentiviral targeting of astrocytes in the central nervous system.* PLoS One, 2013. **8**(10): p. e76092.
200. Wang, L., et al., *Long-term effect of neuronal nitric oxide synthase over-expression on cardiac neurotransmission mediated by a lentiviral vector.* J Physiol, 2009. **587**(Pt 14): p. 3629-37.
201. Pacak, C.A. and B.J. Byrne, *AAV vectors for cardiac gene transfer: experimental tools and clinical opportunities.* Mol Ther, 2011. **19**(9): p. 1582-90.
202. Deyle, D.R. and D.W. Russell, *Adeno-associated virus vector integration.* Curr Opin Mol Ther, 2009. **11**(4): p. 442-7.
203. Huang, S., et al., *Adeno-associated virus Rep-mediated targeting of integrase-defective retroviral vector DNA circles into human chromosome 19.* Biochem Biophys Res Commun, 2012. **417**(1): p. 78-83.
204. Park, F., *Lentiviral vectors: are they the future of animal transgenesis?* Physiol Genomics, 2007. **31**(2): p. 159-73.
205. Westfall, M.V., A.M. Lee, and D.A. Robinson, *Differential contribution of troponin I phosphorylation sites to the endothelin-modulated contractile response.* J Biol Chem, 2005. **280**(50): p. 41324-31.
206. Westfall, M.V., E.M. Rust, and J.M. Metzger, *Slow skeletal troponin I gene transfer, expression, and myofilament incorporation enhances adult cardiac myocyte contractile function.* Proc Natl Acad Sci U S A, 1997. **94**(10): p. 5444-9.

207. Rust, E.M., F.P. Albayya, and J.M. Metzger, *Identification of a contractile deficit in adult cardiac myocytes expressing hypertrophic cardiomyopathy-associated mutant troponin T proteins.* J Clin Invest, 1999. **103**(10): p. 1459-67.
208. Herron, T.J., et al., *Ca2+-independent positive molecular inotropy for failing rabbit and human cardiac muscle by alpha-myosin motor gene transfer.* FASEB J, 2010. **24**(2): p. 415-24.
209. Lang, S.E. and M.V. Westfall, *Gene transfer into cardiac myocytes.* Methods Mol Biol, 2015. **1299**: p. 177-90.
210. Kabaeva, Z., M. Zhao, and D.E. Michele, *Blebbistatin extends culture life of adult mouse cardiac myocytes and allows efficient and stable transgene expression.* Am J Physiol Heart Circ Physiol, 2008. **294**(4): p. H1667-74.
211. Lin, B.L., T. Song, and S. Sadayappan, *Myofilaments: Movers and Rulers of the Sarcomere.* Compr Physiol, 2017. **7**(2): p. 675-692.
212. Solaro, R.J., M. Henze, and T. Kobayashi, *Integration of troponin I phosphorylation with cardiac regulatory networks.* Circ Res, 2013. **112**(2): p. 355-66.
213. Metzger, J.M. and M.V. Westfall, *Covalent and noncovalent modification of thin filament action: the essential role of troponin in cardiac muscle regulation.* Circ Res, 2004. **94**(2): p. 146-58.
214. Bodor, G.S., et al., *Troponin I phosphorylation in the normal and failing adult human heart.* Circulation, 1997. **96**(5): p. 1495-500.
215. Bristow, M.R., et al., *Beta 1- and beta 2-adrenergic-receptor subpopulations in nonfailing and failing human ventricular myocardium: coupling of both receptor subtypes to muscle contraction and selective beta 1-receptor down-regulation in heart failure.* Circ Res, 1986. **59**(3): p. 297-309.
216. Brodde, O.E., et al., *Regional distribution of beta-adrenoceptors in the human heart: coexistence of functional beta 1- and beta 2-adrenoceptors in both atria and ventricles in severe congestive cardiomyopathy.* J Cardiovasc Pharmacol, 1986. **8**(6): p. 1235-42.
217. Tardiff, J.C., *Thin filament mutations: developing an integrative approach to a complex disorder.* Circ Res, 2011. **108**(6): p. 765-82.
218. Murphy, A.M., et al., *Molecular cloning of rat cardiac troponin I and analysis of troponin I isoform expression in developing rat heart.* Biochemistry, 1991. **30**(3): p. 707-12.
219. Subramaniam, A., et al., *Tissue-specific regulation of the alpha-myosin heavy chain gene promoter in transgenic mice.* J Biol Chem, 1991. **266**(36): p. 24613-20.
220. Ballester, M., et al., *Real-time quantitative PCR-based system for determining transgene copy number in transgenic animals.* Biotechniques, 2004. **37**(4): p. 610-3.
221. Yin, F.C., et al., *Use of tibial length to quantify cardiac hypertrophy: application in the aging rat.* Am J Physiol, 1982. **243**(6): p. H941-7.
222. Chen, Y., et al., *Left ventricular failure produces profound lung remodeling and pulmonary hypertension in mice: heart failure causes severe lung disease.* Hypertension, 2012. **59**(6): p. 1170-8.
223. Ojha, N., et al., *Characterization of the structural and functional changes in the myocardium following focal ischemia-reperfusion injury.* Am J Physiol Heart Circ Physiol, 2008. **294**(6): p. H2435-43.

224. Vogel, B., et al., *Determination of collagen content within picrosirius red stained paraffin-embedded tissue sections using fluorescence microscopy.* MethodsX, 2015. **2**: p. 124-34.
225. Martin, A.F., et al., *Identification and functional significance of troponin I isoforms in neonatal rat heart myofibrils.* Circ Res, 1991. **69**(5): p. 1244-52.
226. Waterhouse, N.J., et al., *The (Holey) study of mitochondria in apoptosis.* Methods Cell Biol, 2001. **66**: p. 365-91.
227. Ricci, J.E., R.A. Gottlieb, and D.R. Green, *Caspase-mediated loss of mitochondrial function and generation of reactive oxygen species during apoptosis.* J Cell Biol, 2003. **160**(1): p. 65-75.
228. Eigentler A, D.A., Gnaiger E, *Laboratory Protocol: Citrate synthase a mitochondrial marker enzyme.* Oroboros Protocols Enzymes, 2020.
229. Lopez, R., et al., *Impaired Myocardial Energetics Causes Mechanical Dysfunction in Decompensated Failing Hearts.* Function (Oxf), 2020. **1**(2): p. zqaa018.
230. Brandt, R.R., et al., *Atrial natriuretic peptide in heart failure.* J Am Coll Cardiol, 1993. **22**(4 Suppl A): p. 86A-92A.
231. Cominacini, L., et al., *Endoplasmic reticulum stress and Nrf2 signaling in cardiovascular diseases.* Free Radic Biol Med, 2015. **88**(Pt B): p. 233-242.
232. Quiros, P.M., et al., *Analysis of mtDNA/nDNA Ratio in Mice.* Curr Protoc Mouse Biol, 2017. **7**(1): p. 47-54.
233. Chevtzoff, C., et al., *Reactive oxygen species-mediated regulation of mitochondrial biogenesis in the yeast Saccharomyces cerevisiae.* J Biol Chem, 2010. **285**(3): p. 1733-42.
234. Jezek, J., K.F. Cooper, and R. Strich, *Reactive Oxygen Species and Mitochondrial Dynamics: The Yin and Yang of Mitochondrial Dysfunction and Cancer Progression.* Antioxidants (Basel), 2018. **7**(1).
235. Paradies, G., et al., *Reactive oxygen species affect mitochondrial electron transport complex I activity through oxidative cardiolipin damage.* Gene, 2002. **286**(1): p. 135-41.
236. Slater, T.F., *Free-radical mechanisms in tissue injury.* Biochem J, 1984. **222**(1): p. 1-15.
237. Nissanka, N. and C.T. Moraes, *Mitochondrial DNA heteroplasmy in disease and targeted nuclease-based therapeutic approaches.* EMBO Rep, 2020. **21**(3): p. e49612.
238. Hortmann, M., et al., *The mitochondria-targeting peptide elamipretide diminishes circulating HtrA2 in ST-segment elevation myocardial infarction.* Eur Heart J Acute Cardiovasc Care, 2019. **8**(8): p. 695-702.
239. Chatfield, K.C., et al., *Elamipretide Improves Mitochondrial Function in the Failing Human Heart.* JACC Basic Transl Sci, 2019. **4**(2): p. 147-157.
240. Lu, Q.W., et al., *Phosphorylation of cardiac troponin I at protein kinase C site threonine 144 depresses cooperative activation of thin filaments.* J Biol Chem, 2010. **285**(16): p. 11810-7.
241. Cochran, D.A. and A.J. Doig, *Effect of the N2 residue on the stability of the alpha-helix for all 20 amino acids.* Protein Sci, 2001. **10**(7): p. 1305-11.
242. Koya, D. and G.L. King, *Protein kinase C activation and the development of diabetic complications.* Diabetes, 1998. **47**(6): p. 859-66.
243. Inagaki, K., et al., *Pharmacological inhibition of epsilon-protein kinase C attenuates cardiac fibrosis and dysfunction in hypertension-induced heart failure.* Hypertension, 2008. **51**(6): p. 1565-9.

244. Chen, Z. and P.A. Cole, *Synthetic approaches to protein phosphorylation.* Curr Opin Chem Biol, 2015. **28**: p. 115-22.
245. MacGowan, G.A., et al., *Troponin I protein kinase C phosphorylation sites and ventricular function.* Cardiovasc Res, 2004. **63**(2): p. 245-55.
246. Nakai, H., T.A. Storm, and M.A. Kay, *Recruitment of single-stranded recombinant adeno-associated virus vector genomes and intermolecular recombination are responsible for stable transduction of liver in vivo.* J Virol, 2000. **74**(20): p. 9451-63.
247. King, K.C. and S. Goldstein, *Congestive Heart Failure And Pulmonary Edema*, in *StatPearls*. 2021: Treasure Island (FL).
248. Lang, S.E., et al., *Secondary phosphorylation in myocytes expressing FLAG-tagged and non-tagged phospho-mimetic cardiac troponin I.* Data Brief, 2017. **15**: p. 562-566.
249. Mochly-Rosen, D., K. Das, and K.V. Grimes, *Protein kinase C, an elusive therapeutic target?* Nat Rev Drug Discov, 2012. **11**(12): p. 937-57.
250. Lou, Q., A. Janardhan, and I.R. Efimov, *Remodeling of calcium handling in human heart failure.* Adv Exp Med Biol, 2012. **740**: p. 1145-74.
251. Peoples, J.N., et al., *Mitochondrial dysfunction and oxidative stress in heart disease.* Exp Mol Med, 2019. **51**(12): p. 1-13.
252. Cooke, M.S., et al., *Oxidative DNA damage: mechanisms, mutation, and disease.* FASEB J, 2003. **17**(10): p. 1195-214.
253. Dong, Z., et al., *Mitochondrial Ca(2+) Uniporter Is a Mitochondrial Luminal Redox Sensor that Augments MCU Channel Activity.* Mol Cell, 2017. **65**(6): p. 1014-1028 e7.
254. Li, Y., et al., *Dilated cardiomyopathy and neonatal lethality in mutant mice lacking manganese superoxide dismutase.* Nat Genet, 1995. **11**(4): p. 376-81.
255. Silva, J.P., et al., *SOD2 overexpression: enhanced mitochondrial tolerance but absence of effect on UCP activity.* EMBO J, 2005. **24**(23): p. 4061-70.
256. Allen, M.E., et al., *The cardiolipin-binding peptide elamipretide mitigates fragmentation of cristae networks following cardiac ischemia reperfusion in rats.* Commun Biol, 2020. **3**(1): p. 389.
257. Machiraju, P., et al., *SS-31 Peptide Reverses the Mitochondrial Fragmentation Present in Fibroblasts From Patients With DCMA, a Mitochondrial Cardiomyopathy.* Front Cardiovasc Med, 2019. **6**: p. 167.
258. Butler, J., et al., *Effects of Elamipretide on Left Ventricular Function in Patients With Heart Failure With Reduced Ejection Fraction: The PROGRESS-HF Phase 2 Trial.* J Card Fail, 2020. **26**(5): p. 429-437.
259. Lloyd-Jones, D.M., et al., *Lifetime risk for developing congestive heart failure: the Framingham Heart Study.* Circulation, 2002. **106**(24): p. 3068-72.
260. Manning, E.P., J.C. Tardiff, and S.D. Schwartz, *A model of calcium activation of the cardiac thin filament.* Biochemistry, 2011. **50**(34): p. 7405-13.
261. Risi, C., et al., *Ca(2+)-induced movement of tropomyosin on native cardiac thin filaments revealed by cryoelectron microscopy.* Proc Natl Acad Sci U S A, 2017. **114**(26): p. 6782-6787.
262. Huang, X., et al., *Cardiac troponin I gene knockout: a mouse model of myocardial troponin I deficiency.* Circ Res, 1999. **84**(1): p. 1-8.